Swansea University

2024

High-Grade Serous Ovarian Cancer Drug Development:

Investigating the mechanism of action of PLK1 and BRD4 inhibitors in HGSOC

Submitted to Swansea University in fulfilment of the requirements for the Degree of Master of Science by Research

Agne Baseviciene

BSc (Hons)

Summary

Background. In females, ovarian cancer is the 5th cancer-related death cause and the deadliest gynaecological cancer. High-grade serous ovarian cancer accounts for the majority of ovarian cancer cases and is associated with poor prognosis and high rates of resistance. Although, the majority of new therapeutics show success in preclinical stages they do not provide significant benefits in clinical settings. New treatment strategies relating to cancer hallmarks such as sustained proliferative signalling and non-mutational epigenetic modifications which are regulated through proteins such as polo-like kinase 1, PLK1, and bromodomain-containing protein, BRD4, respectively, hold potential.
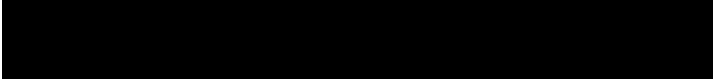
Results. An advanced pre-clinical drug development pipeline was developed, incorporating RNA and ATAC-seq, to identify the mechanism of action of BI 2536 and BI 6727, two compounds that target PLK1 in isolation and/or in combination with BRD4. High-grade ovarian cell lines expressed PLK1 and BRD4 and higher PLK1 expression was associated with greater sensitivity to BI 2536 and BI 6727. Drugs reduced cell viability through induction of G2/M cell cycle arrest, followed by DNA damage and apoptosis. RNA-seq and ATAC-seq results provide evidence for the inhibition of PLK1 function as cell cycle pathways were differentially regulated whereas BRD4 expression and genes were not affected significantly.

Impact. Implementation of functional genomics, involving genomics, transcriptomics, and epigenomics, into drug development and screening, was proven to be a robust strategy to study cancer complexity and result in new druggable target discoveries. Both compounds have undergone clinical trials, with inconsistent classification and an in-depth understanding of their mechanism of action in HGSOC could inform future PLK1 targeting strategies for HGSOC.

Declarations

This work has not previously been accepted in substance for any degree and is not being concurrently submitted in candidature for any degree.
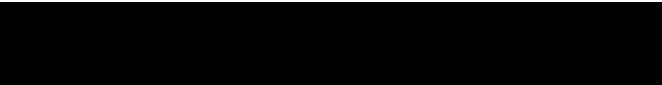
Signed .....

Date ....23/04/2024...

STATEMENT 1

This thesis is the result of my own investigations, except where otherwise stated. Where correction services have been used, the extent and nature of the correction is clearly marked in a footnote(s).

Other sources are acknowledged by footnotes giving explicit references. A bibliography is appended.

Signed ....

Date ......23/04/2024..

STATEMENT 2

I hereby give consent for my thesis, if accepted, to be available online in the University's Open Access Repository and for inter-library loan, and for the title and summary to be made available to outside organisations.

Signed ......

Date ....23/04/2024..

Table of Contents

Acknowledgements

Abbreviations

Abbreviation	Full wording
ATAC-seq	Assay for Transposase-Accessible Chromatin with Sequencing
ATCC	American Type Culture Collection
ATP	Adenosine Triphosphate
BET	Bromodomain and Extra-Terminal Containing Protein
BSA	Bovine Serum Albumin
CA125	Cancer Antigen 125
DMEM	Dulbecco's Modified Eagle Medium
DMSO	Dimethyl Sulfoxide
DNA	Deoxyribonucleic Acid
EGFR	Epidermal growth factor receptor
EOC	Epithelial Ovarian Cancer
FBS	Fetal Bovine Serum
FDR	False Discovery Rate
GAPDH	Glyceraldehyde 3-phosphate dehydrogenase
GSEA	Gene set enrichment analysis
HAT	Histone acetyltransferase
HDAC	Histone deacetylase
HGSOC	High-Grade Serous Ovarian Cancer
IC50	Half Maximal Inhibitory Concentration
IGRF	The insulin-like growth factor receptor
kDa	kilodalton
OC	Ovarian Cancer
ORA	Over-representation analysis
PARP	Poly-ADP Ribose Polymerase
PBD	Polo-Box domain
PLK	Polo-Like Kinase
RNA	Ribonucleic acid
rpm	revolutions per minute
RPMI	Roswell Park Memorial Institute medium

RT	Room Temperature
STC	Solid Tumour Cancer
TBS-T	Tris-Buffered Saline – Tween 20 (Polysorbate 20)
TNBC	Triple-negative breast cancer
VEGF	Vascular Endothelial Growth Factor

List of figures

List of tables

1 Introduction

1.1 Cancer

Cancer is comprised of a group of diverse diseases and is defined by uncontrolled cellular growth and often characterised by an ability to metastasise, i.e., invade other tissues and organs beyond the primary source (World Health Organization, 2019). In 2020, the estimated number of new cancer cases exceeded 18 million worldwide and the number is projected to reach 28 million by 2040 (Cancer Research UK, n.d.-b). It was reported that in 2016 chemotherapy cost £1.4 billion a year which accounted for approximately 10% of the central budget of NHS England (NHS England, 2016). By 2025, the number of people living with cancer in the UK is estimated to reach 3.5 million, increasing the number of families affected, and placing a huge burden on NHS systems and resources (Macmillan Cancer, n.d.).

1.2 Solid tumour cancers

Malignant tumours are classified into solid and liquid tumours. Solid tumour cancers (STCs) can originate in various organs and tissues, including the lung, breast, prostate, colon, ovaries, pancreas, and are defined by the formation of a mass or solid lump of abnormal cells (Weinberg, 2013). Whereas, liquid tumours primarily affect the blood and the immune system; examples include leukaemia (blood), lymphoma (lymphocytes) and myeloma (plasma cells) (Weinberg, 2013). STCs are the leading cancers in cancer-related mortality (Figure 1-1) (World Health Organization, 2020a). In 2020, in both females and males, the highest number of cancer-related deaths was due to lung cancer (World Health Organization, 2020a). The second most deadly cancer in females was breast cancer, in males- prostate, followed by colorectal cancer, in both (World Health Organization,

Estimated number of incident cases and deaths United Kingdom, females, all ages (excl. NMSC)
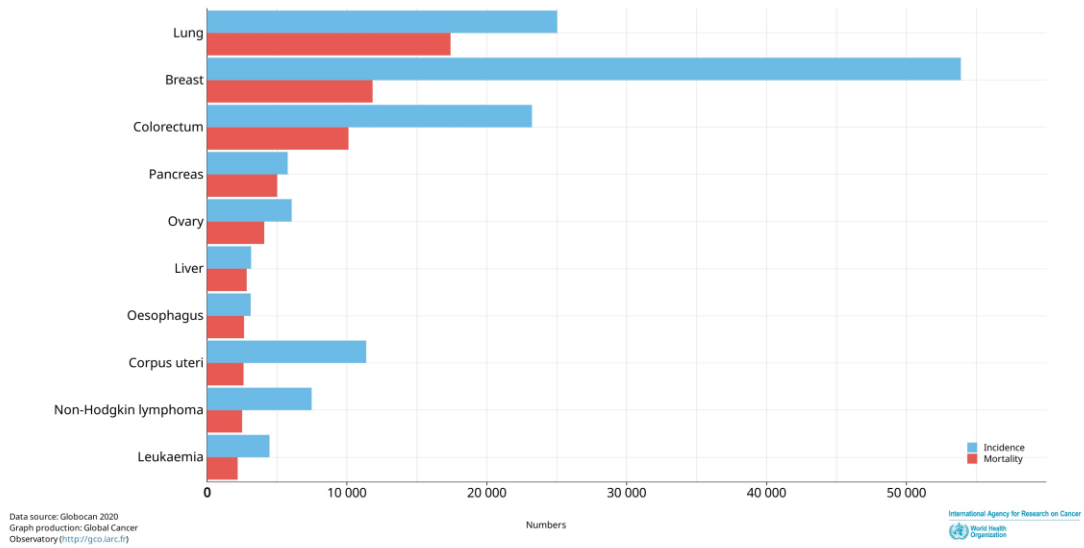
Estimated number of incident cases and deaths United Kingdom, males, all ages (excl. NMSC)
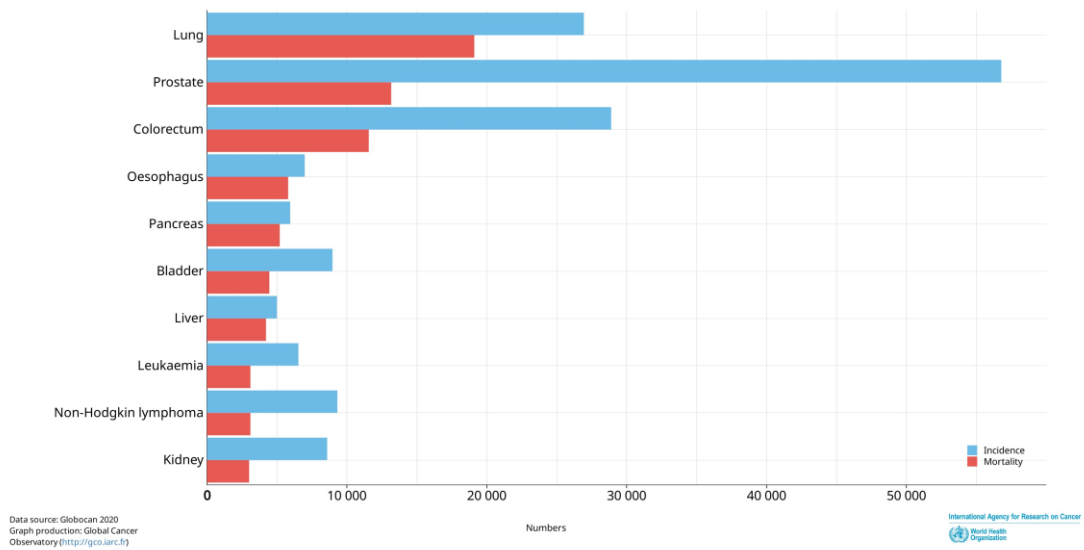
Figure 1-1. Estimated number of cancer incident cases and deaths in females and males in UK. Cancers are ranked by the number of deaths. Incidence rates are in blue, mortality rates- red. Graphs created in https://gco.iarc.fr/ (World Health Organization, 2020a).

2020a). Two gynaecological cancers, ovarian and corpus uteri (endometrial), were among the ten deadliest cancers in females (World Health Organization, 2020a).

1.2.1   Gynaecological Cancers

Gynaecological cancers are one of the deadliest STCs, originating in the female reproductive organs (Cancer Research UK, 2022b). These cancers include cervical,

2

ovarian, uterine, vulvar and vaginal (CDC, 2023). The most common gynaecological cancer is corpus uteri referred to as endometrial cancer, a type of uterine cancer which accounted for over 11 thousand new cases and over 2 thousand UK female deaths in 2020 (World Health Organization, 2020a). The second most common, yet the deadliest gynaecological cancer, is ovarian cancer (OC), followed by less common cervical cancer which has an incidence rate 3 times lower than that of endometrial cancer (World Health Organization, 2020a). The two rarest are vulvar and vaginal cancers with 1500 and 300 new cases in 2020, respectively (World Health Organization, 2020a). The incidence and mortality of all gynaecological cancers are predicted to follow an upward trend to 2040 (Figure 1-2), with ovarian cancer possessing the biggest concern, shown by the smallest difference between new cases and number of deaths (World Health Organization, 2020b).

Estimated numbers from 2020 to 2040, Females, age [0-85+]
United Kingdom

GLOBAL CANCER OBSERVATORY
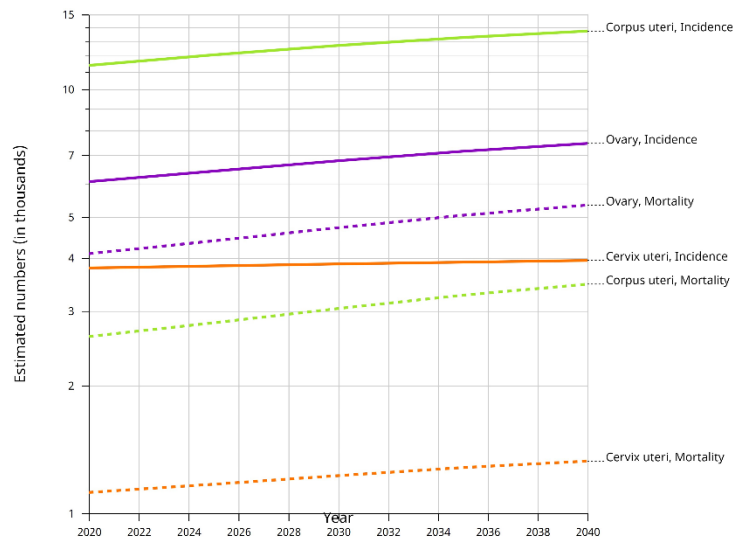
Cancer Tomorrow | IARC - All Rights Reserved 2023 - Data version: 2020

International Agency for Research on Cancer
World Health Organization

Figure 1-2. Estimated number of new cases and deaths from endometrial, ovarian and cervical cancer in females. *Estimated number for the 2020-2040 period. Obtained from World Health Organization (2020b).*

1.3 Ovarian cancer

In 2020, OC ranked 8th in the number of new cancer cases in females worldwide (World Health Organization, 2020a). With over 6000 new cases and over 4000 deaths in the UK, OC ranks 5th among the deadliest cancers in females (World Health Organization, 2020a). The UK Million Women study linked higher mortality rates to the later stages, older age, higher BMI, and smoker status (Gaitskell et al., 2022). Females diagnosed at stage III and stage IV showed a seven-fold and ten-fold higher risk of death, respectively, when compared to early stage I diagnosis (Gaitskell et al., 2022).

1.3.1 Ovarian Cancer Classification

OC is classified into three categories depending on the cell origin (Figure 1-3). The lowest proportion of OC cases is germ cell and sex-cord stromal while approximately 90% of OC
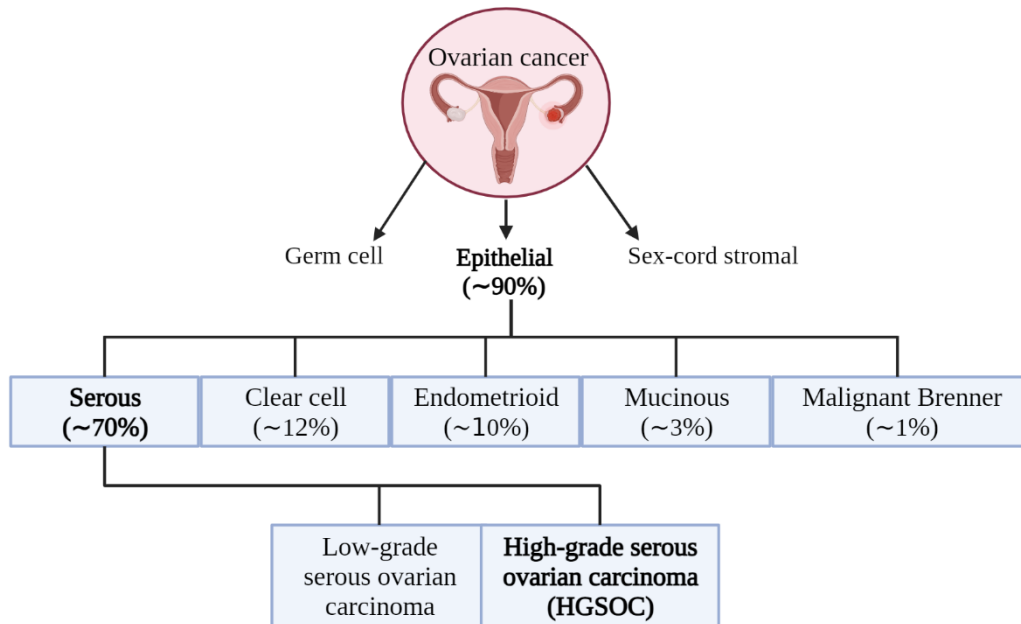
Figure 1-3. Ovarian cancer types by cell origin and histological subtypes of epithelial. *Percentages in the brackets indicate prevalence. Adapted from Rojas et al. (2016). Created in Biorender.*

cases are epithelial (Rojas et al., 2016). Epithelial ovarian cancer (EOC) is further subdivided into five histological subtypes. Starting from the most common, accounting for approximately 70% of all EOC cases is serous OC (Rojas et al., 2016). Other histological subtypes are clear cell (~12%), endometrioid (~10%), mucinous (~3%) and malignant Brenner (~1%)(Rojas et al., 2016). Serous OC is further divided into two grades: high-grade and low-grade serous ovarian cancer (Rojas et al., 2016). High-grade

serous OC (HGSOC) cells are poorly differentiated or undifferentiated, have abnormal appearance and have greater replication and metastasis potential than low-grade serous OC (Rojas et al., 2016).

1.3.2 High-grade serous ovarian cancer

HGSOC is associated with poorer survival compared to low-grade serous OC tumours (Gaitskell et al., 2022; Gockley et al., 2017). Median survival in females with stage III and IV HGSOC was 43.8 and 32.5 months, respectively, in contrast to 98.1 and 55.2 months in low-grade serous OC patients (Gaitskell et al., 2022; Gockley et al., 2017). The majority of HGSOC patients are *TP53* gene mutation carriers, which lessens p53's ability to induce cell cycle arrest for reparation of deoxyribonucleic acid (DNA) damage as well as induce apoptosis in response to DNA damage or mutations (Bell et al., 2011; Ozaki & Nakagawara, 2011).

1.3.3 Diagnosis and treatment

The high rates of mortality in OC are attributed to late diagnosis because of non-specific symptoms, no specific biomarker and resistance to chemotherapy arising at recurrence (Brain et al., 2014; Garzon et al., 2020). To diagnose OC, extensive tests are performed including pelvic exams, imaging such as ultrasound or CT scans, blood tests, sometimes surgery and genetic testing (Cancer Research UK, n.d.-a). Cancer antigen 125 (CA125) is the biomarker that may indicate the presence of OC (Cancer Research UK, n.d.-a). However, its levels can be elevated because of other conditions such as uterine fibroids, endometriosis (Cancer Research UK, n.d.-a). For example, one study examined CA125 levels in females with endometriosis diagnosis and the mean serum CA125 level was 49.93 ± 4.30 U/mL which could lead to false positives OC diagnosis as the normal range is 0-35 U/mL (Karimi-Zarchi et al., 2016). The non-specific symptoms that can include persistent bloating, abdominal pain, and fatigue are often disregarded thus highest percentage of OC diagnoses are of stage III/IV which decreases their survival chances and results in more complex treatment (Torre et al., 2018).

Current treatment strategies may involve surgery, chemotherapy, radiotherapy, hormone and/or targeted therapy (Cancer Research UK, 2022a). The treatment strategy is determined by the following factors: ovarian cancer tumour size, type, location, whether

it had metastasised, i.e. spread further from the primary site, and general patient health (Cancer Research UK, 2022a). Possible surgery options include removal of both ovaries and the fallopian tubes (bilateral salpingo-oophorectomy), removal of cervix and removal of womb (abdominal hysterectomy). Standard chemotherapy is platinum-based or combination therapy (Cancer Research UK, 2022a). The most common chemotherapy is carboplatin alone or in combination with paclitaxel (Taxol) (Cancer Research UK, 2022a).

Platinum-based compounds damage cellular DNA through cross-linkage of DNA molecules, leading to cell death (Bardal et al., 2011). Paclitaxel is an antimicrotubular agent which stabilizes microtubules during mitosis, stopping cells from dividing (Kampan et al., 2015). Despite the initial response to these drugs, the biggest issue that is associated with OC treatment is cancer reoccurrence and resistance to standard chemotherapy (Pokhriyal et al., 2019).

1.3.4 Next-generation drug treatment strategies relating to specific cancer hallmarks

Targeted therapies are being introduced to improve the outcome of OC treatment (Lim & Ledger, 2016). In the development of next-generation drugs, that target specific hallmarks of the disease, it is useful to understand the cancer development process' and how cancer cells differ from normal cells (Hanahan, 2022; Hanahan & Weinberg, 2000; Hanahan & Weinberg, 2011). Targeted therapies according to their effect on cancer can be assigned cancer hallmarks illustrated in Figure 1-4. The following are hallmarks with targets that can be inhibited by targeted therapy: angiogenesis through Vascular endothelial growth factor (VEGF), sustained proliferative signal through Epidermal growth factor receptor (EGFR) and folate receptor, evasion of apoptosis through Insulin-like growth factor receptor (IGFR) and genome instability through poly-ADP ribose polymerase (PARP) (Lim & Ledger, 2016).

Angiogenesis is the formation of new blood vessels crucial for cancer development as it provides cancer with oxygen, nutrients as well as growth factors (Adair & Montani, 2010). VEGF is a molecule which promotes angiogenesis, and its inhibition leads to disrupted angiogenesis (Shibuya, 2011). Currently out of all of the anti-angiogenesis drugs, the VEGF inhibitor -bevacizumab, also known as Avastin® is approved to treat OC patients
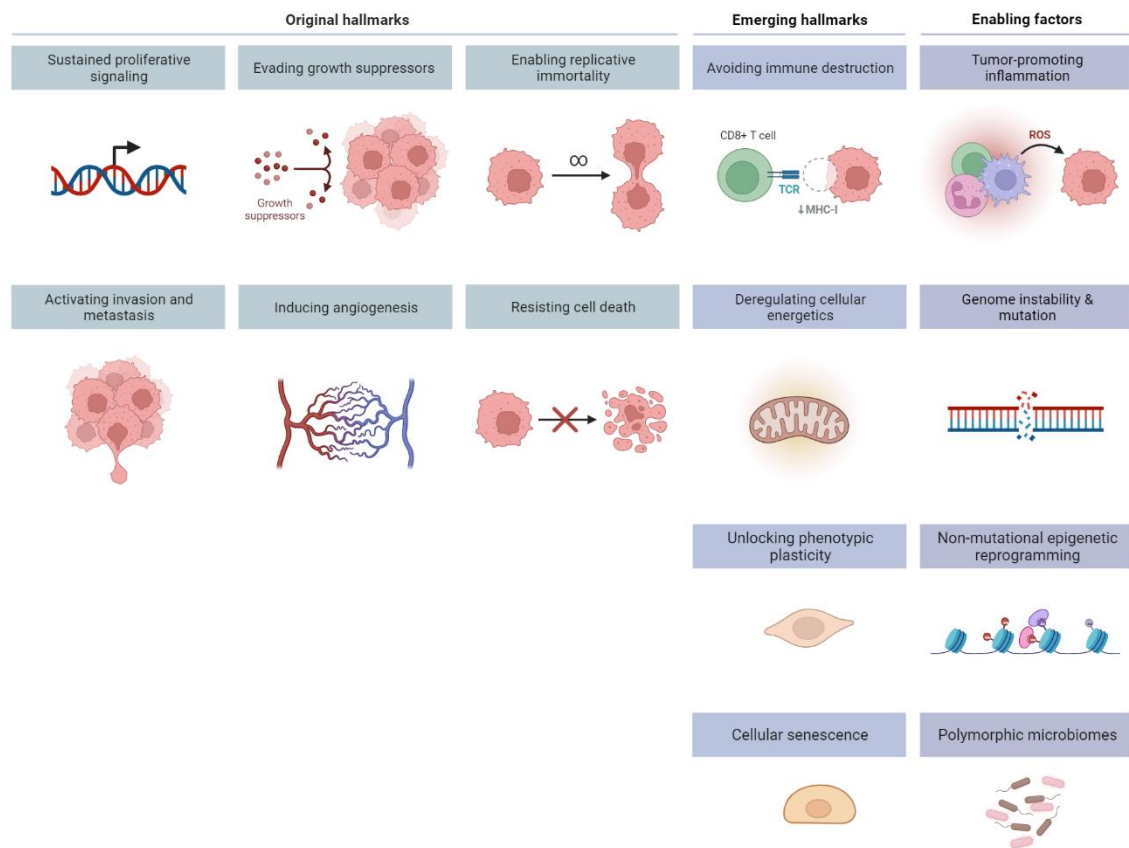
Figure 1-4. Hallmarks of ovarian cancer. *(Hanahan, 2022; Hanahan & Weinberg, 2000; Hanahan & Weinberg, 2011) Created in BioRender.*

(Hall et al., 2020; Hall et al., 2013). DNA damage repair is one of the genome stability-ensuring functions and PARP is one of the key molecules involved (Morales et al., 2014). PARP repairs single-strand DNA breaks via the base excision repair/single-strand break repair pathway (Javle & Curtin, 2011). In OC, when PARP is inhibited, an accumulation of single-strand breaks results in DNA double-strand breaks which cannot be repaired due to alternative DNA repair pathways (Della Pepa et al., 2015). The alternative DNA damage repair pathway is used due to the absence of functional BRCA1 or BRCA2 proteins in OC, causing chromosomal instability resulting in apoptosis (Tangutoori et al., 2015; Ward et al., 2015). Current PARP inhibitors in the clinic are Niraparib (Zejula®), Olaparib (Lynparza®) and Rucaparib (Rubraca®). EGFR promotes proliferative signalling and is overexpressed in approximately 70% of OC cases (Kohler et al., 1992; Mak et al., 2021). Its expression is associated with poor prognosis (Tas et al., 2014). Although EGFR seems to hold potential as a target for inhibition, monoclonal antibodies

against EGFR such as cetuximab and EGFR tyrosine kinase inhibitors such as gefitinib did not show great efficacy as OC treatment (Lim & Ledger, 2016). Folate Receptor α (FRα) is overexpressed in OC which increases available folate levels in cancer cells resulting in tumour growth (Ledermann et al., 2015). FRα inhibitors are not yet approved for OC treatment but hold potential as BGC 954 induced partial response and EC145 in combination with pegylated liposomal doxorubicin was superior to standard therapy, respectively (Banerjee et al., 2022; Naumann et al., 2013). Insulin-like growth factor 1 (IGF1R) promotes cell growth and is involved in the inhibition of apoptosis and is overexpressed in low-grade serous OC representing a minority of OC (King et al., 2011; Weroha & Haluska, 2008). However, anti-IGF-1R mono-antibodies such as teprotumumab, did not have positive effect on STC patients (Qu et al., 2017).

1.4 Role of cell cycle and epigenetic modulators in cancer development

With new treatment strategies emerging, the range of OC resistance, to inhibitors such as PARPi, is also expanding (Miller et al., 2022). Therefore, a better understanding of cancer resistance mechanisms and alternative, new treatment strategies and drugs is required. Targeting sustained proliferative signalling, downregulating proteins involved in the cell cycle, and proteins involved in non-mutational epigenetic reprogramming hold potential because cell cycle proteins such as polo-like kinases (PLK) are overexpressed in OC alongside amplification of epigenetic modulators such as bromodomain and extra-terminal containing proteins (BET) (Liu et al., 2017; Rhyasen et al., 2018). Cell cycle targeting inhibitors such as prexasertib for checkpoint kinases 1 and 2, adavosertib, WEE1 inhibitor, as well as BET inhibitor undergoing clinical trials provide validity that it is a potential treatment strategy and requires further development (Andrikopoulou et al., 2021; Konstantinopoulos et al., 2022; Lheureux et al., 2021).

1.4.1 Polo-like kinases

PLKs are a group of serine/threonine protein kinases that are one of the key regulators of the cell cycle and mitosis (Zitouni et al., 2014). There are five PLKs present in humans, PLK1, PLK2, PLK3, PLK4 and PLK5 (Zitouni et al., 2014). PLKs are characterized by their structural components which are an N-terminal serine/threonine kinase domain, and a C-terminal polo-box domain (PBD) (Figure 1-5). While the kinase domain is a catalytic domain which binds adenosine triphosphate (ATP) (except in PLK5), subcellular localization and catalytic activity regulation of PLKs are regulated by PBD (Barr et al., 2004; Shin et al., 2015; Song et al., 2000). As illustrated in Figure 1-5, PLK1-3 are more homologous in their structure because of their kinase domain but have unique PBDs (Kressin et al., 2021). Whereas PLK4 and PLK5 are structurally and thus functionally different from the rest of the PLK family members.
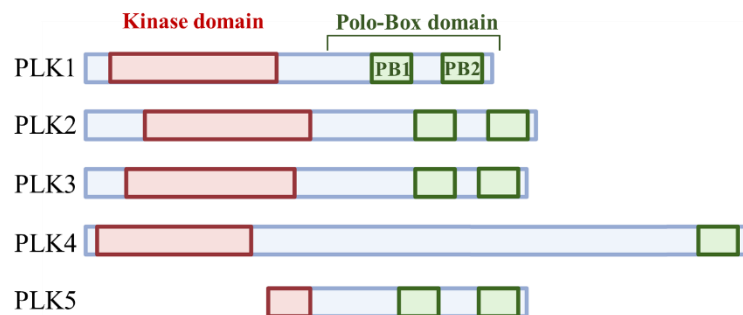
Figure 1-5. Structure of Polo-like kinases. Polo-like kinases (PLK) contain kinase domain (red) and polo-box (PB) domain (green). Adapted from (Xu et al., 2012). Created with BioRender.

PLK1, the most studied PLK, regulates the cell cycle, including G2/M transition and mitosis checkpoints (De Cárcer et al., 2011). During mitosis, Plk1 localization changes as mitosis progresses. Initially in prophase, Plk1 localizes in centrosomes, in prometaphase and metaphase it associates with kinetochores, in anaphase- central spindle and lastly in telophase, PLK1 resides in the midbody (Petronczki et al., 2008). PLK1 promotes mitotic entry as it phosphorylates, and activates Cdk1-cyclin B as well as centrosome maturation, chromosome condensation, spindle assembly, chromosome segregation and cytokinesis-cell and cytoplasm division into two daughter cells (Kagami et al., 2017; Lane & Nigg, 1996; van de Weerdt & Medema, 2006). PLK2 is expressed in the G1 phase and is required together with PLK4 for centriole duplication which is initiated during the G1/S transition (Habedanck et al., 2005; Warnke et al., 2004). PLK3 is activated in response to

oxidative stress, DNA damage and promotes cell cycle arrest and apoptosis (Xie et al., 2005). PLK5 does not have a functional kinase domain but can ectopically be expressed in response to stimuli and induce cell cycle arrest and apoptosis similarly to PLK3 (Andrysik et al., 2010).

In HGSOC, *TP53*, gene coding for p53 protein, is mutated in 97% of HGSOC cases losing its ability to act as a tumour suppressor and regulating genes which regulate cell cycle arrest and apoptosis (Vousden & Prives, 2009; Y. Zhang et al., 2016). The repressor function of p53 on forkhead box M1 (FOXM1) expression is impaired (Barsotti & Prives, 2009; Bell et al., 2011). Therefore, FOXM1 is upregulated which leads to overexpression of its target genes, such as *PLK1*, which has a detrimental role in proliferation (Bell et al., 2011; Zhou et al., 2014). PLK1 overexpression has been detected in several types of cancer tumours, including OC implying that PLK1 upregulation has a role in tumorigenesis (Liu et al., 2017; Weichert et al., 2005; Zhang et al., 2015). Significantly higher expression levels of PLK1 are observed in stage III-IV OC patients with high-grade OC such as HGSOC, which can be expected because overexpressed PLK1 also inhibits p53 function resulting in aggressive tumourigenic status (de Cárcer, 2019; Takai et al., 2001; Zhang et al., 2015). The oncogenic PI3K pathway can also be activated as a result of PLK1 overexpression as it inhibits tumour suppressor, PTEN, leading to an increased cell proliferation rate (de Cárcer, 2019).

1.4.2   Bromodomain containing proteins

BETs are proteins, referred to as epigenetic readers, which bind to acetylated lysine residues on histone tails and transcription factors (Marmorstein & Zhou, 2014). BET family members include BRD2, BRD3, BRD4 and the testis-restricted BRDT (Taniguchi, 2016). BET proteins contain two bromodomains (BD1 and BD2) which recognise N-acetyl residue, an extra-terminal domain which facilitates protein-protein interactions and a C-terminal domain (Marmorstein & Zhou, 2014; Trivedi et al., 2020; Werner et al., 2020). These BETs have an important role in epigenetic regulation, gene expression, and chromatin remodelling. BRD4 directly interacts with, and regulates the recruitment of positive transcription elongation factor b (p-TEFb) to promoters and promotes RNA polymerase II-mediated transcription elongation, the second phase of transcription

initiation (Altendorfer et al., 2022; Jang et al., 2005). BRD4 can also bind the Mediator complex, a coactivator complex, which interacts with transcription factors, recruits, and activates RNA polymerase II (Bhagwat et al., 2016). In addition to these binding functions, BRD4 can phosphorylate RNA polymerase II and function as a histone acetyltransferase (HAT); acetylating histones, thus having a role in chromatin remodelling (Devaiah et al., 2016; Devaiah et al., 2012). BRD2 can bind to the E2F transcription factor and increase transcription of E2F-regulated genes (Denis et al., 2000).

The *BRD4* gene was found to be amplified most frequently in HGSOC patients in contrast to other cancers such as uterine, lung, breast (Rhyasen et al., 2018). *BRD4* is associated with higher expression of oncogenes, such as *NRG1*, *MYC*, *NOTCH3* (Rhyasen et al., 2018; Ucar & Lin, 2015). *BRD4* amplification leads to increased P-TEFb-dependent phosphorylation of RNA polymerase II, which stimulates transcription of oncogenes which is essential for cancer proliferation (Jang et al., 2005). BRD4 binds to promoters, enhancers and super-enhancers- a group of enhancers located near genes such as the *MYC* oncogene and changes in BRD4 expression lead to oncogenic growth (Lovén et al., 2013).

1.5   PLK1 inhibitors

Due to the overexpression and abnormal activity of PLK1 in cancer processes, the specific inhibition of this protein has become a prominent goal in advanced therapeutic development (Su et al., 2022). Normal, or non-cancerous cells, have been shown to exhibit reduced sensitivity to such PLK1 inhibition, demonstrating the potential for less off-target effects (Liu et al., 2006).

There are several selective PLK1 inhibitors in preclinical and clinical trial phases, including Onvansertib (PCM-075, NMS-P937) ATP inhibitor, GSK461364 and TAK-960, N-terminal catalytic domain inhibitors. Onvansertib underwent a phase Ib study in combination therapy for patients with relapsed or refractory acute myeloid leukaemia with planned phase II (Zeidan et al., 2020). Ovansertib is also being studied in the ongoing phase II trial in metastatic colorectal cancer as part of a combination treatment with irinotecan, fluorouracil [5-FU], and leucovorin (FOLFIRI) and bevacizumab (Cardiff Oncology, 2023b). Phase II trial in chronic myelomonocytic leukaemia is in the recruitment stage (Mayo Clinic, 2023). It is also being tested in combination with

paclitaxel for triple-negative breast cancer, to explore synergistic capabilities with paclitaxel (Cardiff Oncology, 2023a). Olmos et al. (2011) reported the results of a phase I clinical trial on GSK461364 treatment for advanced STCs including two cases of OC. The best outcome was stable disease which was also observed in one OC patient. The drug had a short half-life of 9-13 h and the most common grade 3-4 adverse events were venous thrombotic emboli and myelosuppression (Olmos et al., 2011). HMN-214, a PLK1 inhibitor, underwent phase I trial for advanced STCs such as colorectal, non–small cell lung carcinoma, breast carcinoma, and oesophageal carcinoma (Garland et al., 2006). 24% of patients in response to HMN-214 treatment had a stable disease, the rest had a progressive disease. Terminal half-life was dose-dependent and ranged from 10.0 to 11.1 h. Lastly, TAK960, PLK1 inhibitor, efficacy studies were terminated in the phase I trial due to drug ineffectiveness in advanced nonhematologic malignancies and commercial reasons (Millennium Pharmaceuticals, 2014).

Overall, PLK1 inhibition shows promise as an STC treatment strategy, especially, improved, newest-generation inhibitors. Despite that information on OC is lacking and thus more extensive research is required to establish PLK1 inhibition effectiveness.

1.6 Bromodomain inhibitors

The development of bromodomain inhibitors is in relatively early phases, the first bromodomain inhibitor molibresib (GSK525762, I-BET 762) was described only in 2010 (Nicodeme et al., 2010). Since then, the drug has gone to phase II clinical trials but did not achieve predefined clinically significant response rates in any of the STCs tested, including testis carcinoma, small cell lung cancer, castration-resistant prostate cancer, triple-negative breast cancer (Cousin et al., 2022). JQ1 was the second BRD inhibitor described, now it is used in preclinical models only, due to the short half-life (1 h) it is not suitable for clinical trials (Trabucco et al., 2015). ODM-207 underwent Phase 1–2, multicentre, non-randomised open-label in STCs including castration-resistant cancer, melanoma, oestrogen receptor-positive breast cancer where the observed response was a stable disease, progressive disease, or non-measurable disease (Ameratunga et al., 2020). Birabresib (MK-8628/OTX015), BRD2, BRD3, and BRD4 inhibitor, achieved complete and partial responses in several acute leukaemia and diffuse large B-cell lymphoma

patients (Amorim et al., 2016; Berthon et al., 2016). Thrombocytopenia was a common adverse event thus 14 days on, 7 days off scheduled treatment was suggested for further phase II investigation. Birabresib was tested in phase I trial for castrate-resistant prostate cancer and non-small-cell lung cancer half-life of 3.6 -5.3 h (Lewin et al., 2018). The most common adverse event was also thrombocytopenia as previously observed in haematological cancer. 7% of patients partially responded which was the best response and in 60% the disease was stable (Lewin et al., 2018).

1.7   Dual target PLK1 and BRD4 inhibitors: BI 2536 and BI 6727

Next-generation anticancer drugs which have dual action and can target both protein families have been in development. First generation PLK1 and BRD4 inhibitor, BI 2536 and its derivative, second generation - BI 6727 are the two most prominent examples. Although their dual targeting is debatable and, in the literature, they are more commonly classified as selective PLK1 inhibitors rather than dual inhibitors. BI 2536 downregulated the expression of PLK1 protein and mRNA specifically in hepatocellular carcinoma, while also significantly reducing the half-maximal inhibitory concentration (IC50) for adriamycin and other drugs in adriamycin-resistant hepatocellular carcinoma cells (Li et al., 2019). In neuroblastoma cells, the IC50 of BI 2536 ranged between 17 and 28 nM and BI-2536 decreased MCM2 and MCM10 expression levels and induced apoptosis (Hsieh et al., 2022). BI 2536 induced apoptosis in triple-negative breast cancer cells (TNBC) but not in healthy cells (Maire et al., 2013). It also effectively inhibited tumour growth in vivo TNBC-patient-biopsy xenografts models and the combination with chemotherapy agents reduced the time to achieve complete response and prevent recurrence (Maire et al., 2013).

Ciceri et al. (2014) determined the binding constant of BI 2536 (37 $\pm$ 3 nM) and BI 6727 (79 $\pm$ 3 nM) with BRD4, which confirmed the strong interaction and ability of both drugs to bind BRD4. Kinome-wide profiling data showed that BI 2536 was highly selective for PLK1, PLK2, PLK3 and confirmed BI 2536 and BI 6727 ability to interact with BET bromodomains (Ciceri et al., 2014). In stimulated primary human cell types and co-cultures BI-2536 acted differently to selective BET or PLK inhibitors displaying polypharmacology and its profile clustered with both BET and PLK inhibitors (Ciceri et al., 2014). Both BI 2536 and BI 6727 inhibit BRD4 by its displacement from chromatin

which results in suppression of c-MYC expression in B lymphoblast cells (Ciceri et al., 2014). The authors also suggested that the dual targeting inhibitor can have an effect on novel combinations of predictive biomarkers different from those of the PLK/BET only inhibitors. Among 14 kinase inhibitors, BI 2536 had the strongest inhibitory BRD4 ability with the IC50 of 25 nM and its potency closely resembled that of JQ1 (Ember et al., 2014). Interestingly, in a study on HIV-1, both BI 2536 and BI 6727 activated long terminal repeat transcription through BET and not PLK inhibition which reactivates the virus for subsequent killing (Gohda et al., 2018). In acute myeloid leukaemia cells, BI 2536 IC50 values were 88.5 nM and it decreased MYC, a downstream target of transcription mediated by BRD4, protein expression after 12h with 100 nM BI 2536 treatment (Mu et al., 2020). Contrary to that, in another study on acute myeloid leukaemia, a compound with increased BRD4 inhibition potency had a higher viability percentage in comparison to BI 2536, hypothesising that anti-proliferative potential of BI 2536 is due to PLK1 inhibition (Koblan et al., 2016). They confirmed that neither the compound with increased BRD4 potency nor JQ1 had a strong effect on cell cycle while PLK1 selective inhibitors, GSK461364 and BI 2536 induced cell arrest at G2/M (Koblan et al., 2016).

1.7.1 BI 2536 and BI 6727 in ovarian cancer

In preclinical studies BI 2536 inhibited OVCAR-8 growth with IC50 of 7.19 ± 3.60 nM whereas ABCB1-overexpressing human ovary NCI-ADR-RES cells were highly resistant to BI 2536, IC50= 1273.30 ± 191.20 nM (Wu et al., 2013). Only one study used OC cell lines, comparing the BI 6727 effect to JQ1, and found that BI 6727 anti-proliferative activity and effect on OC cell viability closely resembled that of the BRD4 inhibitor (Z. Zhang et al., 2016). Yet the experiments performed with BI 6727 were not extensive, thus authors emphasized the importance of determining precise BI 6727 mechanism of action in advanced OC cases (Z. Zhang et al., 2016).

BI 2536 underwent the multicentric parallel phase II trial in 2010 (Schöffski et al., 2010). Patients had one of five solid tumour types, including ovarian cancer. Despite not moving further, the drug had the greatest effect on OC patients. More than 75% of treated ovarian cancer patients had at least stable disease according to RECIST (Schöffski et al., 2010). Concluding that exploration of the use of PLK1 inhibitors is warranted, BI 2536 derivate,

BI 6727, was created to improve drug efficacy (Schöffski et al., 2010). BI 6727 also reached randomized phase II clinical trials where its efficacy was compared to chemotherapy in platinum-resistant or -refractory OC patients (Pujade-Lauraine et al., 2016). The half-life of BI 6727 was significantly longer than that of BI 2536, 143 h versus 17–34 h respectively. Grade 3 and 4 drug-related haematological adverse events were observed in both trials with lower incidence in BI 6727 treated than BI 2536, but more often than in patients who received chemotherapy (Pujade-Lauraine et al., 2016; Schöffski et al., 2010). Adverse events included neutropenia, thrombocytopenia, febrile neutropenia (33.3% BI 2536 vs. 5.6% BI 6727), anaemia, and pain. Both drugs showed high potential in preclinical models but did not result in satisfactory clinical response, raising the question; why PLK1/BRD4 was more effective in OC patients compared to other STCs?

Indeed, exploring the effect of potential dual inhibition using BI 2536 and BI 6727 as probes may provide insight into the HGSOC development, enabling exploration of the gene expression patterns and functional cancer pathways that are affected in the presence of these drugs. Furthermore, the conflicting literature on the targets of BI 2536 and BI 6727 raises questions about whether these drugs have their effect by targeting and inhibiting PLK1 solely or if they express dual targeting abilities, by targeting BRD4 too. In the majority of research papers outlined previously, the drugs are regarded as PLK1 inhibitors which disregards the potential inhibitory effect on BRD4, thus attributing the mechanism of action on PLK1 rather than joint inhibition. Ember et al. (2014) supported the statement that the use of kinase inhibitors in BET-sensitive cell lines, to probe signalling pathways, could lead to false conclusions if the simultaneous BET inhibition is indeed contributing to the anti-cancer effect.

1.8 Functional genomics and drug development

In the past, cancer research and treatments were unidirectional focusing on and targeting altered single genes and proteins but the number of clinically effective new single druggable targets is close to being depleted (Menghi & Liu, 2022). In addition, with new single-target therapeutics being developed the drug resistance range also increases (Menghi & Liu, 2022; Miller et al., 2022). Moving forward approaches utilising functional genomics are essential to have a better understanding of cancer and its complexity.

Functional genomics encompasses a range of multiplex techniques including transcriptomics RNA seq, epigenetics- Chip-seq for investigation of genome-wide functions, and establishing interactions between genes and proteins instead of the classical gene-by-gene approach (Gasperskaja & Kučinskas, 2017). Using a functional genomics approach, researchers performed genome-scale CRISPR-Cas9 loss-of-function screens across over 800 cancer cell lines and found that overexpression of phosphate importer SLC34A2, observed in OC which was associated with disrupted phosphate efflux leading to the discovery of therapeutic vulnerability in ovarian carcinoma (Bondeson et al., 2022).

In the Genomics of Drug Sensitivity in Cancer project over 200 compounds were tested that were either approved to be used in the clinic, in preclinical stages or experimental drugs, and over 600 statistically significant associations were established between the cancer functions event and compounds tested (Iorio et al., 2016). One of which was that squamous lung cancer cell lines carrying inactivating mutations of MLL2, a chromatin modifier, were sensitive to the anti-androgen compound bicalutamide. These studies represent big-scale data analysis from hundreds of cell lines, however, the same principles can be applied to study several cell lines for instance in this study where they integrated RNA- and ATAC-seq (Assay for Transposase-Accessible Chromatin) for the development of 3-chloropiperidines as a potential anticancer drug in colorectal adenocarcinoma cells (Carraro et al., 2022). This approach helped them potentially identify more susceptible and resistant tumour types for further drug development (Carraro et al., 2022). This research also attempts to utilise functional genomics at a small scale, using RNA-seq and ATAC-seq to better understand OC response to both PLK1 and PLK1/BRD4 inhibiting drugs.

1.9 Hypothesis, Aims and Objectives

As introduced here, the advent of functional genomics and the inclusion of techniques such as Chromatin immunoprecipitation, ATAC-seq and RNA-seq at the genome/transcriptome scale, has enabled a more in-depth understanding of drug compound mechanism of action in early-stage, preclinical drug development. Due to the expression profiles of PLK1 and BRD4 proteins in subtypes of OC, particularly HGSOC, this research aimed to add in-depth cellular and molecular understanding of specific PLK1 inhibitors BI 2536 and BI 6727 on cell line models of HGSOC. The hypothesis states simply that 'The integration of functional genomics, in the form of RNA and ATAC seq, to the drug development pipeline will inform the optimal strategy for PLK1/BRD4 targeting in the future'. To test this hypothesis a series of objectives have been devised:

1. Define the IC50 concentration of BI 2536 and BI 6727 in HGSOC cell lines expressing both PLK1 and BRD4 proteins;
2. Assess the specificity of the drug molecules, in HGSOC cell lines, to define the optimal time exposure for functional genomic screening;
3. Perform RNA-seq analysis of HGSOC cell lines, in the presence of both compounds, to determine the effect on whole transcriptome expression levels;
4. Perform ATAC-seq analysis of HGSOC cell lines, in the presence of both compounds, to determine the effect on the chromatin landscape and specifically changes in chromatin accessibility;
5. Use a series of informatic and cellular, molecular approaches and assays to validate the mechanistic understanding of both compounds in HGSOC.

2 Methods

2.1 Cell culture

2.1.1 Cells

OC cell lines were sourced from ATCC: CAOV3 (HTB-75), OVCAR-3 (HTB-161), UWB1.289 (CRL-2945), SKOV3 (HTB-77). CAOV3 are HGSOC cells isolated from the ovary of ovarian cancer patient (ATCC, n.d.-a). OVCAR3 are HGSOC cells isolated from the malignant ascites of a female with progressive ovarian cancer (ATCC, n.d.-b). SKOV3 are epithelial OC cells which were isolated from the ovary of a 64-year-old (ATCC, n.d.-c). UWB1.289 cells are epithelial OC cells that were isolated from the tumour of papillary serous histology from breast and ovarian cancer patient and has a germline *BRCA1* mutation (ATCC, n.d.-d).

2.1.2 Media

SKOV3 and OVCAR-3 cells were maintained in RPMI 1640 media (Gibco™, 11875093) with 20% of fetal bovine serum (FBS) (Gibco™, 10270106),10 µg/mL of Insulin solution from bovine pancreas (Sigma, I0516), penicillin (100 units/mL)-Streptomycin (100 µg/mL) (P/S) (Gibco™, 15140122). UWB1.289 and CAOV3 were grown in DMEM/F-12, GlutaMAX™ media (Gibco™, 10565018) media with 10% of FBS and same concentration of P/S. Stripped media was also prepared by substituting FBS with charcoal-stripped FBS (Gibco™, 12676029).

2.1.3 Culturing

Cells were stored in liquid nitrogen and brought up for culturing. Cells were thawed rapidly by placing vials in a 37 °C water bath and gently mixed with appropriate media prewarmed to 37 °C and centrifuged for 3 min at 300 g to retrieve cell pellet. The supernatant was discarded, and cells were resuspended in 7 mL of media and transferred to T25 flask. Cells were maintained in the humidified incubator at 37 °C, 5% CO_2. When the confluency of 80 % or above was reached cells were passaged. Media was discarded from the flask and cells were washed with PBS (Gibco™, 10010015). 2 mL of Trypsin-EDTA (Gibco™, 25300062) was added and flask was returned to the incubator for a few minutes till cells were detached from the bottom of the flask. 8 mL of media was added to inactivate the trypsin and cell suspension was transferred to a 15 mL tube and centrifuged

at 300 g for 3 min. The supernatant was removed and cells were resuspended in 15 mL of media and transferred to a T75 flask. Cells were grown until reaching 80% confluency (~2-3 days), whereby the passaging step was repeated again.

2.2 Drug compounds

The compounds of interest BI 2536 (CAY17385) and BI 6727 (CAY18193) where obtained from Cambridge Bioscience. DMSO (Sigma, D8418) was the vehicle control used to dissolve and dilute stock compounds to a working concentration [1 mM]. Staurosporine (Tocris, 1285) was used as a positive control.

2.3 Cell viability Assay

2.3.1 2D

Cells were seeded on white TC treated 96 well plates at a density: 2×10^3 (CAOV3), 3×10^3 (UWB1.289), 2×10^3 (OVCAR-3), 1×10^3 cells per well (SKOV3). Cells were seeded with 100 µL of stripped media and grown for 24 h at 37 °C, 5% CO_2. BI 2536 and BI 6727 were diluted with stripped media to achieve 20 µM, 2 µM, 200 nM, 20 nM, 2 nM concentrations. Staurosporine was diluted to 20 µM concentration. DMSO was diluted in the same ratios to achieve same concentration as in the 20 µM compound solutions. Media was discarded using multichannel pipette from 96 well plate and 50 µL of drug, positive control or DMSO was added per well in triplicates. Luminescence solution was prepared by adding 10 µL of MT Cell Viability Substrate, 1,000X (Promega, G971A) and 10 µL NanoLuc® Enzyme, 1,000X (Promega, E499A) to 4980 µL of stripped media. 50 µL of luminescence solution was added to each well. Plate was incubated for 24 h at 37 °C, 5% CO_2. Luminescence readings were taken by FLUOstar Omega (BMG LABTECH) reader prewarmed to 37 °C at three different timepoints, 24, 48 and 72 h after the treatment. In between the readings plate was kept in the incubator.

2.3.2 3D

Cells were seeded on ultra-low attachment 3D 96-well plates (CLS4520, Sigma) at a density: 2×10^3 (CAOV3), 2×10^3 (UWB1.289), 2×10^3 (OVCAR-3), 1×10^3 (SKOV3) cells per well. Cells were seeded with 100 µL of stripped media and grown for 24 h at 37 °C, 5% CO_2. Drugs and DMSO were prepared as described in 2.3.1. Prior to treatment, 50 µL of media was carefully removed from each well with multichannel pipette without

19

disturbing the spheroids. 50 µL of drug, positive control or DMSO was added per well in triplicates and plate was incubated for 48 h, 5% CO_2. CellTiter-Glo® 3D Reagent (Promega, G9682) was transferred from -20 °C to 4 °C and kept at room temperature (RT) before taking readings, following manufacturer's recommendations. 100 µL of CellTiter-Glo® 3D Reagent were added to each well and plate was shaken for 5 min to disrupt the spheroids. Plate was incubated at room temperature in the dark for 25 min. Luminescence readings were taken by FLUOstar Omega reader.

2.4   Western Blot

Cells were seeded on 6-well plates at a density of 4×10^5 (CAOV3) and 5×10^5 (OVCAR-3) cells per well with stripped media. Plates were incubated for 24 h at 37 °C, 5% CO_2. Media was discarded and cells were treated either with DMSO, 100 nM BI 2536 and 100 nM BI 6727 for 24, 48 and 72 h. Lysis buffer was prepared by adding 3 µL of 1X Halt™ Protease and Phosphatase Inhibitor Cocktail (Thermo Scientific, 1861281) to 300 µL of RIPA buffer (Sigma, R-0278) and kept on ice. Media was discarded and cells were washed 2 times with PBS. 75 µL of lysis buffer was added to each well and cells were scraped with cell scrapers. Lysate was transferred to Eppendorf tubes and tubes were left on ice for 30 min with constant agitation and vortexed every 5 min. Lysate was centrifuged at $8,000 \times g$ for 10 min at 4 °C. The supernatant was transferred to new Eppendorf tubes and protein was stored at -80 °C.

2.4.1   Protein quantification

Protein was quantified using the DC™ Protein Assay Kit II (5000112). 3g of Bovine serum albumin (BSA) (Pan Biotech, P061391050) was dissolved in double distilled water and BSA standards were prepared using the following ratios:

	Concentration	BSA	ddH$_2$O
Stock	300 µg/µL	3 g	10 mL
A	1500 ng/µL	10 µL (Stock)	1990 µL
B	1000 ng/µL	667 µL (A)	333 µL
C	750 ng/µL	500 µL (A)	500 µL
D	500 ng/µL	500 µL (B)	500 µL
E	250 ng/µL	500 µL (D)	500 µL
F	125 ng/µL	500 µL (E)	500 µL
G	75 ng/µL	100 µL (C)	900 µL
H	25 ng/µL	100 µL (E)	900 µL
O	0 ng/µL	0 µL	1000 µl

Table 2-1. BSA standards preparation. *BSA and double distilled H$_2$O proportions were combined to achieve standard concentrations in the second column.*

Samples were diluted 1:4 ratio with nuclease-free water. 5 µL of BSA standards and samples were loaded into 96 well plate in triplicates. 40 µL of Reagent S was mixed with 2 mL of reagent A in a tube. 25 µL of A+S followed by 200 µL of reagent B were added to each well. Plate was protected from light and incubated for 15 min. Absorbance at 750 nm was measured with the FluoStar Omega plate reader. Protein quantities of samples were calculated using the standardised BSA concentration curve in Microsoft Excel.

2.4.2 SDS-PAGE

Samples were diluted with nuclease-free water in PCR tubes to 30 ng of protein. 190 µL of 2X Laemmli Sample Buffer (BioRad, 1610737) was mixed with 10 µL of β-mercaptoethanol in the fume hood and added to diluted samples in 1:1 ratio. PCR tubes were loaded on to the thermal cycler (BioRad) at 95 °C for 5 min to denature protein. 4–20% Mini-PROTEAN® TGX™ Precast Protein Gel (BioRad, 4561094) was placed into the box casket and 1X Running buffer was poured to cover electrodes. 3.5 µL Precision Plus Protein Dual Color Standards (BioRad, 1610374) were loaded into the first and last well of the gel and samples containing 30 ng of protein in between the standard. The electrophoresis was run with the following conditions: 5 min at 100V and then 35 min 170V.

2.4.3 Membrane transfer

Trans-Blot Turbo Transfer System (BioRad) was used to perform protein transfer. The gel was removed from the cast and gently placed on the membrane in between ion reservoir stacks from Trans-Blot Turbo Mini 0.2 µm PVDF Transfer Packs (BioRad, 1704156) in the cassette. The top layer was added to the gel and the remaining air bubbles were removed by rolling. Electrophoresis was run with 1 mini TGX setting at 25V for 3 min.

2.4.4 Antibody incubation

The membrane was blocked in 5% BSA blocking buffer for 1 h on a rocker at RT, followed by the addition of the primary antibody of choice with the manufacturer's recommended dilution. Following antibodies were used anti-PLK1 (Cell Signalling, 4513), anti-phospho Cyclin B1 (Ser133) (Cell Signalling, 4133), anti-BRD4 (Bethyl, A301-985), anti-γH2A.X (Cell Signalling, 2577), anti-cleaved PARP (Cell Signalling, 9541), anti-Phospho-Histone H3 (Ser10) (Cell Signalling,9701) and anti-GAPDH (Santa Cruz, sc-47724). The membrane was incubated with the antibody at 4 °C overnight on a rocker to maintain constant agitation. Antibody was discarded and the membrane was washed with 1X Tris-buffered saline with Tween (TBS-T) for 30 min on a rocker changing buffer every 5 min. HRP-conjugated secondary antibodies either anti-mouse (Cytiva, NA931V) or anti-rabbit (Cytiva, NA934V) diluted (1:2000) in 5% BSA blocking solution and membrane was incubated with secondary antibody for 1 h at RT on the rocker. The secondary antibody was discarded and the washing step with 1X TBS-T described above was repeated. The membrane was taken out of the washing buffer and Clarity™ Western ECL Substrate (BioRad, 1705060) was added to the membrane and incubated for 1 min in the dark. The membrane was imaged on the ChemiDoc MP Imaging system (BioRad).

2.5 Cell cycle assay

Cells were seeded on the 6-well plate at a density of 4×10^5 (CAOV3) and 5×10^5 (OVCAR-3) cells per well with a stripped media. Plate was incubated for 24 h at 37 °C. Media was discarded and cells were treated either with DMSO, 10, 100 nM BI 2536, BI 6727, 100 nM staurosporine (positive control) and kept in the incubator for 24 and 48 h. After 24h media was transferred to 15 mL tubes. Cells were washed once with 1 mL of PBS and PBS was collected in the same tubes. 200 µL of trypsin was added into each well

and incubated till most of the cells were detached. 800 µL of media was added to each well and cell suspension was transferred to the same tubes. Tubes were centrifuged for 7 mins at 200 g at RT. Supernatant was discarded, cell pellet was resuspended in 0.5 mL of PBS and centrifuge 5 minutes at 350 g. Supernatant was discarded and tubes were gently vortexed for cell pellet to detach. 3 mL of freshly prepared 70% ethanol, kept at -20 °C, was slowly added with the dropper to each tube with gentle vortexing in order to fix the cells. Tubes were placed in -20 °C for 2 h and then to 4 °C. These steps were repeated for cells treated for 48 h. All tubes were then centrifuged for 5 min at 200 g, RT. Ethanol was discarded and cells were resuspended in 2 mL of PBS and incubated at RT for 1 min. Tubes were centrifuged for 5min at 400 g, RT and resuspended in 200 µL of DAPI staining solution containing 1 µg/mL of DAPI. Cells were incubated with DAPI stain for 30 minutes in the dark (RT). CellStream® (Luminex) was used to take measurements.

2.6   Apoptosis assay

Cells were seeded, treated, and collected in the tubes as described in 3.5. Tubes were centrifuged for 7 min at 300 g, at 4°C. Supernatant was discarded and cell pellet was resuspended in 1 mL of cold staining buffer (Biolegend®, 420201). Tubes were centrifuged 7 minutes at 300 g 4 °C, and supernatant was discarded. This procedure was repeated once more. DMSO and staurosporine-treated cells were gently resuspended in 200 µL of Annexin V binding buffer (Biolegend®, 422201) and BI 2536, BI 6727-treated cells were resuspended in 100 µL of the binding buffer. Cell suspensions were transferred to 1.5 mL Eppendorf tubes. DMSO and Staurosporine-treated cells were divided into two Eppendorf tubes. One tube with DMSO-treated cells was left unstrained. 5 ul of Annexin V (Biolegend®, 640945) was added to all tubes except one staurosporine treated cells. 10 ul of PI (Biolegend®, 421301) was added to all tubes except to the annexin stained staurosporine-treated cells. Tubes were gently vortexed and incubate 15 min in the dark at RT. Additional 100 µL of Annexin V binding buffer was added to each tube before loading samples onto CellStream flow cytometer.

2.6.1   Flow cytometry

The instrument was initialized and calibrated. New experiment was created and unstained DMSO-treated cells, Staurosporine Annexin only and Staurosporine-cells stained for PI

only cells were used to check saturation of FSC, SSC, 488 lasers and set appropriate settings accordingly. Settings were saved and experiment was closed. New compensation experiment was created unstained and single stained control were loaded again and recorded. Compensation experiment was saved and opened in analysis program to create compensation matrix. Previously created experiment was opened, laser settings were loaded, and compensation matrix was applied. All samples including unstained DMSO, single and double stained samples were loaded, and 10,000 singlets were recorded from each.

2.7   RNA-seq

2.7.1   RNA extraction

Cells were seeded on the 12-well plate at a density of 2×10^5 cells per well and grown for 24 h. Cells were treated with 100 nM BI 6727, 100 nM BI 2536 and DMSO. Cells were maintained at 37 °C, 5% CO_2 for 24 h. RNA was isolated using RNeasy Plus Mini Kit (Qiagen, 74136). Media was discarded and cells were washed with PBS twice. 350 μL of cold RLT lysis buffer was added to the cells and scraped using scraper. RNA samples were transferred to gDNA eliminator spin columns and centrifuged at 8000 g for 30 sec. One volume (350 μL) of freshly prepared 70% ethanol was added to the flow through and transferred to the RNeasy spin column. Tubes with the column were centrifuged and flow through was discarded. Flow through was discarded and columns were then washed with 700 μL of RW1 buffer. Columns were centrifuged at 8000 g for 15 sec and washing was repeated. 700 μL of RPE buffer was added to the columns and centrifuged at 8000 g for 30 sec. Flow through was discarded and 500 μL of RPE buffer was added to the columns and left for 1 min to soak. Columns were centrifuged for 1 min at 8000 g and flow through was discarded. 500 μL of RPE buffer was added once more and columns were centrifuged for 2 min at the same speed. Column were placed in collection tubes and 50 μL of Rnase free water was added. Tubes with columns were centrifuged for 1 min at 8000 g. RNA quality control step was performed using Nanodrop. For high quality RNA 260/280, 230/260 values are supposed be greater than 1.9. Samples with lower numbers were additionally cleaned using RNAClean XP (Beckman Coulter, A63987) magnetic beads according to the manufacturers protocol and quality control step was repeated. Samples were stored in -80 °C.

2.7.2 Sequencing and data analysis

Three biological replicates of RNA extracted from OVCAR-3 and CAOV3 cells treated for 24 h with DMSO, 100 nM BI 2536 and 100 nM BI 6727 were sent off to Novogene for Eukaryotic mRNA library preparation using poly-A enrichment and sequencing (pair-ended reads, 150bps). Novogene performed quality control and sequenced samples. As described in our previous paper quality check was carried out for raw reads FASTQ files using FastQC tool (Andrews, 2019; Quintela et al., 2023). Human genome GRCh38/hg38 was used as a reference to align reads using STAR universal RNA-seq aligner (Dobin et al., 2012). In STAR -quant Mode GeneCounts Table argument was used to create tables with gene counts. For normalisation of gene counts DESeq2 median of means method was used (Love et al., 2014). DESeq2 was used to correct for multiple hypothesis testing and determine significantly modified transcripts between DMSO, control and BI 2536 or BI 6727 experimental samples (FDR < 0.05). Using WebGestalt platform, gene set enrichment analyses (GSEA) and gene set over-representation analyses (ORA) were performed to compare lists of differentially expressed genes between both cell lines treated with BI 2536 and BI 6727 to gene datasets related to major pathway (Liao et al., 2019). Venn diagrams were created from the lists of genes using the Venny website (Oliveros, 2015). Principal component analysis (PCA) was performed using the factoextra package (Lê et al., 2008). Package ggplot2 was used for volcano plots and visualisation of pathways (Wickham, 2016).

2.8 ATAC-seq

Cells were seeded on the 6-well plate at a density of 4×10^5 cells per well with a stripped media. Plate was incubated for 24 h at 37°C. Media was discarded and cells were treated either with DMSO, 100 nM BI 2536 nM and 100 nM BI 6727 for 24 h, Media was discarded, and cells were washed with PBS twice. 0.05% Trypsin-EDTA was added to detach the cells. After cells were detached, trypsin was deactivated with media. Cell suspension was transferred to the 15 mL tube and wells were washed with warm PBS to obtain the remaining cells. The following steps were performed using ATAC-seq kit (Diagenode, C01080002). Cells were centrifuged at 500 x g for 10 min at 4 °C. Resulting supernatant was discarded and cell pellet was resuspended in cold PBS with Proteinase inhibitor cocktail. Total and viable cell number was determined by mixing cell suspension

with Trypan blue in equal ratios and counting cells in the TC20 Automated Cell Counter (Bio-Rad). Volume containing 5×10^4 cells was transferred to the new 1.5 mL Eppendorf tubes. Cells were centrifuged at 500 x g for 10 min at 4 °C. Supernatant was carefully discarded with pipette and cell pellet was gently resuspended in 50 µl of cold ATAC Lysis Buffer 1 + Digitonin on ice. Tubes were incubated for 5 min on ice. To stop lysis, 1 mL of cold ATAC Lysis Buffer 2 was added to each tube. Lysate was centrifuged at 500 x g for 10 min at 4 °C and 1 mL of supernatant was discarded. Lysate was centrifuged again at 500 x g for 5 minutes at 4°C and the remaining supernatant was removed, and pellet was kept on ice. Tagmentation buffer was prepared as per manufacturer's protocol. Nuclei pellet was gently resuspended in 50 µL of tagmentation buffer and tubes were placed into thermomixer (Eppendorf ThermoMixer® C) at 37 °C for 35 min at 350 rpm. DNA binding buffer was added immediately to stop tagmentation reaction and suspension was transferred to DNA binding columns. Columns were centrifuged at 12,000 x g for 30 sec and the flow-through was discarded. 200 µl of DNA Wash Buffer was added to the column and columns were centrifuged at 10,000 x g for 30 sec. Wash step was repeated once again. The column was place in a new 1.5 ml microcentrifuge tube and 12 µl of DNA Elution Buffer was added to the column matrix. Tubes with columns were centrifuged at 10,000 x g for 30 sec.

2.8.1 PCR

10 µl of tagmented libraries were mixed with 25 µL of 2x High-Fidelity Mastermix and 14 µL of nuclease-free water in PCR tubes. 1 µl of Unique dual indexes (UDI) from 24 UDI for Tagmented libraries kit (Diagenode, C01011034) was added to the mix. PCR was run as per protocol for initial 5 cycles.

2.8.2 Additional PCR cycles

qPCR was used to determine number of additional PCR cycles to add to the initial 5 cycles. 5 µL of amplified libraries from 2.8.1 were mixed with 5 µL of 2x High-Fidelity Mastermix, 0.25 µL of UDI 1, 0.15 µL of 100x SYBR and 4.6 µL of nuclease-free water. 20 qPCR cycles were run as per protocol. Fluorescence (y) versus cycles (x) graph was used to find maximum fluorescence intensity. The number was divided by 3 and corresponding number was matched to cycle number. The libraries required 5 more cycles

thus tagmented DNA was amplified for 5 more cycles. qPCR step was only repeated for one biological replicate of each cell line and both required 10 PCR cycles in total.

2.8.3   Double-sided library cleanup

AMPure XP beads (Beckman Coulter, A63880) were used to clean up libraries and remove primer dimers. 22.5 or 25 µL of AMPure XP beads was mixed with 45 or 50 µL of library, respectively, depending on whether the qPCR step was carried out previously. Tubes were incubated for 10 min at RT and placed on the magnetic rack for the magnetic beads to bind the magnet and form pellet. Supernatant was transferred to the new tube and mixed with 58.5 or 65 µL of magnetic beads, respectively and incubated for 10 min at RT. While keeping tubes on the magnetic rack, supernatant was discarded and beads were washed with 100 µL of 80% ethanol twice. Remaining ethanol was discarded with a pipette and beads were left to dry until they had matte appearance. Tubes were then removed from the rack and beads were resuspended in 20 µL of DNA Elution Buffer and incubated for 10 min at RT. Tubes were placed on magnetic rack and supernatant was transferred to DNA LoBind® tubes (Eppendorf, 0030108051) and stored at -20 °C.

2.8.4   Quality control

Double-stranded DNA quantity was measured using Qubit™ 1X dsDNA High Sensitivity (HS) kit (Invitrogen™, Q33230) as per manufacturer's protocol. Bioanalyzer High Sensitivity DNA Analysis kit (Agilent, 5067-4626) was used to visualise library profiles on Agilent Bioanalyzer (G2939A). Successful libraries contained four peaks each representing free DNA, mononucleasomal, dinucleosomal and trinucleosomal DNA. In the presence of additional primer, adapter dimer peaks or >1000 bp peaks, additional size selection was required.

2.8.5   Additional size selection

Samples were brought to 50 µl volume by estimating initial library volume and adding nuclease free water. In the presence of both primer dimers and large fragments double-size selection was repeated as described in 2.8.3. In the presence of primer dimers left-side cleanup was performed. 90 µl of AMPure XP beads was mixed with 50 µl of diluted library and incubated for 10 min. PCR tubes were placed on the magnetic rack and supernatant was carefully discarded. 100 µl of 80% ethanol was added to the tubes and

discarded, this was repeated. Beads were left to dry out and were resuspended in 20 μL of elution buffer. Tubes were incubated for 10 min and placed on a magnetic rack. Eluted DNA was transferred to DNA LoBind® tubes and stored at -20 °C.

2.8.6 Sequencing and data analysis

Prepared libraries were sent for sequencing to Novogene. Quality control was performed for raw read files using FastQC tool (Andrews, 2019). Indexed human genome GRCh38/hg38 was used as a reference to align trimmed reads using Bowtie 2 (Langmead & Salzberg, 2012). SAMTOOLS tool was used to convert SAM files to BAM, sort them, remove blacklist and index them (Danecek et al., 2021). DeepTools2 was used to make bigwig files while peak calling was carried out using MACS2 (Ramírez et al., 2016; Zhang et al., 2008). Peaks and reads were visualized using an IGV genome browser while DiffBind function was used for comparative analysis between control and treatment cells (Gentleman et al., 2004; Robinson et al., 2023).

2.9 Statistical analysis

Analysis of variance was conducted on each dataset following an initial evaluation for normality (Anderson-Darling or Kolmogorov-Smirnov test). Parametric and or non-parametric analysis was then conducted accordingly. FlowJo 10.8.1 was used to perform cell cycle analysis while GraphPad Prism 10.0.2 was used to analyse data. Cell viability curves using the least squares fitting method were produced from means of biological triplicates to calculate IC50 values for the selection of optimal drug doses for further experiments. Basal protein levels from untreated cell line protein lysates were determined by Western blot and quantified using BIO-RAD Image Lab 6.1 and normalized by GAPDH. Further Western blots were used as a qualitative technique. One biological replicate was performed per protein of interest, thus no statistical tests were used. The genome-wide analysis utilised RBGO informatics pipelines, assaying quality control through gene set enrichment and pathway analysis. All statistical values are provided in the results section, p-value < 0.05 represents significant results.

3 Results

3.1 PLK1 and BRD4 are expressed in ovarian cancer tissue

This project focuses on PLK1 and BRD4 dual inhibitors thus it was firstly determined whether these targets are expressed in serous OC. The Human Protein Atlas contains information about the expression of genes coding for proteins such as PLK1 and BRD4 (Figure 3-1). Antibody-stained healthy ovary samples antibody shows low intensity for PLK1 and moderate intensity for BRD4. PLK1 stain intensity ranged from low to high and BRD4 moderate to high in different serous cystadenocarcinoma samples emphasizing
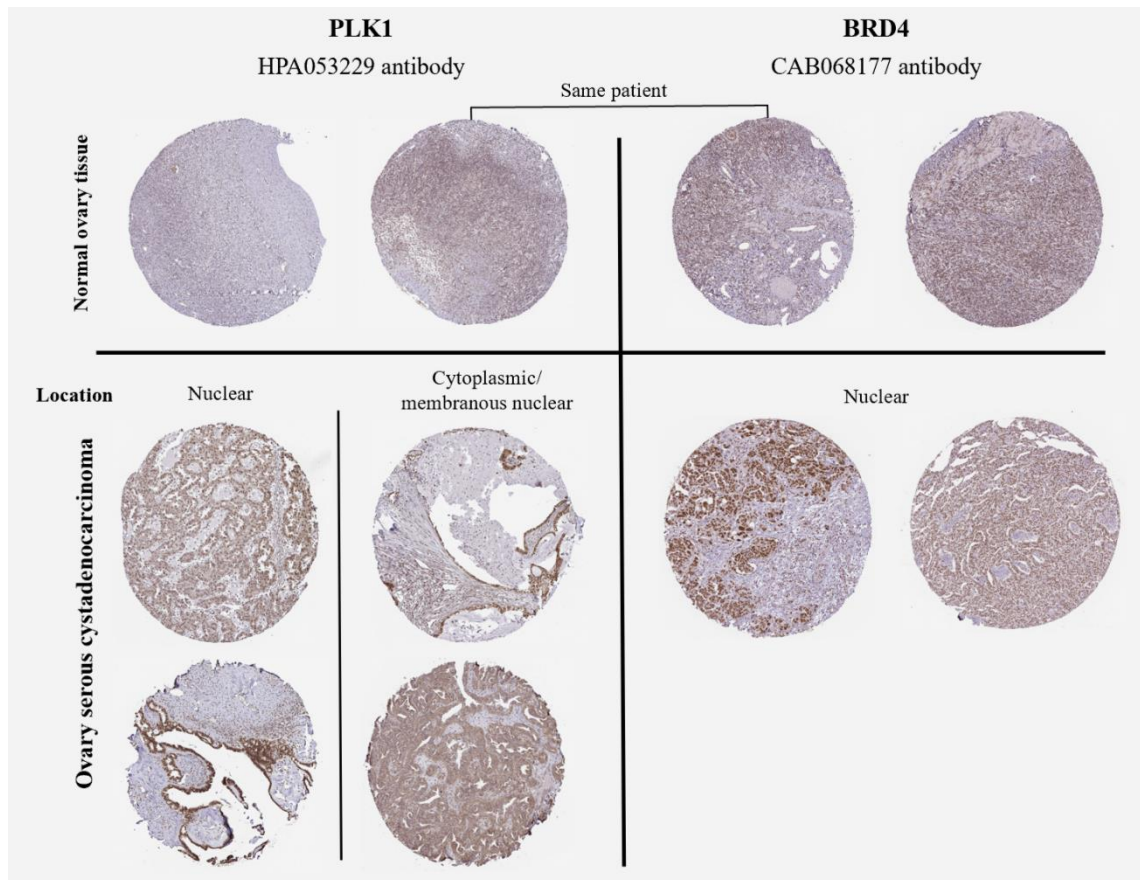
Figure 3-1. Normal ovary tissue and serous cystadenocarcinoma stained with anti-PLK1 and anti-BRD4 antibody. *Tissues stained with HPA053229 antibody for PLK1 and CAB068177 antibody for BRD4. Samples are matched only for one patient. PLK1 and BRD4 staining came from different patients. Localization of proteins is indicated above the samples***.*** *Obtained from the Human Protein Atlas (n.d.-a, n.d.-b).*

the cellular heterogeneity aspect of serous OC. PLK1 stain localization varied between nuclear or cytoplasmic/ membranous nuclear and BRD4 stained was nuclear, corresponding to its function in gene expression through interaction with chromatin.

3.2 BRD4 and PLK1 are expressed in ovarian cancer cell lines

As PLK1 and BRD4, drug targets, are expressed, it confirms that BI 2536 and BI 6727 are appropriate candidates for this study. Model selection was the first step that I undertook to study drug effects on OC cells. For initial exploration and cell line selection experiments OVCAR-3, CAOV3, SKOV3 and UWB1.289 cell lines were chosen. The data from Human Protein Atlas was used to determine PLK1 and BRD4 expression levels (Human Protein Atlas, n.d.-a, n.d.-b). RNA expression levels were used to compare PLK1 and BRD4 expression between the cell lines and the healthy ovarian tissue (Figure 3-2). There was no data for the UWB1.289 cell line.

The number of transcripts for PLK1 in normal ovary tissue, represented as transcripts per million (nTPM), is 2.2 while in OC cell lines that number is significantly greater (OVCAR-3- 47.9, CAOV3- 73.3, SKOV3- 93.6). BRD4 is highly expressed in normal ovary tissue (nTPM = 29.2) but its expression is upregulated in both CAOV3 (31.8) and SKOV3 (48.8) whereas in OVCAR-3, BRD4 nTPM is 26.6.
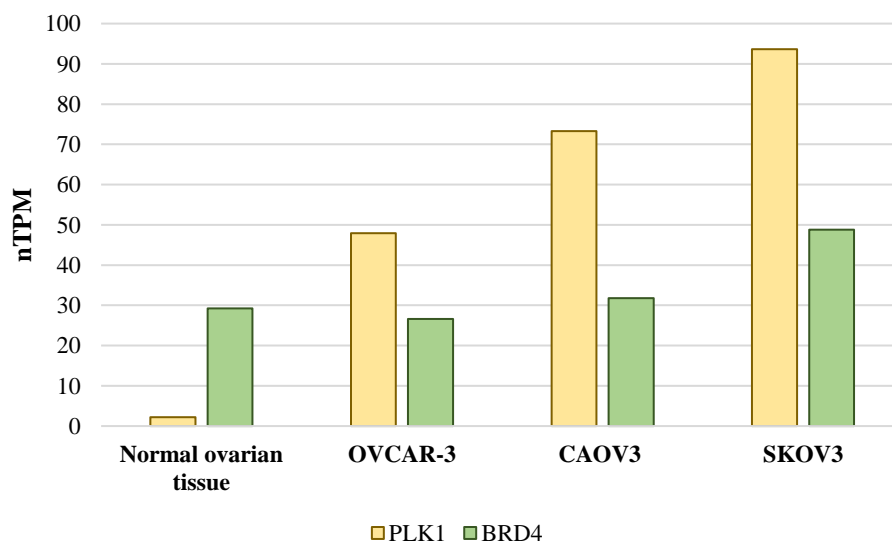
Figure 3-2. PLK1 and BRD4 mRNA expression levels in normal ovarian tissues and OC cancer cell line . Gene expression is quantified as transcripts per million (nTPM), n = 1. Obtained from the Human Protein Atlas (n.d.-a, n.d.-b).

To corroborate the basal protein expression levels of PLK1 and BRD4 *in vitro*, I performed Western Blots. As expected, PLK1, BRD4 and GAPDH band location on the

blot correspond to their molecular weight, 62, 238 and 36 kilodalton (kDa), respectively. As shown in Figure 3-3, BRD4 band is below 250 kDa marker band, on left, and band location correlates to its molecular weight of 238 kDa. Blots (Figure 3-4) were cropped for comparative purposes and to produce Figure .
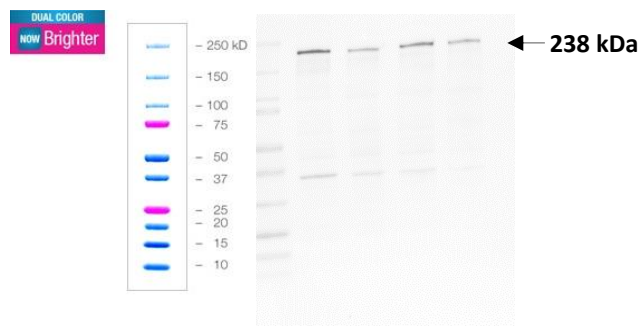
Figure 3-3. Blot of basal BRD4 expression in OC cell lines aligned to standards. *Precision Plus Protein Dual Color Standards (BioRad, 1610374) on the left, basal protein levels in OVCAR-3, CAOV3, SKOV-3 and UWB1.289 grown in media, on right. BRD4 molecular weight is 238 kDa.*
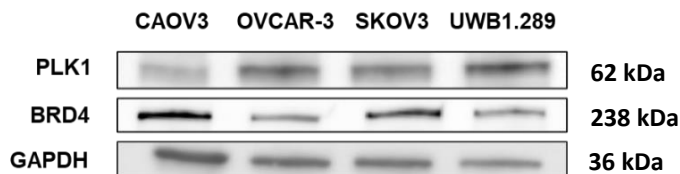
Figure 3-4. Western blot of basal BRD4 and PLK1 expression in OC cell lines protein lysates. *Basal protein levels in OVCAR-3, CAOV3, SKOV-3 and UWB1.289 grown in media. Protein molecular weight is indicated on the right in kilodaltons (kDa). GAPDH (36 kDa) is loading control.*

The graph below summarizes PLK1 and BRD4 expression levels which were normalized by GAPDH expression (Figure 3-5). UWB1.289 had the highest PLK1 and BRD4 expression while CAOV3 exhibited high BRD4 expression and the lowest PLK1 expression in comparison to other OC cell lines. BRD4 expression was lowest in OVCAR-3 and PLK1 was expressed moderately. Whereas SKOV3 highly expressed BRD4 and had moderate PLK1 levels.
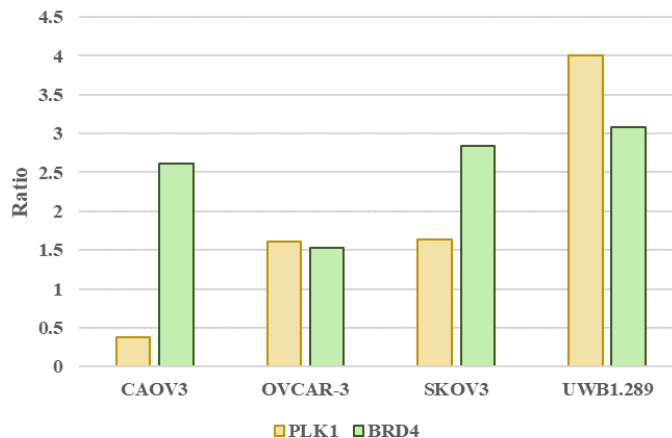
Figure 3-5. Normalized basal BRD4 and PLK1 expression in OC cell lines. *Basal protein levels in protein lysates from OVCAR-3, CAOV3, SKOV-3 and UWB1.289 as determined by Western blot quantified with Image Lab software and normalized by GAPDH expression, n = 1.*

The experimental protein expression levels differed from the Human Protein Atlas gene expression data, while in CAOV3, PLK1 protein levels were lower than in the rest of OC cell lines on transcript level, according to protein atlas data, PLK1 expression was higher in CAOV3 than in OVCAR-3. The BRD4 protein expression trend from experimental data matched the Human Protein Atlas gene expression.

3.3 PLK1/ BRD4 inhibition leads to a significant decrease in cell viability

BI 2536 and its derivative, BI 6727, are classified as dual target PLK1 and BRD4 inhibitors and their inhibitor effect on OC cells was measured using cell viability assay, RTGlo. Graphs show OVCAR-3, CAOV3, SKOV-3 and UWB1.289 viability in the presence and absence of each compound at 48h and 72h (Figure 3-6).

BI 2536 and BI 6727 significantly decreased the viability of all OC cell lines, in a dose-dependent manner. Both drugs significantly inhibited growth of OC cell lines at nanomolar doses, which is consistent with previous findings in EOC cancer (Huo et al., 2022; Raab et al., 2019).
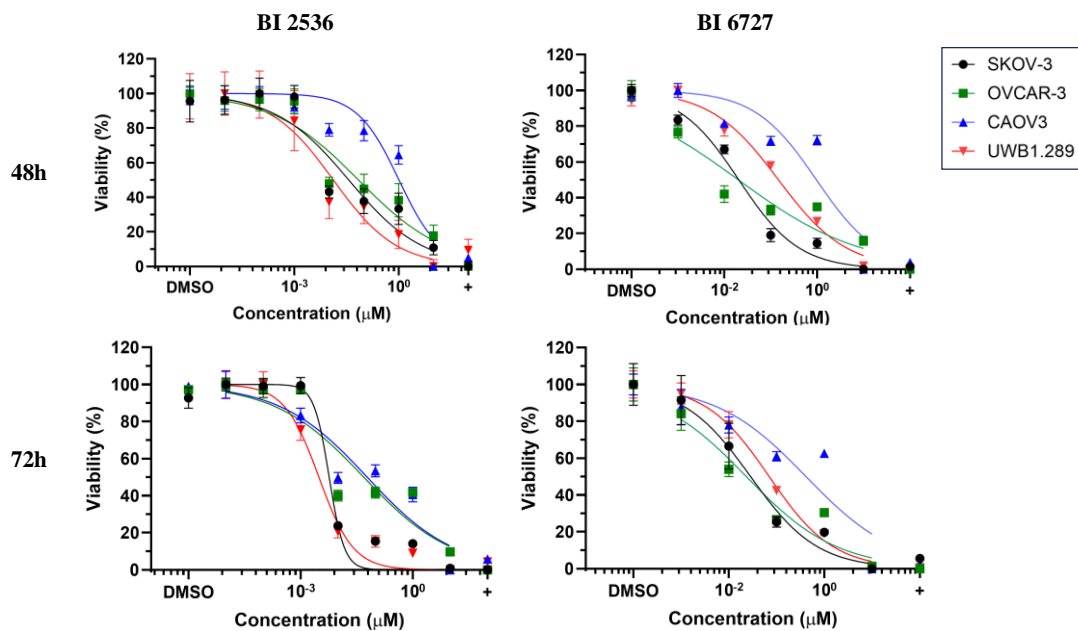
Figure 3-6. OC cell viability dose response curves. *Graphs show OVCAR-3 (green), CAOV3 (blue), SKOV-3 (black) and UWB1.289 (red) cell viability with BI 2536 and BI 6727 treatment at 48h and 72h. Each point represents a mean of biological triplicates, n = 3, error bars are standard error of the mean (SEM). Staurosporine is positive control (+; 0% viability), DMSO is negative control (100% viability). Least squares regression fitting model was used to fit data.*

At 48h in OVCAR-3, SKOV-3 and UWB1.289, BI 2536 inhibited cell growth in a comparable manner. With BI 6727 the highest inhibition percentages at low doses were achieved in OVCAR-3 and SKOV-3. BI 2536 and BI 6727 had a comparable effect on CAOV3 cell viability at 48h but was the least affected cell line compared to other OC cell lines. At 72h, the OVCAR-3 curve did not change significantly but in CAOV3 cells both compounds induced a comparable decrease in viability. Long exposure to BI 2536 had the greatest inhibitory effect on SKOV-3 and UWB1.289 cells and with BI 6727 in OVCAR-3 and SKOV-3.

IC50 values indicate that CAOV3 was the least sensitive to both BI 2536 and BI 6727 compounds with IC50s over 1 and 1 μM at 48h and 60 and 412 nM, respectively (Table 3-1). BI 2536 was more effective in inhibiting CAOV3 growth with lower concentrations at both timepoints. At 48h, IC50 for BI 2536 in UWB1.289 was 13 nM and decreased at 72h to 3 nM, with long exposure BI 6727 IC50 decreased two times, from 147 nM to 70 nM. BI 6727 (IC50 = 20 nM) was more effective in growth inhibition in OVCAR-3 compared to BI 2536 (IC = 70 nM) at 48h and longer exposure (23 nM vs 49 nM). BI 2536 had a significant inhibitory effect on SKOV-3 cells, especially with 72h treatment and BI 6727 had comparable IC50 (48h- 20 nM, 72h- 29 nM) to the OVCAR3 IC50 values.

IC50 (μM)				
	SKOV-3	**OVCAR-3**	**CAOV3**	**UWB1.289**
BI 2536 48h	0.037	0.070	1.025	0.013
BI 6727 48h	0.020	0.020	0.963	0.147
BI 2536 72h	0.006	0.049	0.060	0.003
BI 6727 72h	0.029	0.023	0.412	0.070

Table 3-1. BI 2536 and BI 6727 half-maximal inhibitory concentration (IC50) at 48 and 72 h. IC50 values were determined for OVCAR-3, CAOV3, SKOV-3 and UWB1.289 by fitting least squares regression model.

3.4 BRD4/PLK1 inhibition reduces spheroid viability

3D models allow for the closer resemblance of realistic cell-cell interactions and the 3-dimensional structure of tumours (Kapałczyńska et al., 2018). 3D viability assay was performed at 48h after the treatment with each compound, using the 3D RTGlo assay kit (Figure 3-7).

BI 2536

BI 6727

Legend:
- SKOV-3
- OVCAR-3
- CAOV3
- UWB1.289
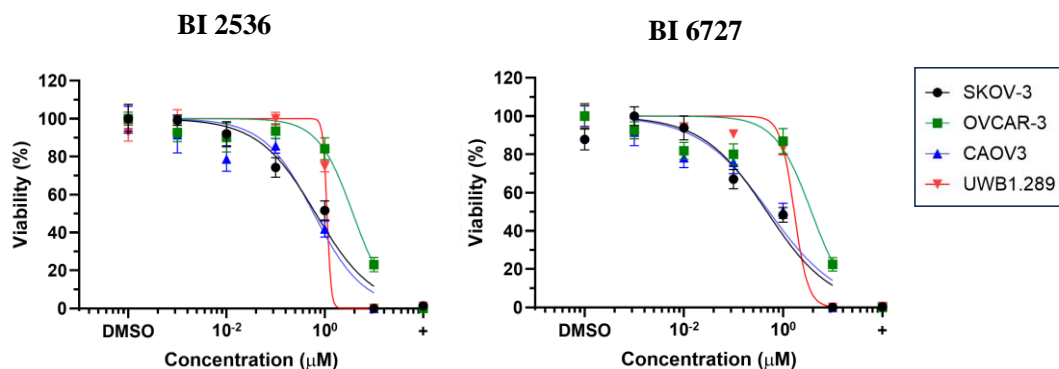
Figure 3-7. OC spheroid viability dose response curves. *Graphs show OVCAR-3 (green), CAOV3 (blue), SKOV-3 (black) and UWB1.289 (red) spheroid viability with BI 2536 and BI 6727 treatment at 48h. Each point represents a mean of biological triplicates, n = 3, error bars are standard error of the mean (SEM). Staurosporine is positive control (+; 0% viability), DMSO is negative control (100% viability). Least squares regression fitting model was used to fit data.*

BI 2536 and BI 6727 similarly inhibited cell growth in 3D spheroids. With both drugs, the greatest inhibitory effect was seen in SKOV-3 (650 nM- BI 2536; 470 nM-BI 6727) and CAOV3 (590 nM- BI 2536; 520 nM-BI 6727) which differs from 2D viability results

IC50 (μM)

	SKOV-3	OVCAR-3	CAOV3	UWB1.289
BI 2536	0.65	3.73	0.59	1.11
BI 6727	0.47	3.71	0.52	1.67

Table 3-2. BI 2536 and BI 6727 half-maximal inhibitory concentration (IC50) at 48 h in spheroids. *IC50 values for OVCAR-3, CAOV3, SKOV-3 and UWB1.289 spheroids were determined by fitting least squares regression model.*

where CAOV-3 cell line was least sensitive to both drugs (Table 3-2). OVCAR-3 had the highest IC50 values for both drugs over 3.7 μM. In UWB1.289 there was a significant variation in BI 2536 and BI 6727 replicates resulting in ambiguous IC50 value which were estimated to be over 1 μM.

Taking into consideration, PLK1 and BRD4 gene and protein expression levels together with cell viability data the research was narrowed to HGSOC cell lines: CAOV3 and OVCAR-3 as models to study mechanism of action of BI 2536 and BI 6727. OVCAR-3 expresses highly PLK1 and moderately BRD4 whereas in CAOV3 PLK1 expression was

low yet cell viability in both cells was reduced with nanomolar doses. Therefore, these cell lines were chosen as high and low PLK1 expression models. Although SKOV3 and UWB1.289 highly expressed BRD4 and PLK1 and responded to the treatments, OVCAR-3 and CAOV3 represent HGSOC better as SKOV3 was determined to poorly resemble HGSOC and it resembled endometrioid or clear cell subtype whereas UWB1.289 cells have *BRCA1* mutation and this subset of serous OC can be treated with PARP inhibitors, therefore, finding drugs for OC which do not carry *BRCA* mutation is intended (Anglesio et al., 2013; Barnes et al., 2021; Beaufort et al., 2014; Domcke et al., 2013).

3.5 BI 2536 and BI 6727 upregulate PLK1 and BRD4 protein expression

Drug dose choice is an important aspect of drug development as the dose has to be optimal to induce detectable changes in protein/ gene expression without inducing cell death or decrease in viability in all the cells. Aiming to partially reduce viability that would range from 20% to 80% of the cells and for the ability to perform comparative analysis between cell line and treatment, 100 nM drug concentration was chosen for further exploration. Western blots were then performed for CAOV3 and OVCAR-3 cells treated with 100 nM BI 2536 and BI 6727 to explore the efficacy and effect of this dose throughout three timepoints: 24, 48 and 72 h. PLK1 and BRD4 were studied as direct BI 2536 and BI 6727
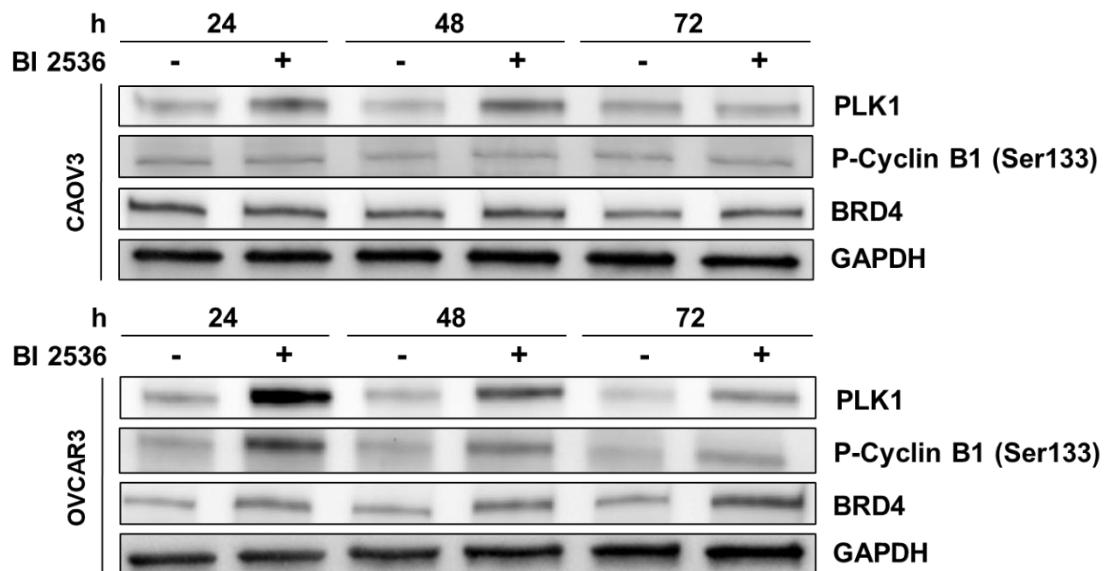
Figure 3-8. Western blot protein expression in BI 2536 and DMSO- treated CAOV3 and OVCAR-3 cells. *PLK1, BRD4 and p-cyclin B1 (Ser133) protein expression levels at 24, 48, 72 h after the treatment. Cells were treated with DMSO (-) or 100 nM BI 2536 (+). GAPDH is a loading control.*

targets as well as phosphorylated cyclin B1 at Ser 133 (p-cyclin B1 (Ser133)) which gets phosphorylated directly by PLK1 (Jackman et al., 2003).

At 24h in CAOV3 and OVCAR-3 PLK1 expression was upregulated upon the treatment with 100 nM BI 2536 and BI 6726 (Figure 3-8). The downstream target of PLK1, p-cyclin B1, upregulated expression correlated to PLK1 expression in OVCAR3 treated with BI 2536, but not in CAOV3 where p-cyclin B1 expression did not change. In OVCAR3, cells exposed to BI 2536 treatment for 48h triggered PLK1 and p-cyclin B1 expression upregulation but resulted in lower expression when compared to 24h, with further decrease in PLK1 and p-cyclin B1 expression at 72h. Whereas in CAOV3, at 24h and 48h timepoints PLK1 expression was upregulated and with longer, 72h drug exposure PLK1 expression decreased. BRD4 expression was not affected by BI 2536 treatment in CAOV3 while in OVCAR3 there was minimal increase in BRD4 expression which peaked at 72h, opposite to PLK1 expression.

 BI 6727 treatment resulted in similar protein expression trends seen in BI 2536 treated cells (Figure 3-9). In both cell lines upon treatment with BI 6727, PLK1 upregulation seen at 24 h decreased with longer exposure. Where p-cyclin B1 expression in CAOV3 was the
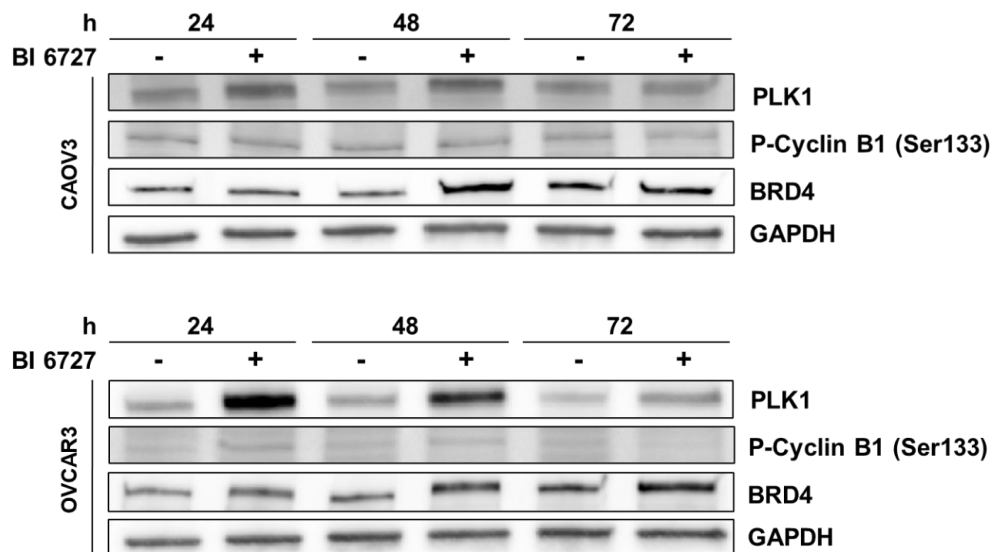
Figure 3-9. Western blot protein expression in BI 6727 and DMSO- treated CAOV3 and OVCAR-3 cells. *PLK1, BRD4 and p-cyclin B1 (Ser133) protein expression levels at 24, 48, 72 h after the treatment. Cells were treated with DMSO (-) or 100 nM BI 6727 (+). GAPDH is a loading control.*

same as in BI 2536 treated cells, in OVCAR3 cells BI 6727 did not induce any expression change. On the protein level, both BI 2536 and BI 6727 resulted in increased levels of PLK1 and BRD4 in both cell lines. The upregulated protein levels of drug targets upon treatment indicate that BI 2536 and BI 6727 do not inhibit expression of PLK1 and BRD4 but as determined by cell viability assay, they decrease cell viability. It raises a question of what the mechanism of action of BI 2536 and BI 6727 is and whether it differs between the drugs. To explore this question, changes in transcriptome level relating to PLK1 inhibition and chromatin level relating to BRD4 function were interrogated using RNA-seq and ATAC-seq, respectively. For these experiments, 24 h treatment was chosen because protein expression changes are observed at 24 h thus it should be an optimal time-point to detect changes in gene expression and chromatin accessibility.

3.6 RNA-seq

RNA sequencing enables to study the transcriptome, mRNA, of the cell and detect treatment-induced changes in gene expression. The experiment aims to study the genome-wide expression patterns and changes in response to the BI 2536 and BI 6727 treatments. This enables detecting genes, and pathways which inform the mechanism of action of these drugs.

CAOV3 and OVCAR-3 cells were grown for 24 h and treated with DMSO, 100 nM of BI 2636 and BI 6727 for 24 h. RNA was extracted and sent to Novogene where libraries were prepared using poly(A) enrichment of the mRNA for pair-ended, 150 bp Illumina Sequencing. Prior to sample sequencing, RNA passed the quality control stage, RNA integrity score for all samples was 10 indicating that RNA was intact.

3.6.1 Sequencing quality control and alignment efficacy
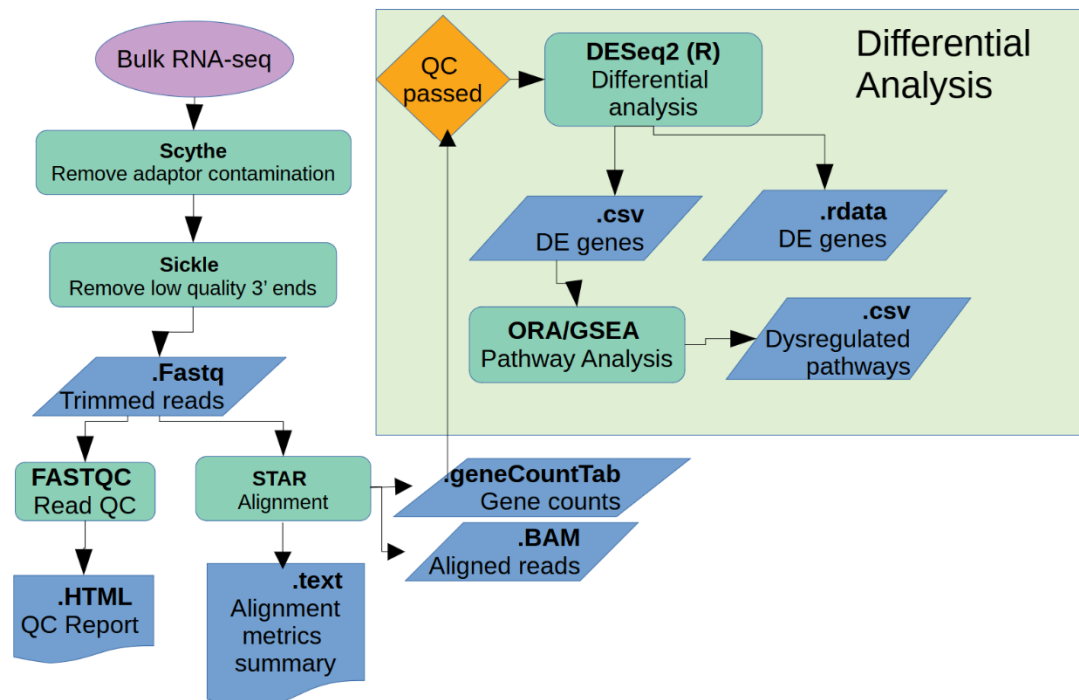
Figure 3-10. RNA-seq data analysis pipeline: from raw reads to pathway analysis. *Raw data is in purple, tools and their functions are in green with the output files in blue.*

Pipeline above was used to carry out RNA-seq analysis (Figure 3-10). Novogene sequenced samples and raw reads were received in fastq files. Scythe tool is usually used to remove adaptor contamination, but it was not necessary because raw reads did not have adapter contamination. Sickle tool was then used for removal of low quality 3'-end of reads resulting in trimmed reads in .fastq format. More than 99% of total reads were pair reads with nearly 0% of pair reads removed whereas half of single reads were kept (0.2%) and half trimmed (0.2%). An example of 2nd replicate of OVCAR-3 treated with BI 2536 is shown in Figure 3-11. From total of almost 76 million of reads, 4682 paired reads were discarded accounting for 0.006% of total reads and 118150- single reads, accounting for 0.16%.

```
PE forward file: /data//OVBI2_1.fq.gz
PE reverse file: /data//OVBI2_2.fq.gz

Total input FastQ records: 75899212 (37949606 pairs)

FastQ paired records kept: 75658230 (37829115 pairs)
FastQ single records kept: 118150 (from PE1: 69454, from PE2: 48696)
FastQ paired records discarded: 4682 (2341 pairs)
FastQ single records discarded: 118150 (from PE1: 48696, from PE2: 69454)
```

Figure 3-11. Sickle adaptive trimming output for the 2nd replicate of OVCAR-3 treated with BI 2536. *PE-pair ended forward and reverse file.*

To determine the accuracy of a sequencing platform the base calling is used because it is possible the given base was called incorrectly by the sequencer (Illumina Technical Note). FASTQC report indicated the high quality of reads with Phred Score equal or greater than

Figure 3-12. FASTQC: mean quality value across each base position in the read. *Phred Quality Score is used for base calling accuracy. Position on x axis is base pairs (bp).*

35 across each base position as shown in Figure 3-12 (Andrews, 2019). All samples passing quality control were aligned to the GRCh38/hg38 human genome using STAR alignment tool (Dobin et al., 2012). The alignment was successful as the percentage of

uniquely mapped reads was in the range of 92-95% (Table 3-3). For instance, OVCAR-3 treated BI 2536 2nd replicate from pair-end reads that were kept, which is 37829115 pairs, 35349782 (93.5%) were mapped uniquely, only 1523776 (4.0%) mapped to too many loci, 37769 (0.1%) unmapped because of too many mismatches, 883796 (2.3%) unmapped

Treatment	Read Length	No. of Reads	% Uniquely Mapped	% Mapped to too many loci	% Unmapped	Coverage
CAOV3 DMSO 1	297	36586289	92.63%	4.02%	3.35%	6.1
CAOV3 DMSO 2	297	30100650	91.98%	4.13%	3.88%	4.98
CAOV3 DMSO 3	297	37069300	92.09%	3.97%	3.95%	6.14
CAOV3 BI 2536 1	297	42999297	92.26%	3.75%	4%	7.14
CAOV3 BI 2536 2	297	43093100	91.54%	4.71%	3.75%	7.1
CAOV3 BI 2536 3	297	28995819	92.86%	3.98%	3.15%	4.85
CAOV3 BI 6727 1	297	30750498	94.50%	3.04%	2.47%	5.23
CAOV3 BI 6727 2	298	35625600	93.86%	3.12%	3.02%	6.04
CAOV3 BI 6727 3	297	34298923	93.67%	2.85%	3.48%	5.78
OVCAR-3 DMSO 1	297	38501891	92.34%	4.54%	3.11%	6.4
OVCAR-3 DMSO 2	298	43348471	93.16%	4.03%	2.81%	7.29
OVCAR-3 DMSO 3	298	35288166	92.86%	4.93%	2.20%	5.92
OVCAR-3 BI 2536 1	297	40821633	92.97%	3.61%	3.43%	6.83
OVCAR-3 BI 2536 2	298	37829115	93.45%	4.03%	2.53%	6.38
OVCAR-3 BI 2536 3	298	40332363	92.07%	5.16%	2.76%	6.71
OVCAR-3 BI 6727 1	297	28260231	94.91%	2.80%	2.29%	4.83
OVCAR-3 BI 6727 2	297	31304108	94.05%	3.04%	2.91%	5.3
OVCAR-3 BI 6727 3	297	35102775	93.23%	3.35%	3.42%	5.89

Table 3-3. Mapping metrics from trimmed reads alignment to reference human genome. Percentages are percentage reads that were either uniquely mapped, mapped to too many loci or unmapped.

because too short and 33992 (0.09%) unmapped because of other reasons. All previous QC checks were successful thus STAR alignment gene count file, .geneCountTab was created for further analysis.

3.6.2 Principal component analysis

Then principal component analysis (PCA) graphs were created from gene counts to study the variance between the treatment groups (Figure 3-13). PCA showed the difference between CAOV3 (left), and OVCAR-3 (right) cell lines gene expression treated with DMSO, 100 nM BI 2536 and 100 nM BI 6727 for 24 h. While in OVCAR-3 all treatments form separate clusters, in CAOV3 just BI 6727 treated samples forms a distinct cluster. Although CAOV3 three replicates with DMSO and BI 2536 treated cells are scattered, the low variance between DMSO and BI 2536 in every replicate separately shows that BI 2536 did not significantly different. The difference in response to BI 2536 treatment

between CAOV3 and OVCAR-3 highlights that HGSOC is a heterogenous and thus result in different effect upon treatment with same drug.
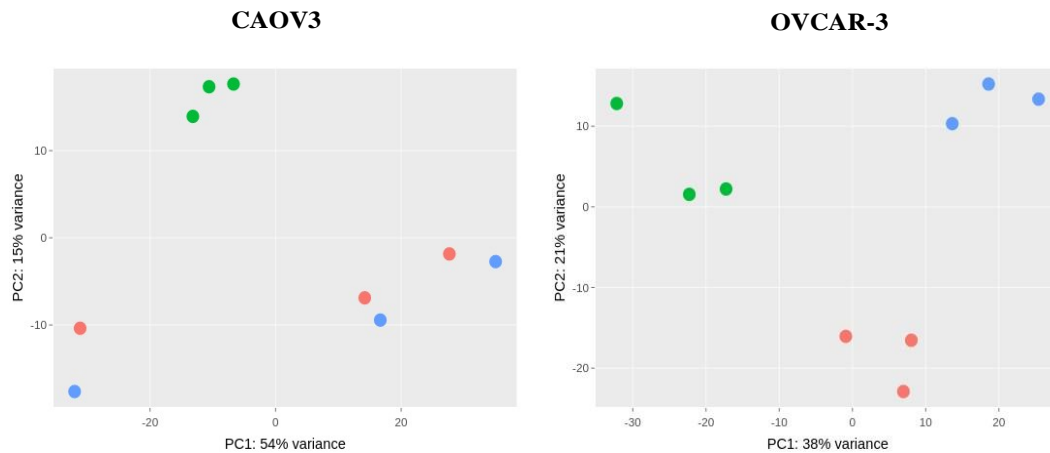
Figure 3-13. Principal component analysis (PCA) showing distribution of RNA-seq data from CAOV3, and OVCAR-3 treated with DMSO, 100 nM BI 2536 or 100 nM BI 6727 for 24 h. *Three biological replicates of each cell line treated with DMSO (blue), 100 nM BI 2536 (red) and 100 nM BI 6727 (green) were sequenced, n = 3. Each point represents one biological replicate.*

3.6.3   Differential analysis

Gene count files were normalized using DESeq2 median of means method by the treatment to output normalized gene counts (Love et al., 2014). DESeq2 was used to determine significantly regulated transcripts between treatment and control. To visualise DESeq2 results volcano plots were produced (Figure 3-14). This analysis enables the

exploration of upregulated and downregulated genes between BI 2536 and BI 6727 treatments and cell lines.
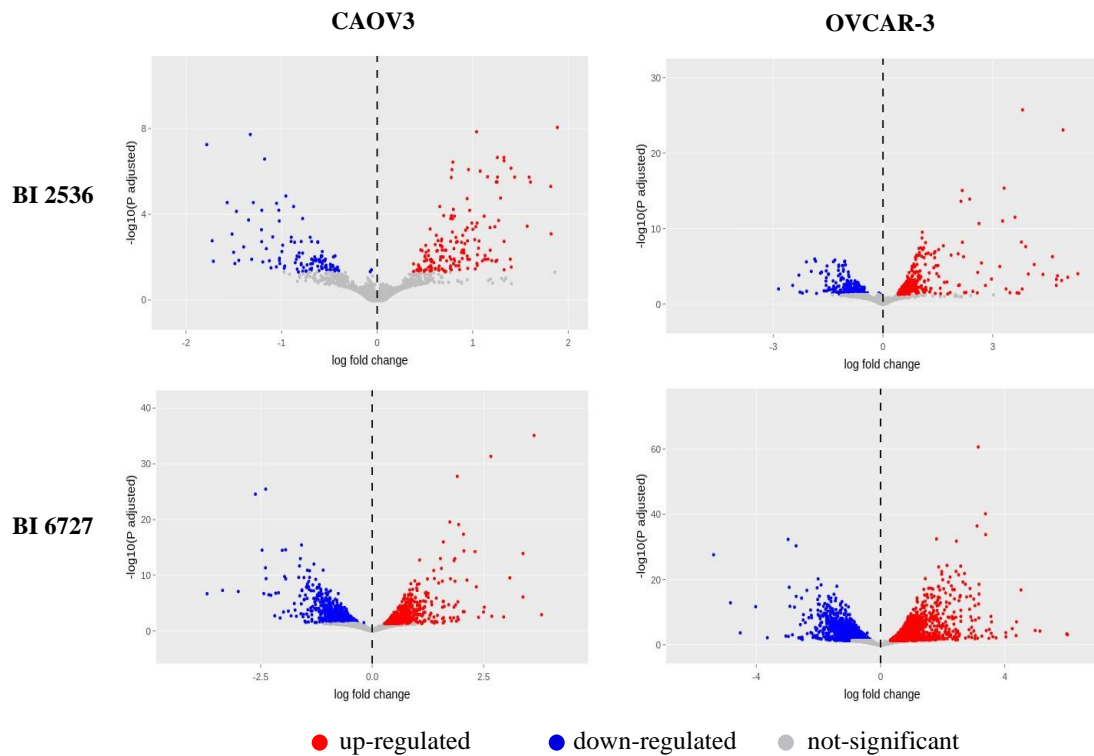
Figure 3-14. Gene transcript levels in CAOV3 and OVCAR-3 in response to BI 2536 and BI 6727 treatment. *Volcano plots illustrate number of gene transcript levels after 24 h 100 nM BI 2536 and 100 nM BI 6727 treatment that are upregulated (red), downregulated (blue), or not changed significantly, (p-value > 0.05; grey). Logarithmic fold change shows the extent of upregulation or downregulation of gene transcripts when compared to DMSO, vehicle control gene expression.*

The higher number of significantly upregulated and downregulated gene transcripts in OVCAR-3 reflects greater variance between clusters in PCA plot (Figure 3-13). Clustering of CAOV3 treatment groups in PCA is also explained by the five-fold greater number of genes with significantly altered expression in BI 6727 (1559 genes) in comparison to BI 2536 (283 genes) treatment. Upon BI 2536 treatment there were 167 and 303 significantly upregulated genes in CAOV3, and OVCAR-3 cell line, respectively. BI 6727 treatment induced significant upregulation of 684 (CAOV3) and 2387 (OVCAR-3) genes. 40% of genes with significant change were downregulated in both cell lines by

BI 2536 treatment whereas BI 6727 treatment downregulated over 55% and 50% genes in CAOV3 and OVCAR-3, respectively.

Figure 3-15 shows gene counts after filtering for genes that have absolute log2fold change greater than 0.58 (absolute fold change > 1.5). In CAOV3 there were 269 (158 upregulated, 111 downregulated) and 892 (342 upregulated, 550 downregulated) differentially expressed genes in BI 2536 and BI 6727 treatment groups, respectively. In OVCAR-3, there were 561 (288 upregulated, 273 downregulated) and 3225 (1600 upregulated and 1625 downregulated), in BI 2536 and BI 6727 treatment groups, respectively.
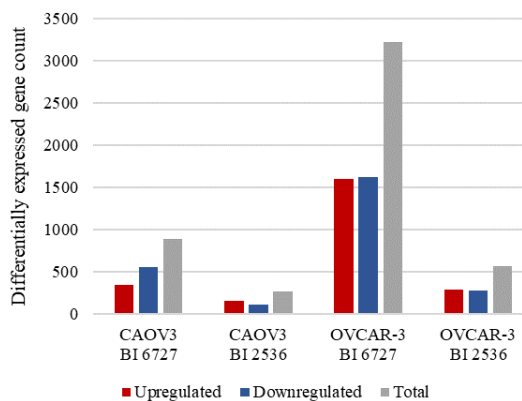
Figure 3-15. Filtered upregulated, downregulated and total gene counts in CAOV3 and OVCAR-3 cells treated with 100 nM BI 2536 and 100 nM BI 6727 for 24 h. Filtered genes have an absolute log2fold change greater than 0.58 (absolute fold change > 1.5) and p-value < 0.05.

The distribution of upregulated and downregulated genes is shown in the Venn diagrams (Figure 3-16). Venn diagrams were produced to find unique and common differentially expressed genes between treatments and cell lines. The highest number of overlapping downregulated genes were between CAOV3 and OVCAR-3 treated with BI 6727, which was 374 accounting for 23% and 68% of total downregulated genes in OVCAR-3 and CAOV3, respectively. BI 6727 induced upregulation of 1379 and downregulation of 1157
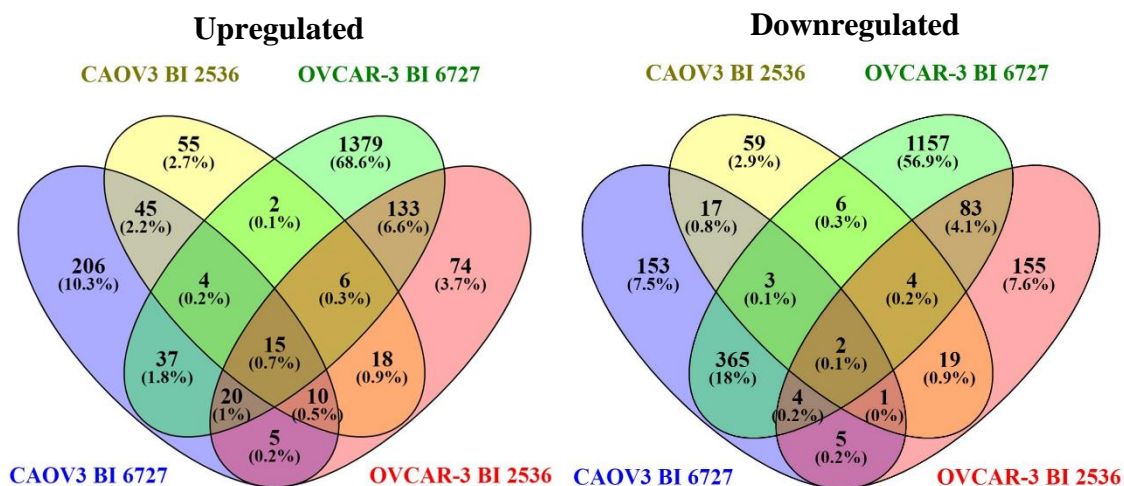
Figure 3-16. Venn diagram comparisons with upregulated and downregulated genes in CAOV3 and OVCAR-3 cells treated with 100 nM BI 2536 and 100 nM BI 6727 for 24 h.

unique genes in OVCAR-3 accounting for approximately 69% and 57% of the total number of upregulated and downregulated genes, respectively. Whereas, BI 2536 induced downregulation in 155 genes including *MYCN*. In CAOV3, BI 6727 treatment resulted in the upregulation of 206 unique genes. There were 15 genes that were upregulated and 2 downregulated in both cell lines in response to both treatments. The 15 upregulated genes were *FAM72B*, *FOS*, *PLK1*, *BUB1*, *ANLN*, *AURKA*, *CDCA8*, *GAS2L3*, *CDCA3*, *IQGAP3*, *SMTN*, *KNSTRN*, *DLGAP5*, *CDCA2*, *CKAP2L* while 2 downregulated were *RP11-469H8.6* and *MAP2K6*. Interestingly, *PLK1* was one of the upregulated genes suggesting a feedback loop as a response to the drug.

3.6.4 Pathway analysis

Gene set enrichment analysis (GSEA) was performed to retrieve differentially regulated pathways. Results in Figure 3-17 showed significantly upregulated pathways that were common in at least two cell lines/treatments and all significantly downregulated pathways.

CAOV3 treated with BI 6727 had upregulated pathways with the highest normalized enrichment ratio which is defined as a normalized number of observed genes divided by the number of expected genes in that pathway (Figure 3-17). Wnt and Notch signalling, reproduction, cellular responses to stress and external stimuli, homology-directed, DNA and DNA double-strand break repair, and deubiquitination were upregulated common pathways in CAOV3 cells treated with BI 2536 and BI 6727 treatment groups. In OVCAR-3, BI 2536 or BI 6727 treatment resulted in upregulation of genes involved in resolution of sister chromatid cohesion, mitotic prometaphase, kinesins, AURKA activation by TPX2 and amplification of signal from the kinetochores. RHO GTPase effectors and cell cycle were only upregulated pathways that common between CAOV3 treated with BI 2536 and BI 6727 and OVCAR-3 with BI 2536 but not OVCAR-3 treated with BI 6727.

Significantly downregulated pathways differed between cell lines and treatments, only RNA metabolism was downregulated in CAOV3 and OVCAR-3 treated with BI 6727.
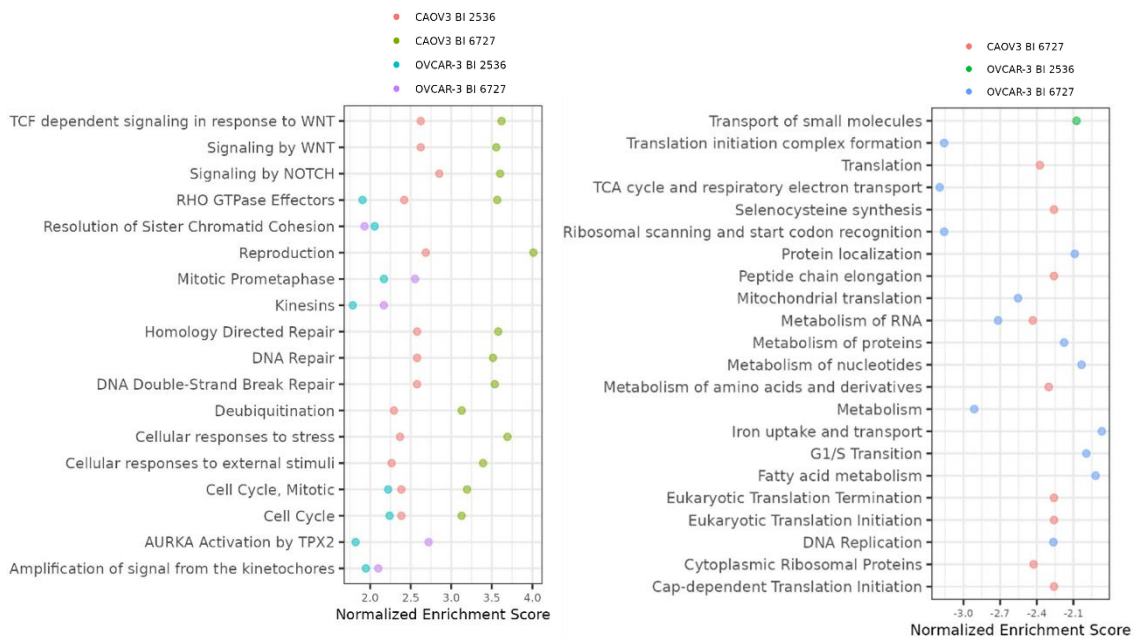
Figure 3-17. Pathways from gene set enrichment analysis (GSEA) of differentially expressed genes in CAOV3 and OVCAR-3 treated with BI 2536 and BI 6727. Significantly upregulated common pathways between at least two cell lines/treatments (left) and significantly downregulated pathways (right). False Discovery Rate (FDR) ≤ 0.05, p-value < 0.05.

There were no significantly downregulated pathways in response to BI 2536 treatment in CAOV3 and small molecule transport was downregulated in OVCAR-3 treated with BI

2536. BI 6727 significantly downregulated genes relating to metabolism of amino acids and derivatives in CAOV3 and metabolism in general, as well as protein, nucleotides and fatty acid metabolism in OVCAR-3. Translation initiation complex formation was downregulated in OVCAR-3 and translation, eukaryotic translation initiation and termination in CAOV3 in response to BI 6727. Genes regulating G1/S transition and DNA replication pathways were downregulated in BI 6727-treated OVCAR-3 cells.

BI 2536 in CAOV3 uniquely upregulated genes in transcriptional regulation by RUNX1, pre-NOTCH transcription, translation, expression and processing, mitotic prophase, and
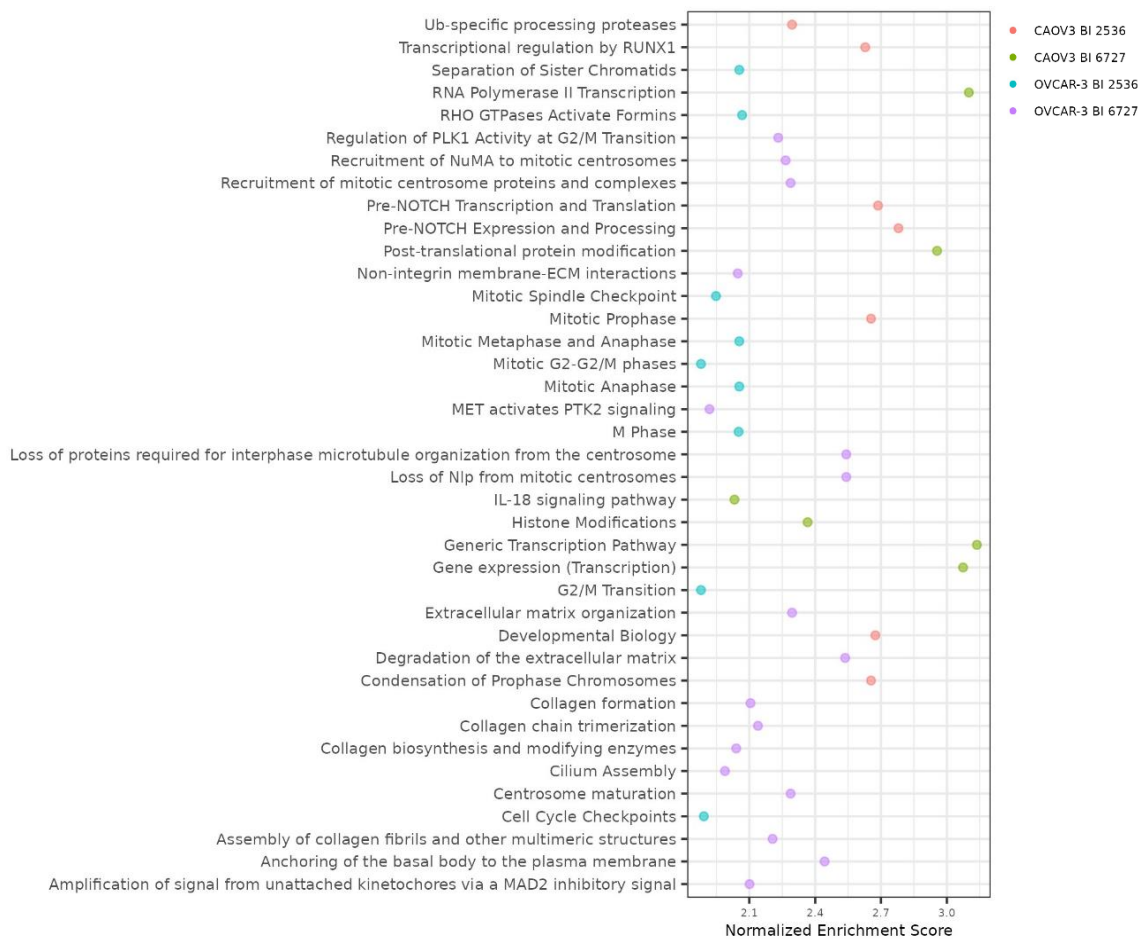
Figure 3-18. Pathways from gene set enrichment analysis (GSEA) of differentially expressed genes in CAOV3 and OVCAR-3 treated with BI 2536 and BI 6727. *Significantly upregulated unique pathways. False Discovery Rate (FDR) ≤ 0.05, p-value < 0.05.*

condensation of prophase chromosomes (Figure 3-18). BI 2536 only in OVCAR-3 significantly upregulated genes related to the separation of sister chromatids, cell cycle checkpoints, G2/M transition, mitosis/M phase-related pathways: mitotic spindle

checkpoints, metaphase and anaphase. BI 6727 in CAOV3 upregulated RNA Polymerase II transcription and gene expression, post-translational protein modification, histone modification. BI 6727 in OVCAR-3 uniquely upregulated genes in regulation of PLK1 activity at G2/M transition, loss of Nlp from mitotic centrosomes, loss of proteins required for interphase microtubule organization from the centrosome, recruitment of mitotic centrosome proteins and complexes, recruitment of NuMA to mitotic centrosomes, centrosome maturation.

Overall, RNA-seq results show that drugs target cell cycle-associated pathways, and gene expression through transcription, translation, and metabolism. Altered transcription and histone modification relate to BRD4 function, validating further exploration of epigenetic changes in response to the drugs.

3.7   ATAC-seq

3.7.1   Protocol optimisation

ATAC-Seq was chosen to explore what effect BI 2536 and BI 6727 have on chromatin level, and how the changes in accessible chromatin regions relate to the gene expression studied with RNA-seq method. ATAC-seq utilises prokaryotic transposon 5 (Tn5) transposase enzyme binds to open chromatin regions and cuts DNA into fragments. The successfully prepared libraries should contain fragments ranging from 200 bp to 1000 bp.

Protocol was optimised because ATAC-seq has never been performed in our lab previously. The table below shows the different conditions such as cell number, tagmentation time and total PCR cycle number that were tested and determined optimal conditions for CAOV3 and OVCAR3 cells (Table 3-4).

Conditions	Tested	Optimal
Number of cells	50,000; 75,000; 100,000	50,000
Tagmentation time	30; 35 min	35 min
Shaking during tagmentation	no shaking; 300 rpm; 1000 rpm	300 rpm
Total PCR cycles	7, 10, 16	10 cycles

Table 3-4. ATAC-seq protocol optimisation. Tested and optimal conditions for ATAC-seq library preparation from CAOV3 and OVCAR-3 cells.

The number of cells has an impact on the fragmentation of DNA because the aim is to have a diverse library with a range of different-size fragments, low cell number leads to overtagmentation where the majority of the library consists of small fragments because the Tn5 transposase will be too high or on the contrary high cell numbers lead to undertagmentation where large fragments comprise the library. The greatest quality libraries were achieved with 50,000 cells which applied to both cell lines. Tagmentation time and shaking can also lead to undertagmentation- too short and overtagmentation- too long. An appropriate number of PCR cycles is essential to avoid oversaturation of libraries and reduce GC and size bias.

Libraries were prepared with optimal conditions from CAOV3 and OVCAR-3 treated with 100 nM BI 2536 and 100 nM BI 6727 for 24 h in biological triplicates. Majority of libraries had primer dimers present as shown in figure below which would show up as peak after lower maker (Figure 3-19).
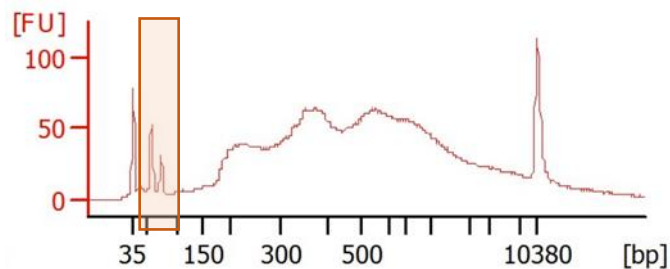
Figure 3-19. Presence of primer dimers in CAOV3 cells treated with 100 nM BI 2536 library. Library profile shows two peaks after the lower maker peak (first peak) representing primer dimer contamination.

Therefore, additional cleanup was required. Below are library profiles showing the size distribution of DNA fragments in prepared libraries 3-20. In all libraries each peak corresponds to nucleosome-free, mononucleosome, dinucleosome and multinucleosome
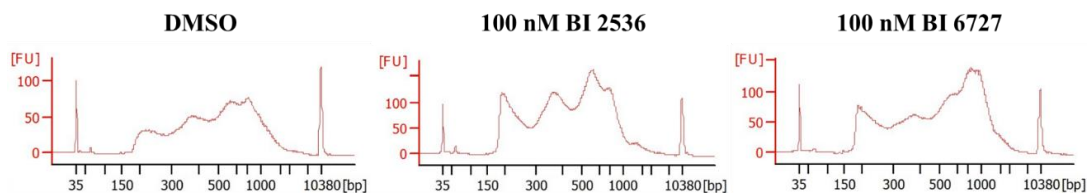
Figure 3-20. ATAC-seq libraries prepared from CAOV3 cells treated with DMSO, 100 nM BI 2536 or BI 6727. Bioanalyzer trace shows lower and upper marker peaks with nucleosome-free, mononucleosome, dinucleosome and multinucleosome peaks in between.

fragments.

3.8 Quality control, alignment and peak calling

All prepared libraries were successfully sequenced, and the following pipeline was used to analyse ATAC-seq raw reads datasets (Figure 3-21).
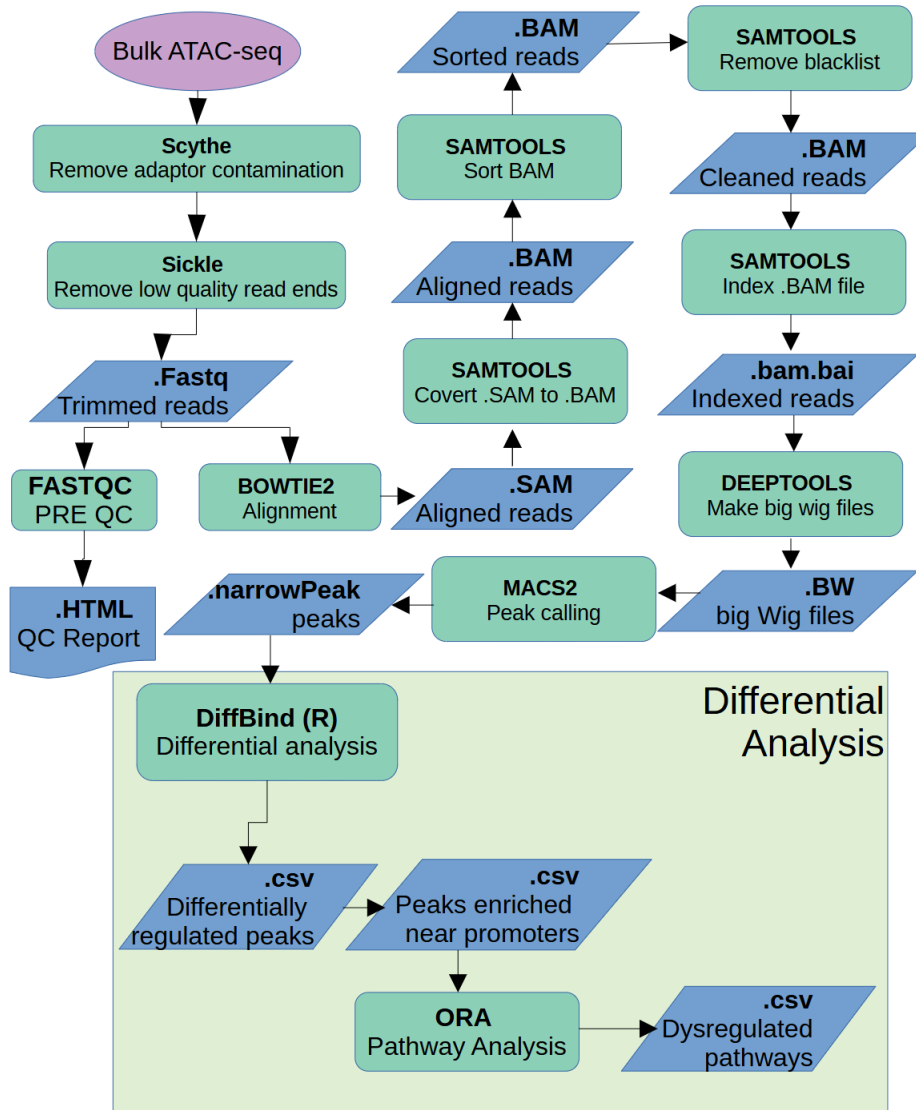
Figure 3-21. ATAC-seq data analysis pipeline: from raw reads to pathway analysis. *Raw data is in purple, tools and their functions are in green with the output files in blue.*

FASTQC tool was used to carry out quality control which showed that Nextera adaptor sequences were present (Figure 3-22). Scythe was used to remove adaptor contamination while Sickle tool was used to remove low quality read ends.
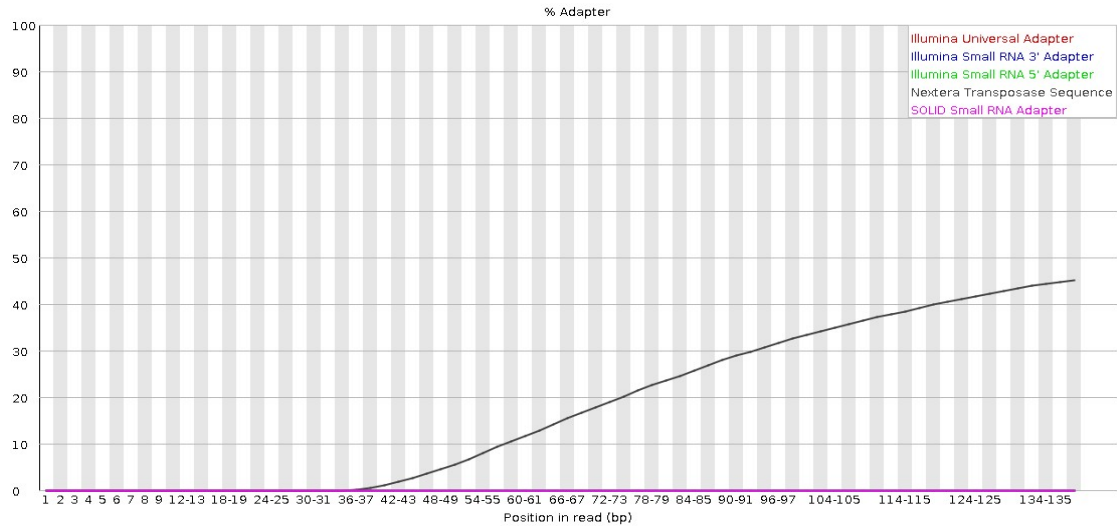
Figure 3-22. Adapter content in CAOV3 treated with DMSO 1st replicate. *Black line represents Nextera Transposase Sequence. Adapter contents show whether fastq files and reads in them have a significant amount of adapter sequences. In the presence of adapters, adapter trimming is performed.*

FASTQC reports showed high quality of samples as shown in Figure 3-23 thus trimmed
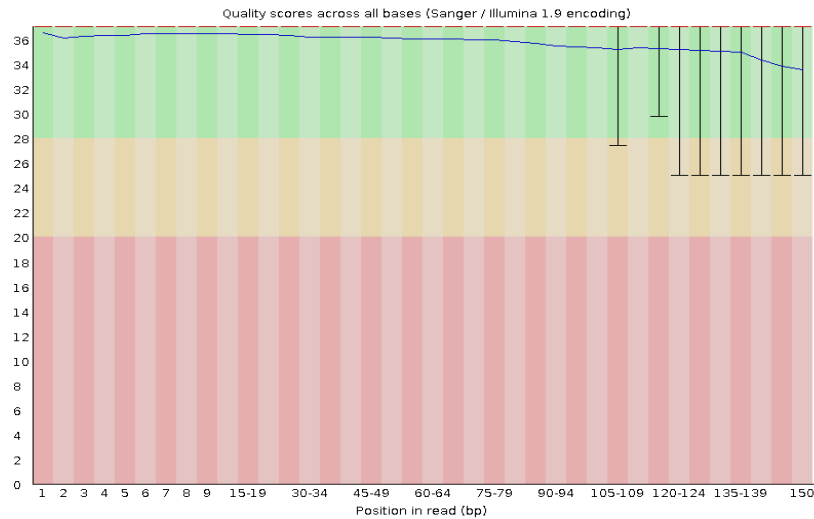
Figure 3-23. Per base sequence quality of CAOV3 treated with DMSO 1st replicate. *Blue line is a mean quality, central red line is the median value and whiskers represent the 10% and 90% points.*

read were aligned to indexed human genome.

Then a series of steps were carried out using SAMTOOLS including SAM file conversion to BAM, sorting BAM files, removing blacklist and indexing BAM file. Peak calling was performed to produce narrowPeak files with called peaks as shown in Figure 3-24.

```
chr1     9896      10575     ATAC_C1_EKDL230009191-1A_HFC7NDSX7_L2_1_bowtie2UPBlkLstRm_MACS2_peak_1      1213    .     15.2479 126.949 121.328 316
chr1     28873     29392     ATAC_C1_EKDL230009191-1A_HFC7NDSX7_L2_1_bowtie2UPBlkLstRm_MACS2_peak_2      703     .     14.6875 74.21   70.3662 290
chr1     29579     30025     ATAC_C1_EKDL230009191-1A_HFC7NDSX7_L2_1_bowtie2UPBlkLstRm_MACS2_peak_3      62      .     3.69401 8.31043 6.21702 243
chr1     34503     34992     ATAC_C1_EKDL230009191-1A_HFC7NDSX7_L2_1_bowtie2UPBlkLstRm_MACS2_peak_4      63      .     4.51411 8.47469 6.3757  137
chr1     79094     79445     ATAC_C1_EKDL230009191-1A_HFC7NDSX7_L2_1_bowtie2UPBlkLstRm_MACS2_peak_5      66      .     5.82336 8.79731 6.6808  142
chr1     96365     97026     ATAC_C1_EKDL230009191-1A_HFC7NDSX7_L2_1_bowtie2UPBlkLstRm_MACS2_peak_6      76      .     6.04882 9.80905 7.66021 231
chr1     180696    181120    ATAC_C1_EKDL230009191-1A_HFC7NDSX7_L2_1_bowtie2UPBlkLstRm_MACS2_peak_7      228     .     6.87778 25.4262 22.8249 211
                                                          ...
chrY     25399190  25399470  ATAC_C1_EKDL230009191-1A_HFC7NDSX7_L2_1_bowtie2UPBlkLstRm_MACS2_peak_75351  146     .     9.22032 17.0361 14.6558 134
chrY     56834183  56834427  ATAC_C1_EKDL230009191-1A_HFC7NDSX7_L2_1_bowtie2UPBlkLstRm_MACS2_peak_75352  22      .     2.64774 4.1189  2.23198 225
chrY     56850325  56851016  ATAC_C1_EKDL230009191-1A_HFC7NDSX7_L2_1_bowtie2UPBlkLstRm_MACS2_peak_75353  71      .     4.62738 9.32652 7.19341 134
chrY     56954013  56954276  ATAC_C1_EKDL230009191-1A_HFC7NDSX7_L2_1_bowtie2UPBlkLstRm_MACS2_peak_75354  37      .     4.36752 5.74204 3.75802 176
chrY     57006585  57007043  ATAC_C1_EKDL230009191-1A_HFC7NDSX7_L2_1_bowtie2UPBlkLstRm_MACS2_peak_75355  99      .     7.2792  12.1638 9.9296  172
chrY     57067553  57068195  ATAC_C1_EKDL230009191-1A_HFC7NDSX7_L2_1_bowtie2UPBlkLstRm_MACS2_peak_75356  591     .     18.5163 62.6848 59.1568 321
chrY     57216578  57217368  ATAC_C1_EKDL230009191-1A_HFC7NDSX7_L2_1_bowtie2UPBlkLstRm_MACS2_peak_75357  1547    .     18.2298 161.625 154.799 506
```

Figure 3-24. Called peaks in CAOV3 treated with DMSO 1ˢᵗ replicate. One row represents one called peak. The first column indicates which chromosome (chr) it is, second- start coordinate of the peak, third- end coordinates, 4ᵗʰ- name, 5ᵗʰ- score, 6ᵗʰ- strand, 7h- signal value, 8ᵗʰ- -log10(pValue), 9ᵗʰ - -log10(qvalue), 10ᵗʰ- peak.

Finally, DiffBind was used to carry out differentially regulated peak analysis.

3.8.1 Differentially regulated peaks

After Peak calling, the comparative analysis showed that there was a difference between control, DMSO-treated cell lines and 100 nM BI 2536 or 100 nM BI 6727 treated cells. Differentially regulated peak counts are shown in Table 3-5. OVCAR-3 had a greater

Cell line	Treatment	Upregulated	Downregulated
CAOV3	BI 2536	45	1797
	BI 6727	24	157
OVCAR-3	BI 2536	219	18870
	BI 6727	81	48486

Table 3-5. Differentially regulated peak counts in CAOV3 and OVCAR-3 treated with 100 nM BI 2536 and 100 nM BI 6727 after 24 h.

number of both upregulated and downregulated peaks in both treatment groups in contrast to CAOV3. Upregulation and downregulation between BI 2536 and BI 6727 treatments differed depending on the cell line. In CAOV3 treated with 100 nM BI 2536, there were over 1800 differentially regulated peaks and less than 200 in BI 6727 treatment. Whereas in OVCAR-2 treated with BI 6727 there were over two-fold greater number (>48000) of differentially regulated in contrast to OVCAR-3 treated with BI 2536 (>19000). Furthermore, the greatest number of differentially regulated peaks were downregulated implying a closed chromatin state in response to the treatment and only a few peaks were upregulated. In CAOV3, BI 2536 treatment resulted in less than 1800 downregulated peaks whereas in OVCAR-3 the peak count was more than ten-fold greater (18870). In OVCAR-3 treated with BI 6727 downregulated peak count was over 48000 when compared to CAOV3 where there were barely any downregulated peaks detected (157).

3.8.2 Differentially regulated peaks enriched near promoters

For further analysis, a gene list was produced from the upregulated and downregulated peaks that were enriched near the promoter region of the corresponding gene. The ATAC-seq analysis was limited to promoter regions because analysis of other regions involves greater complexity. Results shown in Table 3-6 indicate that there were more downregulated peaks enriched at promoter in OVCAR-3 than CAOV3 correlating to total count of differentially regulated peaks. No upregulated peaks enriched at promoter were present in OVCAR-3 whereas in CAOV-3 there 39 and 1 peak in BI 2536 and BI 6727 treatment respectively. Out of 1797 downregulated peaks 86 were enriched the promoter in CAOV3 treated with BI 2536, and 22 out of 157 in BI 6727 treated cells. In OVCAR-3, 3% (601) of downregulated peaks were enriched near promoter in BI 2536 treatment group and almost 4% (1818) in BI 6727.

Cell line	Treatment	Upregulated	Downregulated
CAOV3	BI 2536	39	86
	BI 6727	1	22
OVCAR-3	BI 2536	-	601
	BI 6727	-	1818

Table 3-6. Differentially regulated peak counts enriched near the promoter in CAOV3 and OVCAR-3 treated with 100 nM BI 2536 and 100 nM BI 6727 after 24 h.

Following are the examples of peak differences between control and treatment groups in genes selected from the gene list (Figure 3-25). In DMSO control profile (red) the peaks were higher in comparison to treatment peaks (blue) which indicate accessibility of these genes for transcription.
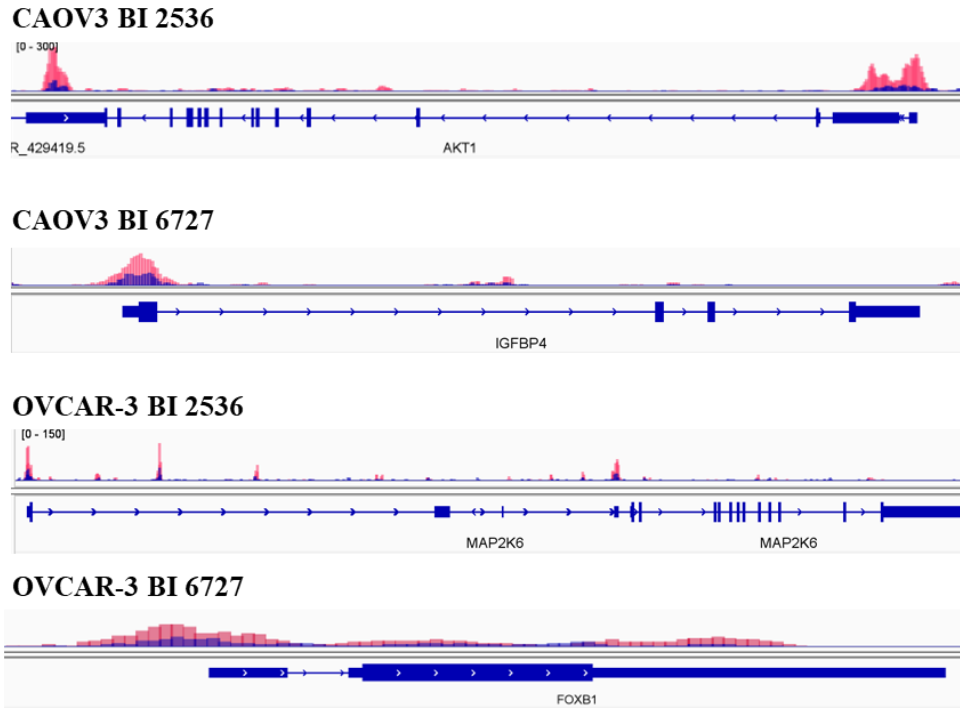
Figure 3-25. DMSO treated CAOV3 and OVCAR-3 peaks overlay from DMSO control and BI 2536 or BI 6727. Red- DMSO, blue- BI 2536/BI 6727.

3.8.3 Transcriptome and chromatin accessibility interlink

The correlation between open chromatin regions from ATAC-seq analysis and gene expression from RNA-seq was explored (Table 3-7).

Cell line	Treatment	ATAC-seq upregulated		ATAC-seq downregulated	
		RNA-seq upregulated	RNA-seq downregulated	RNA-seq upregulated	RNA-seq downregulated
CAOV3	BI 2536	0	0	0	2
	BI 6727	0	1	2	0
OVCAR-3	BI 2536	-	-	5	26
	BI 6727	-	-	146	107

Table 3-7. ATAC-seq and RNA-seq overlapping genes.

In CAOV3 there were 2 genes (*MT1F*, *TFF2*) that were downregulated on transcript level and had downregulated peaks near the promoter in response to BI 2536 treatment. With BI 6727 treatment, *SLC7A2* gene had an upregulated peak near promoter but it was downregulated on transcript level. *FBLN2* and *VGF* were upregulated in RNA-seq but downregulated in ATAC-seq in CAOV3 cells treated with BI 6727. In BI 2536-treated OVCAR-3 there were 5 upregulated genes (*CEL*, *GOLGA8B*, *RNU4ATAC*, *RNVU1-6*,

54

RNVU1-7) but the correlating peaks enriched near promoter were downregulated. In addition, 26 downregulated genes and downregulated peaks enriched near promoter of same gene. These genes included *ADAM21*, *ADGRF1/2*, *AQP5/9*, *BDH2*, *BTC*, *CPM*, *DEF6*, *EDN2*, *GALNT5*, *GRAMD1C*, *HGD*, *HKDC1*, *KRT15*, *MAP2K6*, *PALMD*, *PI15*, *REM2*, *SLC2A9*, *THRSP*, *TNFSF10*, *TNFSF15*, *TRIM22*, *UNC5B-AS1*, *VIT*. In BI 6727 treated OVCAR-3, there were 146 upregulated genes with downregulated peaks and 107 downregulated genes with downregulated peaks. BI 6727 ribosomal proteins.

3.8.4 BI 6727 treatment effect on chromatin accessibility at the promoter of genes involved in cell cycle

ORA pathway analysis was carried out for the differentially regulated peaks enriched near promoters in corresponding genes. Although in CAOV3 there were no significantly upregulated and downregulated pathways (FDR > 0.05) with BI 2536, there was an indication of upregulation in chromatin modifying enzymes and chromatin organization and downregulation of ATP synthesis, TNF signalling pathway. CAOV3 treated with BI 6727 results indicated non-significant downregulation of TNF receptor superfamily members mediating non-canonical NF-kB pathway (FDR=0.5) and post-translational protein phosphorylation (FDR=1). In OVCAR-3, no significantly downregulated pathways in response to BI 2536 treatment. BI 6727 in OVCAR-3 induced downregulation in peaks enriched near the promoter of genes that are involved in the cell cycle including cyclin B2 (*CCNB2*), cell division cycle 27 (*CDC27*), centromere protein E and C (*CENPE*; *CENPC*), *PLK4*, *ALMS1* centrosome and basal body associated protein. Further, significantly downregulated pathways (FDR ≤ 0.05) regulated by genes with downregulated peaks enriched near the promoter of either upregulated or downregulated genes from RNA-seq were explored (Figure 3-26). The downregulated pathways were translation, its initiation and elongation, post-translational protein phosphorylation; cell cycle and mitosis-related pathways such as mitotic G2-G2/M phases, G2/M transition, prometaphase, centrosome maturation, organelle biogenesis and maintenance. These pathways were further validated using a range of different experiments.
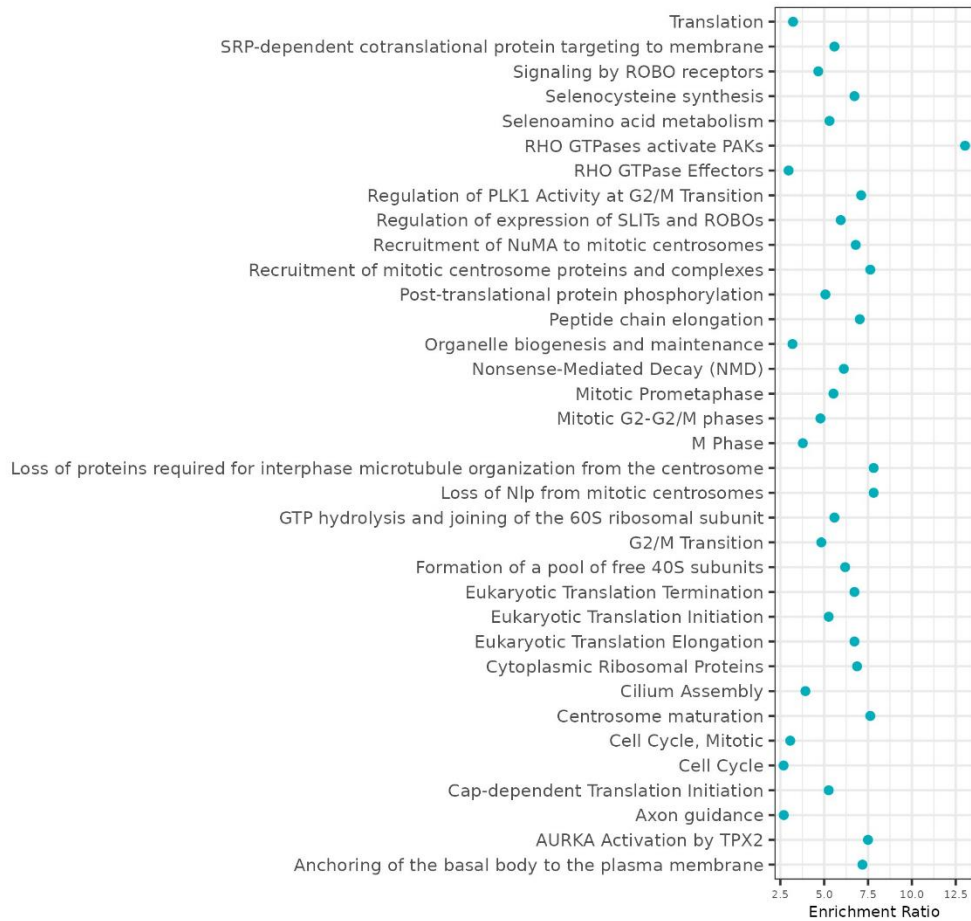
Figure 3-26. Pathways from over-representation analysis of OVCAR-3 treated with BI 6727 with downregulated peaks enriched near promoters of genes that were either upregulated or downregulated in RNA-seq. False discovery rate (FDR) ≤ 0.05, p < 0.05.

3.9 Cell Cycle assay

3.9.1 BI 2536 and BI 6727 induce accumulation of cells in G2/M

RNA-seq and ATAC-seq analysis showed changes in expression genes involved in the cell cycle pathway. Cell cycle assay was performed to study the distribution of cell populations in different cycle phases informing the mechanism of action of BI 2536 and BI 6727. At 24 h, 10 nM BI 2536 treatment induced accumulation of cells in G2 phase in both CAOV3 (32.8%) and OVCAR3 (32.5%) compared to DMSO treated cells (10.7% and 13.1% respectively) as shown in Figure 3-27. Interestingly, same concentration BI 6727 treatment did not induce similar accumulation and G2 cell population in CAOV3 was 17.2% and OVCAR3- 15.8%.
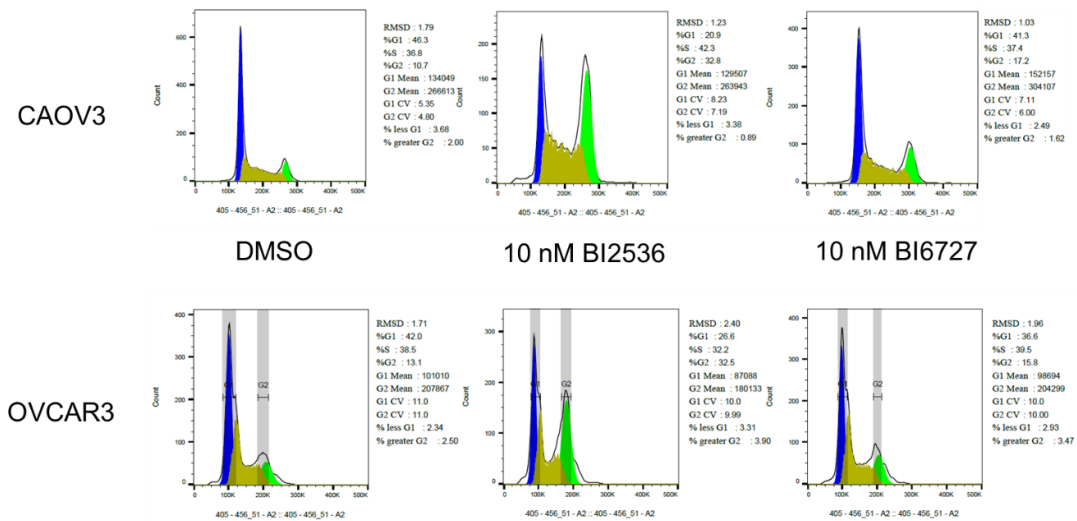
Figure 3-27. Cells distribution in G1, S and G2/M phases. *Flow cytometry cell cycle analysis of CAOV3 and OVCAR3 cells treated with DMSO, 10 nM BI 2536, 10 nM BI6727 for 48h.*

100 nM BI 2536 and BI 6727 treatments induced cell accumulation in the G2 phase at 24 h and 48 h in a similar manner in both cell lines (Figure 3-28). At 24h, 100 nM BI 2536 and BI 6727 treated OVCAR3 cells G2 population was 58% and 51%, respectively, greater than in the control group and G0/G1 phase cell population was 32% and 35% lower. CAOV3 compared to OVCAR3, at 24 h, had less significant changes in G2-phase cell population size, it increased by 28% in 100 nM BI 2536 and 25% in 100 nM BI 6727-treated group. At 48 h, the difference in G2 population increase between CAOV3 and

57

OVCAR3 cell lines was similar 42% vs 55% (BI 2536) and 34% vs 50% (BI 6727) respectively.
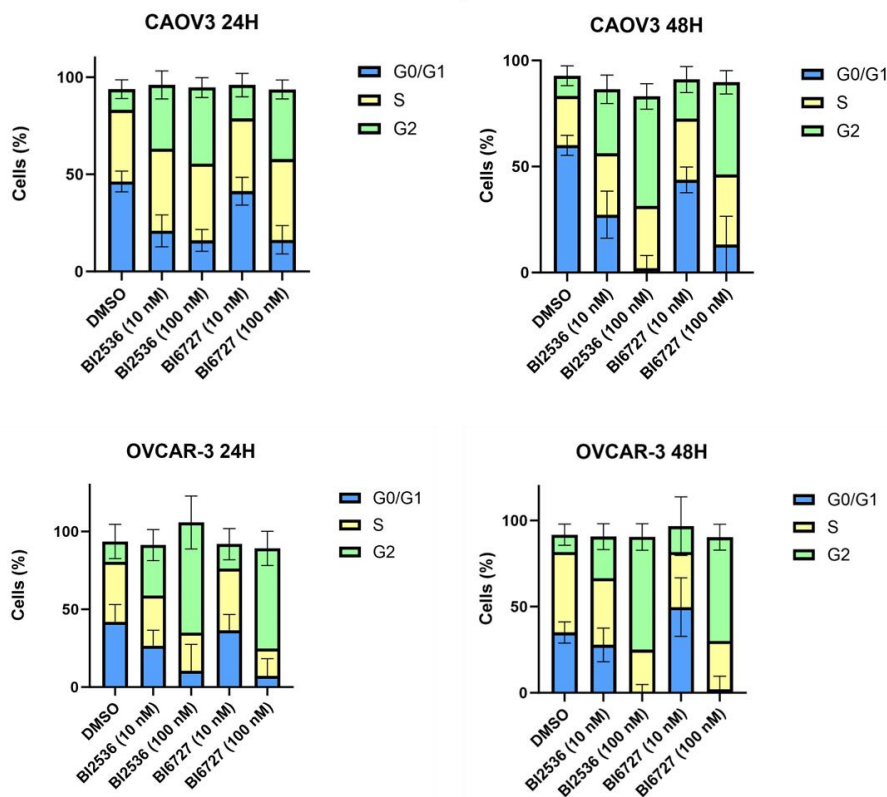
Figure 3-28. Cell cycle at 24 h and 48 h after the 10, 100 nM BI 2536 and BI 6727 treatment on CAOV3 and OVCAR-3. *Error bars are coefficient of variation (CV).*

3.10 Pathway exploration

3.10.1 PLK1 inhibitors induce DNA damage, cell cycle arrest and apoptosis

To further inform the mechanism of action of dual target inhibitor Western Blots were performed to determine what effect the inhibitor has on the expression of target protein and downstream proteins. RNA-seq indicated that cells were undergoing DNA damage, and as γH2AX is phosphorylated in response to DNA double-strand breaks, it was used to measure DNA damage induced by the treatments (Mah et al., 2010). Indication of G2/M phase arrest in RNA-seq, ATAC-seq and cell cycle was further explored through phosphorylated histone H3 expression as it gets phosphorylated when chromatin is condensing at G2 early M phase (Hightower et al., 2012). The decrease in cell viability observed in the viability assay was further interrogated through PARP expression which

is cleaved by caspases during apoptosis and can be also indicative of another form of cell death, pyroptosis (Boulares et al., 1999).

BI 2536 induced γH2AX upregulation in both CAOV3 and OVCAR3 within 24h (Figure 3-29). In CAOV3, the upregulation was lower than in OVCAR-3 at all timepoints. With longer exposure, at 48 h and 72 h γH2AX was highly expressed in OVCAR3. In both cell
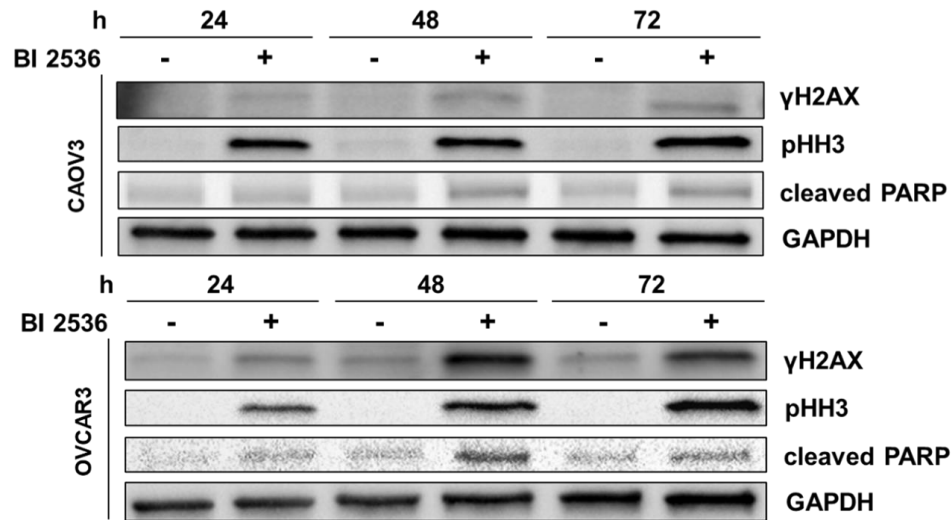
Figure 3-29. Western blot protein expression in BI 2536 and DMSO-treated CAOV3 and OVCAR-3 cells. *Protein expression levels at 24, 48, 72 h after the treatment. Cells were treated with DMSO (-) or 100 nM BI 2536 (+). GAPDH is a loading control.*

lines both BI 2536 and BI 6727 induced pHH3 upregulation from 24h and with long exposure (Figure 3-30).

In contrast to BI 2536-treated CAOV3 cells, BI 6727 upregulated pHH3 expression at 24 h but the upregulation decreased at 48 h and further at 72h after the treatment. The moderate upregulation of γH2AX and cleaved PARP in response to BI 6727 was consistent with the expression of BI 2536-treated CAOV3 cells. OVCAR3 cells treated with 100 nM BI 6727 followed similar expression trends as seen in cells treated with BI 2536. At 24h, BI 6727 induced moderate accumulation of γH2AX and cleaved PARP in OVACR-3 cells and a significant increase in pHH3. γH2AX was highly upregulated with longer exposure to BI 6727 treatment in OVCAR-3 cells. In OVCAR-3 at 48h, cleaved PARP expression peaked but decreased at 72 h whereas pHH3 expression remained upregulated throughout all timepoints.
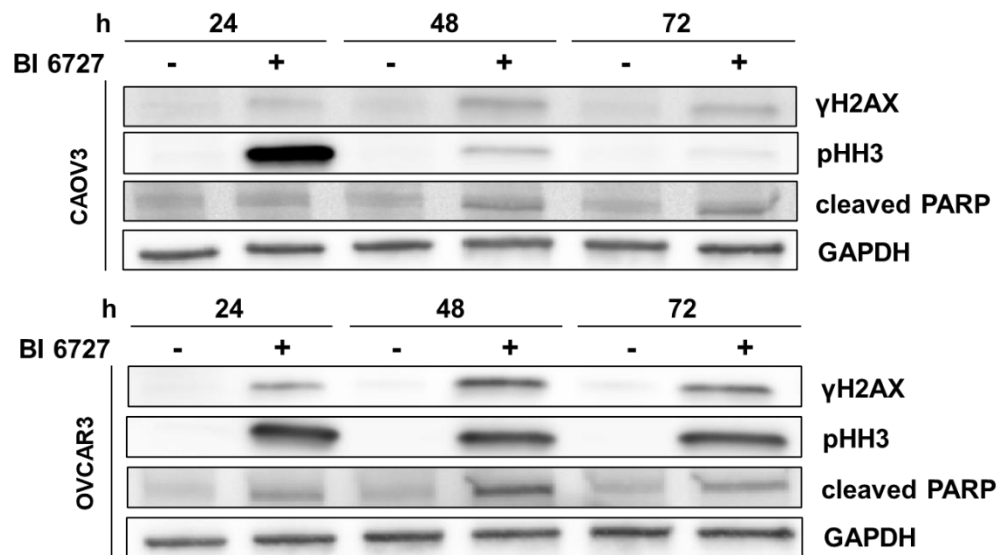
Figure 3-30. Western blot protein expression in BI 6727 and DMSO-treated CAOV3 and OVCAR3 cells. *Protein expression levels at 24, 48, 72 h after the treatment. Cells were treated with DMSO (-) or 100 nM BI 6727(+). GAPDH is a loading control.*

Overall, Western blot analysis showed that drugs induce G2/M arrest, followed by DNA damage and cell death.

3.11 Apoptosis assay

3.11.1 BI 2536 and BI 6727 inhibition induces early and late apoptosis

Viability assay and increase in PARP protein expression implied that cell viability decreased upon the treatment and potentially induced apoptosis. Cells were stained with Propidium iodide and Annexin V-FITC to detect early and late apoptotic cell populations in response to BI 2536 and BI 6727. An important aspect of successful population

differentiation is the compensation of the laser. Because same laser is used to detect both stains compensation is required to separate different populations. As shown in Figure 3-31, at 48h CAOV3 live, apoptotic and late apoptotic populations are well defined showing that compensation was successful. Whereas OVCAR3 same populations are less defined implying that the applied compensation matrix was not effective and it is more difficult to compare these populations.
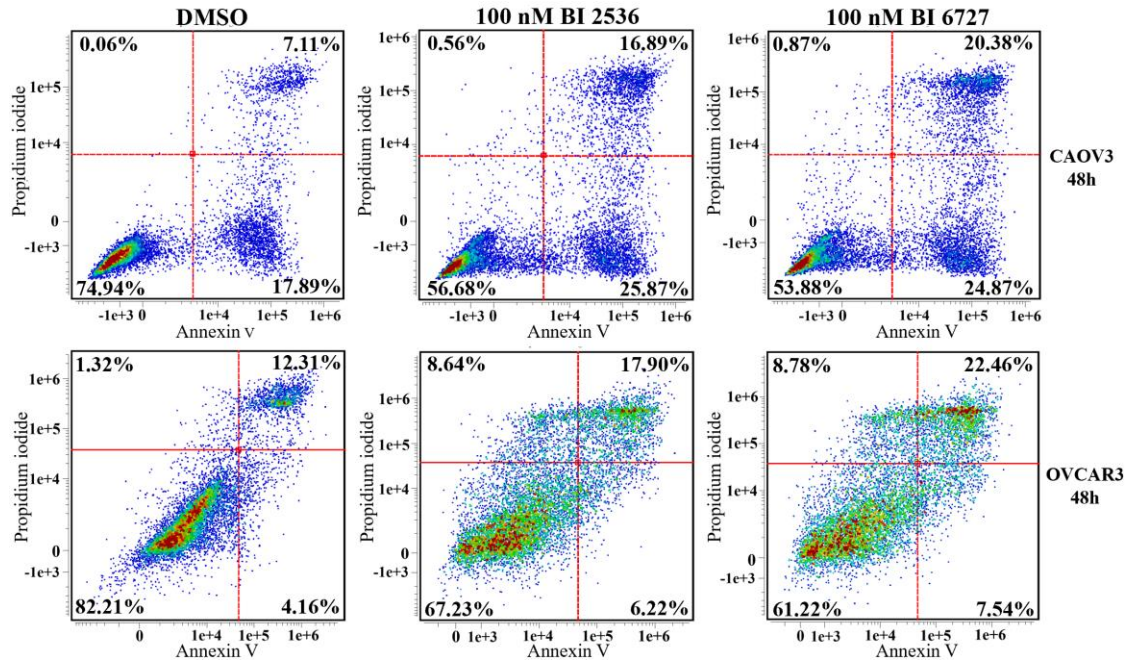
Figure 3-31. Flow cytometry apoptosis assay with 100 nM BI 2536 and BI 6727 treatment at 48 h in CAOV3 and OVCAR-3. *Apoptotic cells are in the bottom right quadrant and necrotic cells are in the top right quadrant. Healthy cells are in the bottom left quadrant.*

At 48h there was an 8% and 7% increase in CAOV3 early apoptotic population size with 100 nM BI 2536 and 100 nM BI 6727, respectively. Upon treatment with 100 nM BI 2536 late apoptotic/necrotic cell population size doubled and with 100 nM BI 6727 it has increased approximately three times. In OVCAR3, BI 2536 induced a 5% increase in late apoptotic/necrotic cell population while BI 6727 treated cell population was twice the size of DMSO treated cells. Less than a 5% increase was detected in early apoptotic cell populations in both treatment groups compared to DMSO control. Results indicate that in response to BI 2536 and BI 6727 cells can undergo early apoptosis as well as late apoptosis- necrosis or pyroptosis.

3.12 Results summary

Findings are summarized in the following table (Table 3-8).

Cell line	CAOV3		OVCAR-3	
Basal PLK1 expression	Low/moderate (+/−)		High (+/+)	
Basal BRD4 expression	High (+/+)		Moderate (+/−)	
Treatment	**BI 2536**	**BI 6727**	**BI 2536**	**BI 6727**
2D: Cell viability	Moderate sensitivity	Moderate sensitivity	Sensitive	Sensitive
Exposure when most sensitive	Long exposure	Long exposure	Short exposure	Short exposure
3D: Cell viability	Sensitive	Sensitive	Moderate sensitivity	Moderate sensitivity
PLK1	↑ - 24, 48 h, relative ↓- 72 h	↑ - 24, 48 h, relative ↓- 72 h	↑ - 24 h, relative ↓ 48, 72 h	↑ - 24 h, relative ↓ 48, 72h
BRD4	↑ long exposure	↑ long exposure	↑ long exposure	↑ long exposure
p-cyclin B1	No change	No change	↑ - 24 h, relatively ↓ 48, 72 h	No change
RNA-seq: ranking by the highest number of differentially expressed genes	4	2	3	1
RNA-seq: Upregulated pathways	Cell cycle, WNT, NOTCH signalling, DNA damage repair, stress response	Cell cycle, WNT, NOTCH signalling, DNA damage repair, stress response, transcription, histone modification	Cell cycle, mitosis, G2/M transition AURKA signalling	Mitosis, AURKA signalling, PLK1 regulation at G2/M transition
RNA-seq: Downregulated pathways	-	Translation, metabolism	Transport of small molecules	Translation, metabolism
ATAC-seq: ranking by the highest number of	3	4	2	1

differentially regulated peaks				
Downregulated pathways	-	-	-	Mitosis, G2/M transition, translation
Cell cycle	↑ G2/M	↑ G2/M	↑ G2/M	↑ G2/M
pHH3	↑	↑ - 24 h, relative ↓ 48, 72 h	↑	↑
γH2AX	↑	↑	↑	↑
Cleaved PARP	↑	↑	↑	↑
Cell death	Early and late apoptosis	Early and late apoptosis	Late apoptosis	Late apoptosis

Table 3-8. Summary of experimental results: CAOV3 and OVCAR-3 response to BI 2536 and BI 6727 treatment.

4 Discussion

OC is the deadliest gynaecological cancer, which is linked to late detection, lack of effective treatment, and recurrence with associated resistance (Chandra et al., 2019). After decades of stagnation in OC cancer treatment strategies newest drugs such as PARP inhibitors for *BRCA1* mutation carriers were introduced (Tangutoori et al., 2015). Despite observed positive results in preclinical stages new drugs often fail in clinical trials. One example of this can be seen in small molecule inhibitors targeting PLK1. PLK1 is a protein of which high expression is linked to high grade, including HGSOC, and OC stage, and is associated with sustained proliferative signalling, invasion, and resisting cell death that are the hallmarks of the disease (Takai et al., 2001). Drugs targeting PLK1 are generally described as monotherapies or dual inhibitors those targeting both PLK1 and BRD4. BRD4 is an epigenetic reader, also overexpressed in OC and its amplification is linked to overexpression of oncogenes such as *MYC*, *NRG1* and is associated with nonmutational epigenetic reprogramming, cancer hallmark, resulting in sustained proliferative signalling, genome instability, invasion and metastasis (Bell et al., 2011; Drumond-Bock & Bieniasz, 2021). In this project, an interdisciplinary, multi-omics-based analysis was conducted on BI 2536 and BI 6727, two inhibitors targeting PLK1 and BRD4, and their associated pathways, that have shown positive results *in vitro* but stagnated in clinical trial progression due to not unsatisfactory response as a monotherapy and hematologic toxicities (Schöffski et al., 2010). BI 6727 was derived from BI 2536 to improve its efficacy which resulted in several cases of partial response and most cases had stable disease compared to BI 2536 which only achieved stable disease yet BI 6727 was not superior to chemotherapy (Pujade-Lauraine et al., 2016; Schöffski et al., 2010). Researchers also suggested patient screening to identify biomarkers in patients who were more sensitive to the treatment (Pujade-Lauraine et al., 2016).

This research was focused on transcriptomic, RNA-seq, and epigenetic, ATAC-seq, approaches trying to understand how they interlink. Proteomic analysis was used as a qualitative technique to validate observed effects on protein level. CAOV3 and OVCAR-3 were chosen as HGSOC cell models. Choosing cell lines with different basal expression of drug targets allows exploration of basal expression as a prognostic marker to determine response to PLK1/BRD4 inhibition. With reference to the Table 3-8, summarizing results,

OVCAR3 had high basal PLK1 and moderate BRD4 expression and was more sensitive to both BI 2536 and BI 6727 treatments with lower IC50 values than CAOV3. Whereas in CAOV3, PLK1 expression was low and BRD4 high and was more sensitive to BI 6727 than BI 2536. PLK1 and BRD4 protein levels were increased in response to both treatments. The greatest response represented by the number of differentially regulated gene and peaks was observed in OVCAR-3 treated with BI 6727 with associated downregulated translation, G2/M transition and metabolism. BI 2536 and BI 6727 induced cell cycle arrest at G2/M arrest leading to DNA damage relating to upregulated γH2AX levels. Both cell lines underwent cell death including early and late apoptosis. Multi-omics approach provided an insight into the mechanism of action at three different levels: chromatin, transcriptome and protein, and observations were mostly interlinked between these levels.

The overlap between ATAC and RNA approaches can further be interrogated but was not done for the purpose of this project as it was aimed at trying to optimise and adapt the approach for drug screening in HGSOC. More detailed analysis is warranted as ATAC-seq has more layers to it, containing information on transcription factor binding dynamics, and differential regulation of peaks at gene enhancers not only promoters (Bentsen et al., 2020; Crump et al., 2021). The differences between transcript levels and accessible chromatin regions between cell lines in response to the same drugs as seen in my findings show that a multi-omics approach can be developed further to identify biomarkers, signatures and new targets and then used on tumour samples to choose the correct treatment strategy as we move closer to personalised treatments (Gallo Cantafio et al., 2018).

The novelty of this research is that it is the first attempt to use RNA-seq and ATAC-seq for both selective PLK1 or dual PLK1/BRD4 inhibitor testing. In a recent study, ATAC-seq and RNA-seq were used to study platinum resistance in HGSOC which was determined to be driven by chromatic changes at DNA regions in between the coding genes resulting in altered gene expression (Gallon et al., 2021). To strengthen my findings and the multi-omics approach, other HGSOC cell lines should be included such as KURAMOCHI and OVSAHO as PLK1 inhibition holds potential in OC treatment (Mei

et al., 2021). Learning from this project's findings and clinical trial results, a bigger HGSOC population needs to be interrogated to gain a better understanding of prognostic makers in HGSOC which would then translate into the clinic and allow for the evaluation of patient suitability for PLK1 inhibitor treatment.

4.1   Cellular heterogeneity

Cellular heterogeneity is one of the most challenging OC characteristics despite that OC is mostly treated as a homogenous disease. The aim of comparing two cell lines was to attempt to understand whether the same drug can lead to different outcomes. The cellular heterogeneity indeed was apparent as OVCAR-3 cells were more sensitive to both BI 2536 and BI 6727 treatments in comparison to CAOV3. The higher basal expression of PLK1 and moderate BRD4 expression in OVCAR-3 but PLK1 low expression and high BRD4 expression in CAOV3 provides evidence for their diverse sensitivity as well as the first insight into mechanism of action of the drugs. As they are both known PLK1 inhibitors, greater response in OVCAR-3 correlates with high basal PLK1 expression in contrast to CAOV3 with low PLK1 expression. Both BI 2536 and BI 6727 reduced OVCAR-3 cell viability in 2D cell viability assay. OVCAR-3 were more sensitive with short exposure while CAOV3 required longer exposure to achieve similar IC50 values. On the contrary, OVCAR-3 spheroids were less sensitive than CAOV3 to both drugs. 3D cell viability assay in OVCAR-3 showed a worse response suggesting that more complex spheroid structure and physiological differences in contrast to monolayer culture increase resistance to both drugs as previously established in the literature (Jensen & Teng, 2020). The differences in the drug response are further seen in protein expression as well as on transcript level where at 24h PLK1 expression increased but protein levels decreased relatively at 48 h time point in OVCAR-3 and later, at 72 h, in CAOV3. Initial surge in PLK1 protein in CAOV3 takes longer for PLK1 to decrease correlating with cell viability assay findings where CAOV3 required longer exposure to achieve similar IC50s as in OVCAR-3. In neuroblastoma cells, greater response to BI 2536 in terms of cell viability decrease and lower IC50s was partially associated with high basal PLK1 expression confirming that basal expression does have a prognostic potential for cell response (Z. Li et al., 2020).

4.2 Mechanism of action

4.2.1 PLK1 inhibition related effects

Upon PLK1 inhibition, PLK1 protein and mRNA expression increased, suggesting that drugs do not inhibit PLK1 expression but rather its function. Initial accumulation of PLK1 protein also suggests that there is a compensatory feedback loop occurring. Drugs are binding to PLK1 but not degrading it as they are not degraders which in the short term results production of more PLK1 to compensate for its loss of function. Therefore PLK1 accumulated in the cell which is visible in the first 24 h after the treatment. As PLK1 is highly involved in centrosome maturation, downregulation of this pathway as indicated by ATAC-seq on OVCAR-3 treated with BI 6727 suggests that PLK1 function is impaired. In addition, Plk1 directly promotes mitotic entry by phosphorylating cyclin B1 (Toyoshima-Morimoto et al., 2001). As shown by Western blots, there is a slight indication of cyclin B1 phosphorylation in BI 2536 where it is first upregulated and then downregulated in OVCAR-3. Whereas in CAOV3 as well as in both cell lines in response to BI 6727, there is no change in p-cyclin B1 expression suggesting that PLK1 function is impaired, and cells struggle to enter mitosis.

4.2.2 BRD4 inhibition-related effect

BRD4 protein expression is upregulated after long exposure (72 h) with both drugs which correlated with previous findings where upon treatment with BET inhibitors, BRD4 accumulated as well we inefficiently inhibited c-MYC and required longer exposure with higher concentration to achieve protein inhibition (Lu et al., 2015). If BI 2536 and BI 6727 are binding BRD4 but inhibition is not effective enough it can potentially trigger cell defence and compensation mechanisms, as drugs are not selective enough to inhibit BRD4 and expression of downstream targets such as c-MYC but enough to disrupt cells to synthesis more BRD4.

As drugs in cell-free assay were less selective to BRD4 than PLK1, the increase in BRD4 expression after longer exposure suggests that both BI 2536 and BI 6727 bind to PLK1 and exert their inhibitory effect whereas their potential BRD4 inhibition takes longer and thus its inhibition effect on cells is moderate and additive rather than primary and causing the changes observed. This theory correlates with CAOV3 higher expression of BRD4

and being less sensitive to both drugs. Because if BRD4 inhibition would be the cause of the effect that were observed, BI 2536, with a better ability to bind BRD4, would have a greater effect than BI 6727 in CAOV3. However, BI 6727 is less selective to BRD4 than BI 2536 and has greater effect on CAOV3 suggesting that the effect that is seen in CAOV3 is primarily because of PLK1 inhibition rather than BRD4. Interestingly, *ALDH1A1* expression downregulation is linked to BET inhibitors, JQ1 and i-BET726 and was downregulated in OVCAR-3 upon treatment with BI 6727 (Yokoyama et al., 2016). However, when compared to OVCAR-3 expression in response to I-BET151 and I-BET585, BI 2536 and BI 6727 did not induce significant downregulation in genes related to BRD4 including *MYCN*, *NRG1*, as well as *HEXIM1*, an established biomarker for evaluation of BET inhibition efficacy in OC (Quintela et al., 2023). Whereas *FOXM1*, *PLK1* which shows opposite response than BET inhibitors in OC as they were upregulated on transcript level (Z. Zhang et al., 2016). *FOS* expression was also upregulated upon BI 2536, BI 6727 and I-BET treatments (Quintela et al., 2023).

Transcription was upregulated as determined by RNA-seq but cell viability was decreasing, thus ATAC-seq assay was used to interrogate changes in chromatin accessibility as BRD4 is epigenetic reader but also functions as HAT. If BRD4 binding to chromatin is disrupted, histone deacetylases (HDAC) no longer compete for acetylated lysine site and can exert their function, remove acetyl residues. While HATs and HDACs are displaced from condensed chromatin during mitosis, BRD4 is present and acts as HAT to de-compact chromatin at its target loci in later mitosis stages to promote trasncription (Devaiah et al., 2016; Kruhlak et al., 2001). Thus when BRD4 acts as HAT and is inhibited then histones do not get re-acetylated. ATAC-seq results showed that there more downregulated peaks than upregulated indicating closing on the chromatin thus supposedly preventing transcription factors and RNA Polymerase II to access genes. Indeed, I-BET inhibitors were shown to reduce histone acetylation levels at promoter regions by blocking BRD4 interaction with histones which supports my findings on downregulation of peaks enriched at gene promoter (Nicodeme et al., 2010).

4.2.3 Cell cycle arrest

RNA-seq and ATAC-seq data indicating differentially expressed genes and differentially regulated peaks near the promoter of genes involved in the cell cycle, more specifically G2/M transition, and early mitosis led to cell cycle exploration by flow cytometry. BI 2536 and BI 6727 induced cell cycle arrest as cells were accumulating in the G2/M phase correlating with previous findings where BI 2536 induced cell cycle arrest at G2/M in A2780, epithelial endometroid OC (Huo et al., 2022). Interestingly, BI 2536 induced cell accumulation in the G2/M phase at a lower dose, 10 nM in comparison to BI 6727 but at a higher dose both drugs induced comparable accumulation.

Indication of G2/M arrest which relates to PLK1 function led to the exploration of expression of mitotic marker, pHH3, a protein phosphorylated during chromatin condensation in mitosis. The histone H3 phosphorylation is initiated in the late G2 phase, early prophase while its dephosphorylation gradually occurs throughout late anaphase, early telophase, therefore, mitotic cells in metaphase express high levels of pHH3 (Lee et al., 2014). Because PLK1 is involved in G2/M transition and mitotic entry, an increase in pHH3 expression observed in CAOV3 treated with BI 2536 and OVCAR-3 treated with BI 2536 and BI 6727 at 24, 48 and 72 h indicate that PLK1 inhibition affects cells and leads to accumulation in late G2 phase, early phases of mitosis when chromatin is in a condensed state as phosphorylation of cyclin B1 is also impaired as discussed previously.

Through PLK1 inhibition cell cycle is stopped permanently with the chromatin not undergoing decondensed which can be linked back to BRD4 as HAT loss of function which contributes to the loss of PLK1 function thus cells are stuck at G2/M phase unable to mediate further mitosis progression. As chromatin is condensed, transcription is not reactivated leading to downregulated translation, and protein synthesis as seen in RNA-seq and ATAC-seq. Yet, the BRD4 inhibition role in cell cycle arrest at G2/M is rather debatable. BI 2536 induced G2/M arrest similarly to selective PLK1 inhibitor, GSK461364, in lymphoma cells while JQ1 did not have a strong effect on cell cycle and HBL-4, a potent BRD4 and PLK1 degrader, induced G0/G1 arrest in acute myeloid leukaemia suggesting that BI 2536 effect on cell cycle and viability primarily to PLK1 inhibition and not BRD4 (Koblan et al., 2016; Mu et al., 2020). Compared to finding from

our previous paper, upon treatment with BI 2536 and BI 6727 both CAOV3 and OVCAR-3 had significantly higher G2/M cell population than I-BET 151 or I-BET 858 treated cells which confirms that PLK1 inhibition leads to cell cycle arrest (Quintela et al., 2023).

4.2.4 DNA damage and apoptosis

Downregulated peaks enriched near promoter of genes in organelle biogenesis and maintenance as well as upregulation in genes related to DNA damage response indicate that cells are undergoing stress and potentially DNA damage which was confirmed through upregulated γH2AX expression. As cell viability was decreased upon the treatment with both drugs, cleaved PARP expression was studied and found to be upregulated indicating induction of apoptosis. Apoptosis assay was also performed which showed that there were two populations of cells: some undergoing early apoptosis and others late apoptosis, or necrosis, pyroptosis which has been previously observed in OC where BI 2536 induced both apoptosis and gasdermin E-dependent pyroptosis (Huo et al., 2022).

4.2.5   Proposed mechanism of action
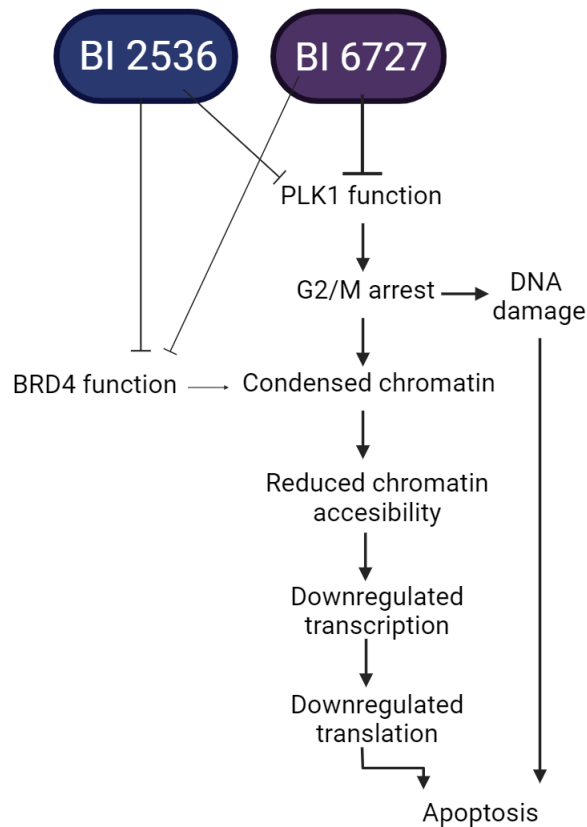
Figure 4-1. Proposed mechanism of action of BI 2536 and BI 6727 in HGSOC.

Even though PLK1 protein is upregulated at 24 h and its mRNA expression is also upregulated in all cell lines, at 48-72h its protein expression starts decreasing which can be a consequence of this cascade (Figure 4-1). PLK1 function but not expression is impaired by both BI 2536 and BI 6727 leading to cell cycle arrest as indicated by cell cycle assay and pHH3 protein accumulation at G2/M, early mitosis which indicates chromatin condensation thus downregulation in chromatin accessibility as seen by ATAC-seq downregulated peak which can also be linked to partial BRD4 inhibition. Cell cycle arrest leads to DNA damage coupled with downregulated transcription which was not indicated by RNA-seq showing only 24 h gene transcript levels and transcription was potentially reduced later at 48-72 h. Both, ATAC-seq and RNA-seq, findings suggest the downregulation of ribosomal proteins and translation, in other terms protein synthesis is downregulated which ultimately leads to cell death in the form of apoptosis or necrosis/pyroptosis.

4.3 Limitations

RNA-seq differentially regulated genes and ATAC-seq differentially regulated peaks enriched near promoters overlapped only partially. Timepoint selection could have led to these findings, thus to improve, two time points similar to Carraro et al. (2022) study should be compared to make proper correlations between epigenetic and transcriptomic landscapes.

Techniques such as single-cell RNA-seq and ATAC-seq would provide a more detailed view in comparison to bulk RNA and ATAC-seq approaches that were used in this study. Even at the cell line level, the response to the drugs varies between the same cell line cells while some populations are more sensitive and undergo cell death others can resist the treatment which could result in broader terms result in relapse. Therefore, using scRNA-seq and scATAC-seq would enable us to explore distinct cell populations and determine which are more resistant to the treatment and determine prognostic signatures of HGSOC (Kagohara et al., 2020; Van de Sande et al., 2023).

Lastly, single cell lines are only indicative of what might be occurring in real OC tumours as they lack complexity. Implementing 3-dimensional co-culture OC models with cells such as immune cells, cancer-associated fibroblasts in combination with a single-cell omics approach would allow a better platform for drug testing and increase the quality of preclinical studies (Tofani et al., 2021).

4.4 Further research

4.4.1 Dual target inhibitors versus combination treatment

CAOV3 and OVCAR-3's higher sensitivity to BI 6727 explains better trial outcomes with BI 6727 compared to BI 2536 yet the outcomes of the trial were not satisfactory for drug to move further at least as a monotherapy. The effectiveness of BI 6727 and its lower binding affinity to BRD4 also shows that targeting BRD4 and PLK1 at least with a dual inhibitor does not necessarily lead to a better response. It is not to be said that targeting PLK1 and BRD4 in combination is ineffective. Therefore, further studies need to be conducted to compare the advantages of improved dual PLK1/BRD4 inhibitors over selective PLK1 or BRD4 inhibitors as well as their combination. A few points that need to be considered are cost-effective: whether more potent PLK1/BRD4 dual inhibitors are

more cost-effective than drug combinations as well as how adverse events compare in dual inhibition versus drug combinations.

4.4.2   RP11-469H8.6

Although, HGSOC signatures were not a predefined outcome of this project one of two downregulated genes that was present in both cell lines and both treatments was *RP11-469H8.6*. It is a long non-coding RNA which has recently been associated with epithelial-mesenchymal transition in endometrioid cancer (Jin et al., 2023). Interestingly, *RP11-469H8.6* was also found to be downregulated in OVCAR-3 upon 24 h I-BET151 and I-BET858 treatment (Quintela et al., 2023). Microprotein inhibiting actin cytoskeleton was identified to be encoded by *RP11-469H8.6* and its downregulated expression in head and neck squamous cell carcinoma and renal cell carcinoma was positively correlated with disease (M. Li et al., 2020; Li et al., 2022). In OC, changes in long non-coding RNAs' expression and mutation have a significant effect on various OC aspects including tumorigenesis, metastasis as well as prognosis and diagnosis (Zhan et al., 2018). For instance, the expression of *RP11-284N8.3.1* can be used to differentiate late-stage OC patients into high-risk (low *RP11-284N8.3.1* expression) and low-risk (high *RP11-284N8.3.1* expression) (Guo et al., 2015). This observation raises questions for further studies of whether *RP11-469H8.6* differential regulation has any prognostic or therapeutic potential in HGSOC.

5 Conclusion

BI 2536 and BI 6727 exert their therapeutic effect mainly through PLK1 inhibition. BRD4 inhibition effects are not definite but suggest that the drugs may have polypharmacological characteristics. BI 6727 successful inhibition of both OVCAR-3 and CAOV3 shows that the lower BRD4 binding capacities may be more beneficial in terms of decreased cell viability and apoptosis induction in comparison to BI 2536. The research findings also show that HGSOC cannot be treated as a homogenous subtype and thus treatment should be chosen based on basal expression and prognostic biomarkers which are yet to be identified. Just as PARP inhibitors are used in OC-carrying *BRCA* mutation patients, tumours could be tested for PLK1 expression and correlation can be established in response to next-generation PLK1 inhibitors. Lastly, the multi-omics approach provides an interesting overlap between chromatin landscape and transcriptome and gives valid insights that can be further confirmed with qualitative experiments such as Western blots. With further optimisation, the multi-omics approach possesses great potential in larger-scale drug screening for HGSOC and other cancers.

6 References

Adair, T. H., & Montani, J.-P. (2010). Overview of Angiogenesis. *Nih.gov*. https://www.ncbi.nlm.nih.gov/books/NBK53238/

Altendorfer, E., Mochalova, Y., & Mayer, A. (2022). BRD4: a general regulator of transcription elongation. *Transcription*, *13*(1-3), 70-81. https://doi.org/10.1080/21541264.2022.2108302

Ameratunga, M., Braña, I., Bono, P., Postel-Vinay, S., Plummer, R., Aspegren, J., Korjamo, T., Snapir, A., & de Bono, J. S. (2020). First-in-human Phase 1 open label study of the BET inhibitor ODM-207 in patients with selected solid tumours. *Br J Cancer*, *123*(12), 1730-1736. https://doi.org/10.1038/s41416-020-01077-z

Amorim, S., Stathis, A., Gleeson, M., Iyengar, S., Magarotto, V., Leleu, X., Morschhauser, F., Karlin, L., Broussais, F., Rezai, K., Herait, P., Kahatt, C., Lokiec, F., Salles, G., Facon, T., Palumbo, A., Cunningham, D., Zucca, E., & Thieblemont, C. (2016). Bromodomain inhibitor OTX015 in patients with lymphoma or multiple myeloma: a dose-escalation, open-label, pharmacokinetic, phase 1 study. *Lancet Haematol*, *3*(4), e196-204. https://doi.org/10.1016/s2352-3026(16)00021-1

Andrews, S. (2019). Babraham Bioinformatics - FastQC A Quality Control tool for High Throughput Sequence Data. *Babraham.ac.uk*. https://www.bioinformatics.babraham.ac.uk/projects/fastqc/

Andrikopoulou, A., Liontos, M., Koutsoukos, K., Dimopoulos, M.-A., & Zagouri, F. (2021). Clinical perspectives of BET inhibition in ovarian cancer. *Cellular Oncology*, *44*(2), 237-249. https://doi.org/10.1007/s13402-020-00578-6

Andrysik, Z., Bernstein, W. Z., Deng, L., Myer, D. L., Li, Y. Q., Tischfield, J. A., Stambrook, P. J., & Bahassi el, M. (2010). The novel mouse Polo-like kinase 5 responds to DNA damage and localizes in the nucleolus. *Nucleic Acids Res*, *38*(9), 2931-2943. https://doi.org/10.1093/nar/gkq011

Anglesio, M. S., Wiegand, K. C., Melnyk, N., Chow, C., Salamanca, C., Prentice, L. M., Senz, J., Yang, W., Spillman, M. A., Cochrane, D. R., Shumansky, K., Shah, S. P., Kalloger, S. E., & Huntsman, D. G. (2013). Type-specific cell line models for type-specific ovarian cancer research. *PLoS One*, *8*(9), e72162. https://doi.org/10.1371/journal.pone.0072162

ATCC. (n.d.-a). Caov-3 [Caov3] - HTB-75 | ATCC. *www.atcc.org*. https://www.atcc.org/products/htb-75#product-references

ATCC. (n.d.-b). NIH:OVCAR-3 [OVCAR3] | ATCC. *www.atcc.org*. https://www.atcc.org/products/htb-161

ATCC. (n.d.-c). *SK-OV-3 [SKOV-3; SKOV3] | ATCC*. https://www.atcc.org/products/htb-77#product-references

ATCC. (n.d.-d). UWB1.289 - CRL-2945 | ATCC. *www.atcc.org*. https://www.atcc.org/products/crl-2945

Banerjee, S., Michalarea, V., Ang, J. E., Ingles Garces, A., Biondo, A., Funingana, I. G., Little, M., Ruddle, R., Raynaud, F., Riisnaes, R., Gurel, B., Chua, S., Tunariu, N., Porter, J. C., Prout, T., Parmar, M., Zachariou, A., Turner, A., Jenkins, B., . . . Banerji, U. (2022). A Phase I Trial of CT900, a Novel α-Folate Receptor-Mediated Thymidylate Synthase Inhibitor, in Patients with Solid Tumors with Expansion Cohorts in Patients with High-Grade Serous Ovarian Cancer. *Clin Cancer Res*, *28*(21), 4634-4641. https://doi.org/10.1158/1078-0432.Ccr-22-1268

Bardal, S. K., Waechter, J. E., & Martin, D. S. (2011). Chapter 20 - Neoplasia. In S. K. Bardal, J. E. Waechter, & D. S. Martin (Eds.), *Applied Pharmacology* (pp. 305-324). W.B. Saunders. https://doi.org/https://doi.org/10.1016/B978-1-4377-0310-8.00020-8

Barnes, B. M., Nelson, L., Tighe, A., Burghel, G. J., Lin, I. H., Desai, S., McGrail, J. C., Morgan, R. D., & Taylor, S. S. (2021). Distinct transcriptional programs stratify ovarian cancer

cell lines into the five major histological subtypes. *Genome Med*, *13*(1), 140. https://doi.org/10.1186/s13073-021-00952-5

Barr, F. A., Silljé, H. H. W., & Nigg, E. A. (2004). Polo-like kinases and the orchestration of cell division. *Nature Reviews Molecular Cell Biology*, *5*(6), 429-441. https://doi.org/10.1038/nrm1401

Barsotti, A. M., & Prives, C. (2009). Pro-proliferative FoxM1 is a target of p53-mediated repression. *Oncogene*, *28*(48), 4295-4305. https://doi.org/10.1038/onc.2009.282

Beaufort, C. M., Helmijr, J. C., Piskorz, A. M., Hoogstraat, M., Ruigrok-Ritstier, K., Besselink, N., Murtaza, M., van IJcken, W. F., Heine, A. A., Smid, M., Koudijs, M. J., Brenton, J. D., Berns, E. M., & Helleman, J. (2014). Ovarian cancer cell line panel (OCCP): clinical importance of in vitro morphological subtypes. *PLoS One*, *9*(9), e103988. https://doi.org/10.1371/journal.pone.0103988

Bell, D., Berchuck, A., Birrer, M., Chien, J., Cramer, D. W., Dao, F., Dhir, R., DiSaia, P., Gabra, H., Glenn, P., Godwin, A. K., Gross, J., Hartmann, L., Huang, M., Huntsman, D. G., Iacocca, M., Imielinski, M., Kalloger, S., Karlan, B. Y., . . . Data coordination, c. (2011). Integrated genomic analyses of ovarian carcinoma. *Nature*, *474*(7353), 609-615. https://doi.org/10.1038/nature10166

Bentsen, M., Goymann, P., Schultheis, H., Klee, K., Petrova, A., Wiegandt, R., Fust, A., Preussner, J., Kuenne, C., Braun, T., Kim, J., & Looso, M. (2020). ATAC-seq footprinting unravels kinetics of transcription factor binding during zygotic genome activation. *Nature Communications*, *11*(1), 4267. https://doi.org/10.1038/s41467-020-18035-1

Berthon, C., Raffoux, E., Thomas, X., Vey, N., Gomez-Roca, C., Yee, K., Taussig, D. C., Rezai, K., Roumier, C., Herait, P., Kahatt, C., Quesnel, B., Michallet, M., Recher, C., Lokiec, F., Preudhomme, C., & Dombret, H. (2016). Bromodomain inhibitor OTX015 in patients with acute leukaemia: a dose-escalation, phase 1 study. *Lancet Haematol*, *3*(4), e186-195. https://doi.org/10.1016/s2352-3026(15)00247-1

Bhagwat, A. S., Roe, J. S., Mok, B. Y. L., Hohmann, A. F., Shi, J., & Vakoc, C. R. (2016). BET Bromodomain Inhibition Releases the Mediator Complex from Select cis-Regulatory Elements. *Cell Rep*, *15*(3), 519-530. https://doi.org/10.1016/j.celrep.2016.03.054

Bondeson, D. P., Paolella, B. R., Asfaw, A., Rothberg, M. V., Skipper, T. A., Langan, C., Mesa, G., Gonzalez, A., Surface, L. E., Ito, K., Kazachkova, M., Colgan, W. N., Warren, A., Dempster, J. M., Krill-Burger, J. M., Ericsson, M., Tang, A. A., Fung, I., Chambers, E. S., . . . Golub, T. R. (2022). Phosphate dysregulation via the XPR1-KIDINS220 protein complex is a therapeutic vulnerability in ovarian cancer. *Nat Cancer*, *3*(6), 681-695. https://doi.org/10.1038/s43018-022-00360-7

Boulares, A. H., Yakovlev, A. G., Ivanova, V., Stoica, B. A., Wang, G., Iyer, S., & Smulson, M. (1999). Role of poly(ADP-ribose) polymerase (PARP) cleavage in apoptosis. Caspase 3-resistant PARP mutant increases rates of apoptosis in transfected cells. *The Journal of biological chemistry*, *274*(33), 22932-22940. https://doi.org/10.1074/jbc.274.33.22932

Brain, K. E., Smits, S., Simon, A. E., Forbes, L. J., Roberts, C., Robbé, I. J., Steward, J., White, C., Neal, R. D., & Hanson, J. (2014). Ovarian cancer symptom awareness and anticipated delayed presentation in a population sample. *BMC Cancer*, *14*, 171. https://doi.org/10.1186/1471-2407-14-171

Cancer Research UK. (2022a). Treatment | Ovarian cancer | Cancer Research UK. *Cancerresearchuk.org*. https://www.cancerresearchuk.org/about-cancer/ovarian-cancer/treatment

Cancer Research UK. (2022b). Women's cancers (gynaecological cancer) | Cancer Research UK. *www.cancerresearchuk.org*. https://www.cancerresearchuk.org/about-cancer/womens-cancer

Cancer Research UK. (n.d.-a). Tests to diagnose | Ovarian cancer | Cancer Research UK. *www.cancerresearchuk.org*. https://www.cancerresearchuk.org/about-cancer/ovarian-cancer/getting-diagnosed/tests

Cancer Research UK. (n.d.-b). *Worldwide cancer statistics*. https://www.cancerresearchuk.org/health-professional/cancer-statistics/worldwide-cancer

Cardiff Oncology. (2023a). Onvansertib + Paclitaxel In TNBC. *clinicaltrials.gov*. https://classic.clinicaltrials.gov/ct2/show/NCT05383196

Cardiff Oncology. (2023b). Study of Onvansertib in Combination With FOLFIRI and Bevacizumab Versus FOLFIRI and Bevacizumab for Second Line Treatment of Metastatic Colorectal Cancer in Participants With a Kirsten Rat Sarcoma Virus Gene (KRAS) or Neuroblastoma-RAS (NRAS) Mutation - Full Text View - ClinicalTrials.gov. *clinicaltrials.gov*. https://classic.clinicaltrials.gov/ct2/show/NCT05593328

Carraro, C., Bonaguro, L., Schulte-Schrepping, J., Horne, A., Oestreich, M., Warnat-Herresthal, S., Helbing, T., De Franco, M., Haendler, K., Mukherjee, S., Ulas, T., Gandin, V., Goettlich, R., Aschenbrenner, A. C., Schultze, J. L., & Gatto, B. (2022). Decoding mechanism of action and sensitivity to drug candidates from integrated transcriptome and chromatin state. *eLife*, *11*, e78012. https://doi.org/10.7554/eLife.78012

CDC. (2023). *Basic Information About Gynecologic Cancers*. https://www.cdc.gov/cancer/gynecologic/basic_info/index.htm#:~:text=The%20five%20main%20types%20of,treatment%20can%20be%20most%20effective

Chandra, A., Pius, C., Nabeel, M., Nair, M., Vishwanatha, J. K., Ahmad, S., & Basha, R. (2019). Ovarian cancer: Current status and strategies for improving therapeutic outcomes. *Cancer Med*, *8*(16), 7018-7031. https://doi.org/10.1002/cam4.2560

Ciceri, P., Müller, S., O'Mahony, A., Fedorov, O., Filippakopoulos, P., Hunt, J. P., Lasater, E. A., Pallares, G., Picaud, S., Wells, C., Martin, S., Wodicka, L. M., Shah, N. P., Treiber, D. K., & Knapp, S. (2014). Dual kinase-bromodomain inhibitors for rationally designed polypharmacology. *Nature Chemical Biology*, *10*(4), 305-312. https://doi.org/10.1038/nchembio.1471

Cousin, S., Blay, J. Y., Garcia, I. B., de Bono, J. S., Le Tourneau, C., Moreno, V., Trigo, J., Hann, C. L., Azad, A. A., Im, S. A., Cassier, P. A., French, C. A., Italiano, A., Keedy, V. L., Plummer, R., Sablin, M. P., Hemming, M. L., Ferron-Brady, G., Wyce, A., . . . Piha-Paul, S. A. (2022). Safety, pharmacokinetic, pharmacodynamic and clinical activity of molibresib for the treatment of nuclear protein in testis carcinoma and other cancers: Results of a Phase I/II open-label, dose escalation study. *Int J Cancer*, *150*(6), 993-1006. https://doi.org/10.1002/ijc.33861

Crump, N. T., Ballabio, E., Godfrey, L., Thorne, R., Repapi, E., Kerry, J., Tapia, M., Hua, P., Lagerholm, C., Filippakopoulos, P., Davies, J. O. J., & Milne, T. A. (2021). BET inhibition disrupts transcription but retains enhancer-promoter contact. *Nature Communications*, *12*(1), 223. https://doi.org/10.1038/s41467-020-20400-z

Danecek, P., Bonfield, J. K., Liddle, J., Marshall, J., Ohan, V., Pollard, M. O., Whitwham, A., Keane, T., McCarthy, S. A., Davies, R. M., & Li, H. (2021). Twelve years of SAMtools and BCFtools. *Gigascience*, *10*(2). https://doi.org/10.1093/gigascience/giab008

de Cárcer, G. (2019). The Mitotic Cancer Target Polo-Like Kinase 1: Oncogene or Tumor Suppressor? *Genes (Basel)*, *10*(3). https://doi.org/10.3390/genes10030208

De Cárcer, G., Manning, G., & Malumbres, M. (2011). From Plk1 to Plk5. *Cell Cycle*, *10*(14), 2255-2262. https://doi.org/10.4161/cc.10.14.16494

Della Pepa, C., Tonini, G., Pisano, C., Di Napoli, M., Cecere, S. C., Tambaro, R., Facchini, G., & Pignata, S. (2015). Ovarian cancer standard of care: are there real alternatives? *Chin J Cancer*, *34*(1), 17-27. https://doi.org/10.5732/cjc.014.10274

Denis, G. V., Vaziri, C., Guo, N., & Faller, D. V. (2000). RING3 kinase transactivates promoters of cell cycle regulatory genes through E2F. *Cell Growth Differ*, *11*(8), 417-424.

Devaiah, B. N., Case-Borden, C., Gegonne, A., Hsu, C. H., Chen, Q., Meerzaman, D., Dey, A., Ozato, K., & Singer, D. S. (2016). BRD4 is a histone acetyltransferase that evicts nucleosomes from chromatin. *Nat Struct Mol Biol*, *23*(6), 540-548. https://doi.org/10.1038/nsmb.3228

Devaiah, B. N., Lewis, B. A., Cherman, N., Hewitt, M. C., Albrecht, B. K., Robey, P. G., Ozato, K., Sims, R. J., 3rd, & Singer, D. S. (2012). BRD4 is an atypical kinase that phosphorylates serine2 of the RNA polymerase II carboxy-terminal domain. *Proc Natl Acad Sci U S A*, *109*(18), 6927-6932. https://doi.org/10.1073/pnas.1120422109

Dobin, A., Davis, C. A., Schlesinger, F., Drenkow, J., Zaleski, C., Jha, S., Batut, P., Chaisson, M., & Gingeras, T. R. (2012). STAR: ultrafast universal RNA-seq aligner. *Bioinformatics*, *29*(1), 15-21. https://doi.org/10.1093/bioinformatics/bts635

Domcke, S., Sinha, R., Levine, D. A., Sander, C., & Schultz, N. (2013). Evaluating cell lines as tumour models by comparison of genomic profiles. *Nature Communications*, *4*(1), 2126. https://doi.org/10.1038/ncomms3126

Drumond-Bock, A. L., & Bieniasz, M. (2021). The role of distinct BRD4 isoforms and their contribution to high-grade serous ovarian carcinoma pathogenesis. *Mol Cancer*, *20*(1), 145. https://doi.org/10.1186/s12943-021-01424-5

Ember, S. W., Zhu, J. Y., Olesen, S. H., Martin, M. P., Becker, A., Berndt, N., Georg, G. I., & Schönbrunn, E. (2014). Acetyl-lysine binding site of bromodomain-containing protein 4 (BRD4) interacts with diverse kinase inhibitors. *ACS Chem Biol*, *9*(5), 1160-1171. https://doi.org/10.1021/cb500072z

Gaitskell, K., Hermon, C., Barnes, I., Pirie, K., Floud, S., Green, J., Beral, V., & Reeves, G. K. (2022). Ovarian cancer survival by stage, histotype, and pre-diagnostic lifestyle factors, in the prospective UK Million Women Study. *Cancer Epidemiology*, *76*, 102074. https://doi.org/https://doi.org/10.1016/j.canep.2021.102074

Gallo Cantafio, M. E., Grillone, K., Caracciolo, D., Scionti, F., Arbitrio, M., Barbieri, V., Pensabene, L., Guzzi, P. H., & Di Martino, M. T. (2018). From Single Level Analysis to Multi-Omics Integrative Approaches: A Powerful Strategy towards the Precision Oncology. *High Throughput*, *7*(4). https://doi.org/10.3390/ht7040033

Gallon, J., Loomis, E., Curry, E., Martin, N., Brody, L., Garner, I., Brown, R., & Flanagan, J. M. (2021). Chromatin accessibility changes at intergenic regions are associated with ovarian cancer drug resistance. *Clinical Epigenetics*, *13*(1), 122. https://doi.org/10.1186/s13148-021-01105-6

Garzon, S., Laganà, A. S., Casarin, J., Raffaelli, R., Cromi, A., Franchi, M., Barra, F., Alkatout, I., Ferrero, S., & Ghezzi, F. (2020). Secondary and tertiary ovarian cancer recurrence: what is the best management? *Gland Surg*, *9*(4), 1118-1129. https://doi.org/10.21037/gs-20-325

Gasperskaja, E., & Kučinskas, V. (2017). The most common technologies and tools for functional genome analysis. *Acta Med Litu*, *24*(1), 1-11. https://doi.org/10.6001/actamedica.v24i1.3457

Gentleman, R. C., Carey, V. J., Bates, D. M., Bolstad, B., Dettling, M., Dudoit, S., Ellis, B., Gautier, L., Ge, Y., Gentry, J., Hornik, K., Hothorn, T., Huber, W., Iacus, S., Irizarry, R., Leisch, F., Li, C., Maechler, M., Rossini, A. J., . . . Zhang, J. (2004). Bioconductor: open software development for computational biology and bioinformatics. *Genome Biology*, *5*(10), R80. https://doi.org/10.1186/gb-2004-5-10-r80

Gockley, A., Melamed, A., Bregar, A. J., Clemmer, J. T., Birrer, M., Schorge, J. O., Del Carmen, M. G., & Rauh-Hain, J. A. (2017). Outcomes of Women With High-Grade and Low-Grade Advanced-Stage Serous Epithelial Ovarian Cancer. *Obstet Gynecol*, *129*(3), 439-447. https://doi.org/10.1097/aog.0000000000001867

Gohda, J., Suzuki, K., Liu, K., Xie, X., Takeuchi, H., Inoue, J. I., Kawaguchi, Y., & Ishida, T. (2018). BI-2536 and BI-6727, dual Polo-like kinase/bromodomain inhibitors, effectively reactivate latent HIV-1. *Sci Rep*, *8*(1), 3521. https://doi.org/10.1038/s41598-018-21942-5

Guo, Q., Cheng, Y., Liang, T., He, Y., Ren, C., Sun, L., & Zhang, G. (2015). Comprehensive analysis of lncRNA-mRNA co-expression patterns identifies immune-associated lncRNA biomarkers in ovarian cancer malignant progression. *Scientific Reports*, *5*(1), 17683. https://doi.org/10.1038/srep17683

Habedanck, R., Stierhof, Y. D., Wilkinson, C. J., & Nigg, E. A. (2005). The Polo kinase Plk4 functions in centriole duplication. *Nat Cell Biol*, *7*(11), 1140-1146. https://doi.org/10.1038/ncb1320

Hall, M., Bertelli, G., Li, L., Green, C., Chan, S., Yeoh, C. C., Hasan, J., Jones, R., Ograbek, A., & Perren, T. J. (2020). Role of front-line bevacizumab in advanced ovarian cancer: the OSCAR study. *Int J Gynecol Cancer*, *30*(2), 213-220. https://doi.org/10.1136/ijgc-2019-000512

Hall, M., Gourley, C., McNeish, I., Ledermann, J., Gore, M., Jayson, G., Perren, T., Rustin, G., & Kaye, S. (2013). Targeted anti-vascular therapies for ovarian cancer: current evidence. *Br J Cancer*, *108*(2), 250-258. https://doi.org/10.1038/bjc.2012.541

Hanahan, D. (2022). Hallmarks of Cancer: New Dimensions. *Cancer Discov*, *12*(1), 31-46. https://doi.org/10.1158/2159-8290.Cd-21-1059

Hanahan, D., & Weinberg, R. A. (2000). The Hallmarks of Cancer. *Cell*, *100*(1), 57-70. https://doi.org/10.1016/s0092-8674(00)81683-9

Hanahan, D., & Weinberg, R. A. (2011). Hallmarks of cancer: the next generation. *Cell*, *144*(5), 646-674. https://doi.org/10.1016/j.cell.2011.02.013

Hightower, E., Cabanillas, M. E., Fuller, G. N., McCutcheon, I. E., Hess, K. R., Shah, K., Waguespack, S. G., Corley, L. J., & Devin, J. K. (2012). Phospho-histone H3 (pHH3) immuno-reactivity as a prognostic marker in non-functioning pituitary adenomas. *Pituitary*, *15*(4), 556-561. https://doi.org/10.1007/s11102-011-0367-3

Hsieh, C.-H., Yeh, H.-N., Huang, C.-T., Wang, W.-H., Hsu, W.-M., Huang, H.-C., & Juan, H.-F. (2022). BI-2536 Promotes Neuroblastoma Cell Death via Minichromosome Maintenance Complex Components 2 and 10. *Pharmaceuticals*, *15*(1), 37. https://www.mdpi.com/1424-8247/15/1/37

Human Protein Atlas. (n.d.-a). BRD4 protein expression summary - The Human Protein Atlas. *www.proteinatlas.org*. https://www.proteinatlas.org/ENSG00000141867-BRD4

Human Protein Atlas. (n.d.-b). PLK1 protein expression summary - The Human Protein Atlas. *www.proteinatlas.org*. https://www.proteinatlas.org/ENSG00000166851-PLK1

Huo, J., Shen, Y., Zhang, Y., & Shen, L. (2022). BI 2536 induces gasdermin E-dependent pyroptosis in ovarian cancer. *Front Oncol*, *12*, 963928. https://doi.org/10.3389/fonc.2022.963928

Iorio, F., Knijnenburg, T. A., Vis, D. J., Bignell, G. R., Menden, M. P., Schubert, M., Aben, N., Gonçalves, E., Barthorpe, S., Lightfoot, H., Cokelaer, T., Greninger, P., van Dyk, E., Chang, H., de Silva, H., Heyn, H., Deng, X., Egan, R. K., Liu, Q., . . . Garnett, M. J. (2016). A Landscape of Pharmacogenomic Interactions in Cancer. *Cell*, *166*(3), 740-754. https://doi.org/https://doi.org/10.1016/j.cell.2016.06.017

Jackman, M., Lindon, C., Nigg, E. A., & Pines, J. (2003). Active cyclin B1-Cdk1 first appears on centrosomes in prophase. *Nat Cell Biol*, *5*(2), 143-148. https://doi.org/10.1038/ncb918

Jang, M. K., Mochizuki, K., Zhou, M., Jeong, H. S., Brady, J. N., & Ozato, K. (2005). The bromodomain protein Brd4 is a positive regulatory component of P-TEFb and stimulates RNA polymerase II-dependent transcription. *Mol Cell*, *19*(4), 523-534. https://doi.org/10.1016/j.molcel.2005.06.027

Javle, M., & Curtin, N. J. (2011). The role of PARP in DNA repair and its therapeutic exploitation. *Br J Cancer*, *105*(8), 1114-1122. https://doi.org/10.1038/bjc.2011.382

Jensen, C., & Teng, Y. (2020). Is It Time to Start Transitioning From 2D to 3D Cell Culture? *Front Mol Biosci*, *7*, 33. https://doi.org/10.3389/fmolb.2020.00033

Jin, Y., Qiu, Y., Li, Y., Jiang, Z., Hu, S., & Dai, H. (2023). A novel epithelial-mesenchymal transition-related lncRNA signature predicts prognosis and immune status in endometrioid endometrial cancer. *Medicine (Baltimore)*, *102*(26), e34126. https://doi.org/10.1097/md.0000000000034126

Kagami, Y., Ono, M., & Yoshida, K. (2017). Plk1 phosphorylation of CAP-H2 triggers chromosome condensation by condensin II at the early phase of mitosis. *Sci Rep*, *7*(1), 5583. https://doi.org/10.1038/s41598-017-05986-7

Kagohara, L. T., Zamuner, F., Davis-Marcisak, E. F., Sharma, G., Considine, M., Allen, J., Yegnasubramanian, S., Gaykalova, D. A., & Fertig, E. J. (2020). Integrated single-cell and bulk gene expression and ATAC-seq reveals heterogeneity and early changes in pathways associated with resistance to cetuximab in HNSCC-sensitive cell lines. *British Journal of Cancer*, *123*(1), 101-113. https://doi.org/10.1038/s41416-020-0851-5

Kampan, N. C., Madondo, M. T., McNally, O. M., Quinn, M., & Plebanski, M. (2015). Paclitaxel and Its Evolving Role in the Management of Ovarian Cancer. *Biomed Res Int*, *2015*, 413076. https://doi.org/10.1155/2015/413076

Kapałczyńska, M., Kolenda, T., Przybyła, W., Zajączkowska, M., Teresiak, A., Filas, V., Ibbs, M., Bliźniak, R., Łuczewski, Ł., & Lamperska, K. (2018). 2D and 3D cell cultures - a comparison of different types of cancer cell cultures. *Arch Med Sci*, *14*(4), 910-919. https://doi.org/10.5114/aoms.2016.63743

Karimi-Zarchi, M., Dehshiri-Zadeh, N., Sekhavat, L., & Nosouhi, F. (2016). Correlation of CA-125 serum level and clinico-pathological characteristic of patients with endometriosis. *Int J Reprod Biomed*, *14*(11), 713-718.

King, E. R., Zu, Z., Tsang, Y. T., Deavers, M. T., Malpica, A., Mok, S. C., Gershenson, D. M., & Wong, K. K. (2011). The insulin-like growth factor 1 pathway is a potential therapeutic target for low-grade serous ovarian carcinoma. *Gynecol Oncol*, *123*(1), 13-18. https://doi.org/10.1016/j.ygyno.2011.06.016

Koblan, L. W., Buckley, D. L., Ott, C. J., Fitzgerald, M. E., Ember, S. W., Zhu, J. Y., Liu, S., Roberts, J. M., Remillard, D., Vittori, S., Zhang, W., Schonbrunn, E., & Bradner, J. E. (2016). Assessment of Bromodomain Target Engagement by a Series of BI2536 Analogues with Miniaturized BET-BRET. *ChemMedChem*, *11*(23), 2575-2581. https://doi.org/10.1002/cmdc.201600502

Kohler, M., Bauknecht, T., Grimm, M., Birmelin, G., Kommoss, F., & Wagner, E. (1992). Epidermal growth factor receptor and transforming growth factor alpha expression in human ovarian carcinomas. *Eur J Cancer*, *28a*(8-9), 1432-1437. https://doi.org/10.1016/0959-8049(92)90538-d

Konstantinopoulos, P. A., Lee, J. M., Gao, B., Miller, R., Lee, J. Y., Colombo, N., Vergote, I., Credille, K. M., Young, S. R., McNeely, S., Wang, X. A., Lin, A. B., & Shapira-Frommer, R. (2022). A Phase 2 study of prexasertib (LY2606368) in platinum resistant or refractory recurrent ovarian cancer. *Gynecol Oncol*. https://doi.org/10.1016/j.ygyno.2022.09.019

Kressin, M., Fietz, D., Becker, S., & Strebhardt, K. (2021). Modelling the Functions of Polo-Like Kinases in Mice and Their Applications as Cancer Targets with a Special Focus on Ovarian Cancer. *Cells*, *10*(5), 1176. https://www.mdpi.com/2073-4409/10/5/1176

Kruhlak, M. J., Hendzel, M. J., Fischle, W., Bertos, N. R., Hameed, S., Yang, X. J., Verdin, E., & Bazett-Jones, D. P. (2001). Regulation of global acetylation in mitosis through loss of histone acetyltransferases and deacetylases from chromatin. *The Journal of biological chemistry*, *276*(41), 38307-38319. https://doi.org/10.1074/jbc.M100290200

Lane, H. A., & Nigg, E. A. (1996). Antibody microinjection reveals an essential role for human polo-like kinase 1 (Plk1) in the functional maturation of mitotic centrosomes. *J Cell Biol*, *135*(6 Pt 2), 1701-1713. https://doi.org/10.1083/jcb.135.6.1701

Langmead, B., & Salzberg, S. (2012). Bowtie 2: fast and sensitive read alignment. *bowtie-bio.sourceforge.net*. https://bowtie-bio.sourceforge.net/bowtie2/index.shtml

Lê, S., Josse, J., & Husson, F. (2008). FactoMineR: an R package for multivariate analysis. *Journal of statistical software*, *25*, 1-18.

Ledermann, J. A., Canevari, S., & Thigpen, T. (2015). Targeting the folate receptor: diagnostic and therapeutic approaches to personalize cancer treatments. *Ann Oncol*, *26*(10), 2034-2043. https://doi.org/10.1093/annonc/mdv250

Lewin, J., Soria, J.-C., Stathis, A., Delord, J.-P., Peters, S., Awada, A., Aftimos, P. G., Bekradda, M., Rezai, K., Zeng, Z., Hussain, A., Perez, S., Siu, L. L., & Massard, C. (2018). Phase Ib Trial With Birabresib, a Small-Molecule Inhibitor of Bromodomain and Extraterminal Proteins, in Patients With Selected Advanced Solid Tumors. *Journal of Clinical Oncology*, *36*(30), 3007-3014. https://doi.org/10.1200/jco.2018.78.2292

Lheureux, S., Cristea, M. C., Bruce, J. P., Garg, S., Cabanero, M., Mantia-Smaldone, G., Olawaiye, A. B., Ellard, S. L., Weberpals, J. I., Wahner Hendrickson, A. E., Fleming, G. F., Welch, S., Dhani, N. C., Stockley, T., Rath, P., Karakasis, K., Jones, G. N., Jenkins, S., Rodriguez-Canales, J., . . . Oza, A. M. (2021). Adavosertib plus gemcitabine for platinum-resistant or platinum-refractory recurrent ovarian cancer: a double-blind, randomised, placebo-controlled, phase 2 trial. *The Lancet*, *397*(10271), 281-292. https://doi.org/https://doi.org/10.1016/S0140-6736(20)32554-X

Li, M., Li, X., Zhang, Y., Wu, H., Zhou, H., Ding, X., Zhang, X., Jin, X., Wang, Y., Yin, X., Li, C., Yang, P., & Xu, H. (2020). Micropeptide MIAC Inhibits HNSCC Progression by Interacting with Aquaporin 2. *Journal of the American Chemical Society*, *142*(14), 6708-6716. https://doi.org/10.1021/jacs.0c00706

Li, M., Liu, G., Jin, X., Guo, H., Setrerrahmane, S., Xu, X., Li, T., Lin, Y., & Xu, H. (2022). Micropeptide MIAC inhibits the tumor progression by interacting with AQP2 and inhibiting EREG/EGFR signaling in renal cell carcinoma. *Molecular Cancer*, *21*(1), 181. https://doi.org/10.1186/s12943-022-01654-1

Li, Z., Yang, C., Li, X., Du, X., Tao, Y., Ren, J., Fang, F., Xie, Y., Li, M., Qian, G., Xu, L., Cao, X., Wu, Y., Lv, H., Hu, S., Lu, J., & Pan, J. (2020). The dual role of BI 2536, a small-molecule inhibitor that targets PLK1, in induction of apoptosis and attenuation of autophagy in neuroblastoma cells. *J Cancer*, *11*(11), 3274-3287. https://doi.org/10.7150/jca.33110

Liao, Y., Wang, J., Jaehnig, E. J., Shi, Z., & Zhang, B. (2019). WebGestalt 2019: gene set analysis toolkit with revamped UIs and APIs. *Nucleic Acids Research*, *47*(W1), W199-W205. https://doi.org/10.1093/nar/gkz401

Lim, H. J., & Ledger, W. (2016). Targeted therapy in ovarian cancer. *Womens Health (Lond)*, *12*(3), 363-378. https://doi.org/10.2217/whe.16.4

Liu, X., Lei, M., & Erikson, R. L. (2006). Normal cells, but not cancer cells, survive severe Plk1 depletion. *Mol Cell Biol*, *26*(6), 2093-2108. https://doi.org/10.1128/mcb.26.6.2093-2108.2006

Liu, Z., Sun, Q., & Wang, X. (2017). PLK1, A Potential Target for Cancer Therapy. *Transl Oncol*, *10*(1), 22-32. https://doi.org/10.1016/j.tranon.2016.10.003

Love, M. I., Huber, W., & Anders, S. (2014). Moderated estimation of fold change and dispersion for RNA-seq data with DESeq2. *Genome Biology*, *15*(12), 550. https://doi.org/10.1186/s13059-014-0550-8

Lovén, J., Hoke, H. A., Lin, C. Y., Lau, A., Orlando, D. A., Vakoc, C. R., Bradner, J. E., Lee, T. I., & Young, R. A. (2013). Selective inhibition of tumor oncogenes by disruption of super-enhancers. *Cell*, *153*(2), 320-334. https://doi.org/10.1016/j.cell.2013.03.036

Lu, J., Qian, Y., Altieri, M., Dong, H., Wang, J., Raina, K., Hines, J., Winkler, James D., Crew, Andrew P., Coleman, K., & Crews, Craig M. (2015). Hijacking the E3 Ubiquitin Ligase

Cereblon to Efficiently Target BRD4. *Chemistry & Biology*, *22*(6), 755-763. https://doi.org/https://doi.org/10.1016/j.chembiol.2015.05.009

Macmillan Cancer, S. (n.d.). Cancer prevalence - Macmillan Cancer Support. *www.macmillan.org.uk*. https://www.macmillan.org.uk/about-us/what-we-do/research/cancer-prevalence#:~:text=There%20are%203%20million%20people

Mah, L. J., El-Osta, A., & Karagiannis, T. C. (2010). γH2AX: a sensitive molecular marker of DNA damage and repair. *Leukemia*, *24*(4), 679-686. https://doi.org/10.1038/leu.2010.6

Maire, V., Némati, F., Richardson, M., Vincent-Salomon, A., Tesson, B., Rigaill, G., Gravier, E., Marty-Prouvost, B., De Koning, L., Lang, G., Gentien, D., Dumont, A., Barillot, E., Marangoni, E., Decaudin, D., Roman-Roman, S., Pierré, A., Cruzalegui, F., Depil, S., . . . Dubois, T. (2013). Polo-like kinase 1: a potential therapeutic option in combination with conventional chemotherapy for the management of patients with triple-negative breast cancer. *Cancer Res*, *73*(2), 813-823. https://doi.org/10.1158/0008-5472.Can-12-2633

Mak, V. C. Y., Li, X., Rao, L., Zhou, Y., Tsao, S.-W., & Cheung, L. W. T. (2021). p85β alters response to EGFR inhibitor in ovarian cancer through p38 MAPK-mediated regulation of DNA repair. *Neoplasia*, *23*(7), 718-730. https://doi.org/https://doi.org/10.1016/j.neo.2021.05.009

Marmorstein, R., & Zhou, M. M. (2014). Writers and readers of histone acetylation: structure, mechanism, and inhibition. *Cold Spring Harb Perspect Biol*, *6*(7), a018762. https://doi.org/10.1101/cshperspect.a018762

Mayo Clinic. (2023). Onvansertib for the Treatment of Recurrent or Refractory Chronic Myelomonocytic Leukemia. *clinicaltrials.gov*. https://clinicaltrials.gov/study/NCT05549661

Mei, J., Tian, H., Huang, H. S., Hsu, C. F., Liou, Y., Wu, N., Zhang, W., & Chu, T. Y. (2021). Cellular models of development of ovarian high-grade serous carcinoma: A review of cell of origin and mechanisms of carcinogenesis. *Cell Prolif*, *54*(5), e13029. https://doi.org/10.1111/cpr.13029

Menghi, F., & Liu, E. T. (2022). Functional genomics of complex cancer genomes. *Nature Communications*, *13*(1), 5908. https://doi.org/10.1038/s41467-022-33717-8

Millennium Pharmaceuticals. (2014). Study of Orally Administered TAK-960 in Patients With Advanced Nonhematologic Malignancies. *clinicaltrials.gov*. https://classic.clinicaltrials.gov/ct2/show/NCT01179399?intr=TAK-960&draw=2&rank=1

Miller, R. E., El-Shakankery, K. H., & Lee, J. Y. (2022). PARP inhibitors in ovarian cancer: overcoming resistance with combination strategies. *J Gynecol Oncol*, *33*(3), e44. https://doi.org/10.3802/jgo.2022.33.e44

Morales, J., Li, L., Fattah, F. J., Dong, Y., Bey, E. A., Patel, M., Gao, J., & Boothman, D. A. (2014). Review of poly (ADP-ribose) polymerase (PARP) mechanisms of action and rationale for targeting in cancer and other diseases. *Crit Rev Eukaryot Gene Expr*, *24*(1), 15-28. https://doi.org/10.1615/critreveukaryotgeneexpr.2013006875

Mu, X., Bai, L., Xu, Y., Wang, J., & Lu, H. (2020). Protein targeting chimeric molecules specific for dual bromodomain 4 (BRD4) and Polo-like kinase 1 (PLK1) proteins in acute myeloid leukemia cells. *Biochemical and Biophysical Research Communications*, *521*(4), 833-839. https://doi.org/https://doi.org/10.1016/j.bbrc.2019.11.007

Naumann, R. W., Coleman, R. L., Burger, R. A., Sausville, E. A., Kutarska, E., Ghamande, S. A., Gabrail, N. Y., Depasquale, S. E., Nowara, E., Gilbert, L., Gersh, R. H., Teneriello, M. G., Harb, W. A., Konstantinopoulos, P. A., Penson, R. T., Symanowski, J. T., Lovejoy, C. D., Leamon, C. P., Morgenstern, D. E., & Messmann, R. A. (2013). PRECEDENT: a randomized phase II trial comparing vintafolide (EC145) and pegylated liposomal doxorubicin (PLD) in combination versus PLD alone in patients with platinum-resistant

ovarian cancer. *J Clin Oncol*, *31*(35), 4400-4406. https://doi.org/10.1200/jco.2013.49.7685

NHS England. (2016). *Chemo drug optimisation to improve patient experience of cancer treatment*. https://www.england.nhs.uk/2016/05/chemo-drug-optimisation/

Nicodeme, E., Jeffrey, K. L., Schaefer, U., Beinke, S., Dewell, S., Chung, C.-w., Chandwani, R., Marazzi, I., Wilson, P., Coste, H., White, J., Kirilovsky, J., Rice, C. M., Lora, J. M., Prinjha, R. K., Lee, K., & Tarakhovsky, A. (2010). Suppression of inflammation by a synthetic histone mimic. *Nature*, *468*(7327), 1119-1123. https://doi.org/10.1038/nature09589

Oliveros, J. C. (2015). Venny 2.1.0. *bioinfogp.cnb.csic.es*. https://bioinfogp.cnb.csic.es/tools/venny/

Olmos, D., Barker, D., Sharma, R., Brunetto, A. T., Yap, T. A., Taegtmeyer, A. B., Barriuso, J., Medani, H., Degenhardt, Y. Y., Allred, A. J., Smith, D. A., Murray, S. C., Lampkin, T. A., Dar, M. M., Wilson, R., de Bono, J. S., & Blagden, S. P. (2011). Phase I study of GSK461364, a specific and competitive Polo-like kinase 1 inhibitor, in patients with advanced solid malignancies. *Clin Cancer Res*, *17*(10), 3420-3430. https://doi.org/10.1158/1078-0432.Ccr-10-2946

Ozaki, T., & Nakagawara, A. (2011). Role of p53 in Cell Death and Human Cancers. *Cancers (Basel)*, *3*(1), 994-1013. https://doi.org/10.3390/cancers3010994

Petronczki, M., Lénárt, P., & Peters, J. M. (2008). Polo on the Rise-from Mitotic Entry to Cytokinesis with Plk1. *Dev Cell*, *14*(5), 646-659. https://doi.org/10.1016/j.devcel.2008.04.014

Pokhriyal, R., Hariprasad, R., Kumar, L., & Hariprasad, G. (2019). Chemotherapy Resistance in Advanced Ovarian Cancer Patients. *Biomark Cancer*, *11*, 1179299x19860815. https://doi.org/10.1177/1179299x19860815

Pujade-Lauraine, E., Selle, F., Weber, B., Ray-Coquard, I.-L., Vergote, I., Sufliarsky, J., Del Campo, J. M., Lortholary, A., Lesoin, A., Follana, P., Freyer, G., Pardo, B., Vidal, L., Tholander, B., Gladieff, L., Sassi, M., Garin-Chesa, P., Nazabadioko, S., Marzin, K., . . . Joly, F. (2016). Volasertib Versus Chemotherapy in Platinum-Resistant or -Refractory Ovarian Cancer: A Randomized Phase II Groupe des Investigateurs Nationaux pour l'Etude des Cancers de l'Ovaire Study. *Journal of Clinical Oncology*, *34*(7), 706-713. https://doi.org/10.1200/jco.2015.62.1474

Qu, X., Wu, Z., Dong, W., Zhang, T., Wang, L., Pang, Z., Ma, W., & Du, J. (2017). Update of IGF-1 receptor inhibitor (ganitumab, dalotuzumab, cixutumumab, teprotumumab and figitumumab) effects on cancer therapy. *Oncotarget*, *8*(17), 29501-29518. https://doi.org/10.18632/oncotarget.15704

Quintela, M., James, D. W., Pociute, A., Powell, L., Edwards, K., Coombes, Z., Garcia, J., Garton, N., Das, N., Lutchman-Singh, K., Margarit, L., Beynon, A. L., Rioja, I., Prinjha, R. K., Harker, N. R., Gonzalez, D., Conlan, R. S., & Francis, L. W. (2023). Bromodomain inhibitor i-BET858 triggers a unique transcriptional response coupled to enhanced DNA damage, cell cycle arrest and apoptosis in high-grade ovarian carcinoma cells. *Clinical Epigenetics*, *15*(1). https://doi.org/10.1186/s13148-023-01477-x

Raab, M., Sanhaji, M., Zhou, S., Rödel, F., El-Balat, A., Becker, S., & Strebhardt, K. (2019). Blocking Mitotic Exit of Ovarian Cancer Cells by Pharmaceutical Inhibition of the Anaphase-Promoting Complex Reduces Chromosomal Instability. *Neoplasia*, *21*(4), 363-375. https://doi.org/https://doi.org/10.1016/j.neo.2019.01.007

Ramírez, F., Ryan, D. P., Grüning, B., Bhardwaj, V., Kilpert, F., Richter, A. S., Heyne, S., Dündar, F., & Manke, T. (2016). deepTools2: a next generation web server for deep-sequencing data analysis. *Nucleic Acids Research*, *44*(W1), W160-W165. https://doi.org/10.1093/nar/gkw257

Rhyasen, G. W., Yao, Y., Zhang, J., Dulak, A., Castriotta, L., Jacques, K., Zhao, W., Gharahdaghi, F., Hattersley, M. M., Lyne, P. D., Clark, E., Zinda, M., Fawell, S. E., Mills, G. B., & Chen, H. (2018). BRD4 amplification facilitates an oncogenic gene expression program in high-grade serous ovarian cancer and confers sensitivity to BET inhibitors. *PLoS One*, *13*(7), e0200826. https://doi.org/10.1371/journal.pone.0200826

Robinson, J. T., Thorvaldsdottir, H., Turner, D., & Mesirov, J. P. (2023). igv.js: an embeddable JavaScript implementation of the Integrative Genomics Viewer (IGV). *Bioinformatics*, *39*(1). https://doi.org/10.1093/bioinformatics/btac830

Rojas, V., Hirshfield, K. M., Ganesan, S., & Rodriguez-Rodriguez, L. (2016). Molecular Characterization of Epithelial Ovarian Cancer: Implications for Diagnosis and Treatment. *International Journal of Molecular Sciences*, *17*(12), 2113. https://www.mdpi.com/1422-0067/17/12/2113

Schöffski, P., Blay, J. Y., De Greve, J., Brain, E., Machiels, J. P., Soria, J. C., Sleijfer, S., Wolter, P., Ray-Coquard, I., Fontaine, C., Munzert, G., Fritsch, H., Hanft, G., Aerts, C., Rapion, J., Allgeier, A., Bogaerts, J., & Lacombe, D. (2010). Multicentric parallel phase II trial of the polo-like kinase 1 inhibitor BI 2536 in patients with advanced head and neck cancer, breast cancer, ovarian cancer, soft tissue sarcoma and melanoma. The first protocol of the European Organization for Research and Treatment of Cancer (EORTC) Network Of Core Institutes (NOCI). *Eur J Cancer*, *46*(12), 2206-2215. https://doi.org/10.1016/j.ejca.2010.03.039

Shibuya, M. (2011). Vascular Endothelial Growth Factor (VEGF) and Its Receptor (VEGFR) Signaling in Angiogenesis: A Crucial Target for Anti- and Pro-Angiogenic Therapies. *Genes Cancer*, *2*(12), 1097-1105. https://doi.org/10.1177/1947601911423031

Shin, S. B., Woo, S. U., & Yim, H. (2015). Differential Cellular Effects of Plk1 Inhibitors Targeting the ATP-binding Domain or Polo-box Domain. *J Cell Physiol*, *230*(12), 3057-3067. https://doi.org/10.1002/jcp.25042

Song, S., Grenfell, T. Z., Garfield, S., Erikson, R. L., & Lee, K. S. (2000). Essential function of the polo box of Cdc5 in subcellular localization and induction of cytokinetic structures. *Mol Cell Biol*, *20*(1), 286-298. https://doi.org/10.1128/mcb.20.1.286-298.2000

Su, S., Chhabra, G., Singh, C. K., Ndiaye, M. A., & Ahmad, N. (2022). PLK1 inhibition-based combination therapies for cancer management. *Transl Oncol*, *16*, 101332. https://doi.org/10.1016/j.tranon.2021.101332

Takai, N., Miyazaki, T., Fujisawa, K., Nasu, K., Hamanaka, R., & Miyakawa, I. (2001). Expression of polo-like kinase in ovarian cancer is associated with histological grade and clinical stage. *Cancer Letters*, *164*(1), 41-49. https://doi.org/https://doi.org/10.1016/S0304-3835(00)00703-5

Tangutoori, S., Baldwin, P., & Sridhar, S. (2015). PARP inhibitors: A new era of targeted therapy. *Maturitas*, *81*(1), 5-9. https://doi.org/10.1016/j.maturitas.2015.01.015

Taniguchi, Y. (2016). The Bromodomain and Extra-Terminal Domain (BET) Family: Functional Anatomy of BET Paralogous Proteins. *International Journal of Molecular Sciences*, *17*(11), 1849. https://www.mdpi.com/1422-0067/17/11/1849

Tas, F., Karabulut, S., Serilmez, M., Ciftci, R., & Duranyildiz, D. (2014). Increased serum level of epidermal growth factor receptor (EGFR) is associated with poor progression-free survival in patients with epithelial ovarian cancer. *Cancer Chemotherapy and Pharmacology*, *73*(3), 631-637. https://doi.org/10.1007/s00280-014-2396-x

Tofani, L. B., Sousa, L. O., Luiz, M. T., Abriata, J. P., Marchetti, J. M., Leopoldino, A. M., & Swiech, K. (2021). Generation of a Three-Dimensional in Vitro Ovarian Cancer Co-Culture Model for Drug Screening Assays. *J Pharm Sci*, *110*(7), 2629-2636. https://doi.org/10.1016/j.xphs.2021.04.003

Torre, L. A., Trabert, B., DeSantis, C. E., Miller, K. D., Samimi, G., Runowicz, C. D., Gaudet, M. M., Jemal, A., & Siegel, R. L. (2018). Ovarian cancer statistics, 2018. *CA Cancer J Clin*, *68*(4), 284-296. https://doi.org/10.3322/caac.21456

Toyoshima-Morimoto, F., Taniguchi, E., Shinya, N., Iwamatsu, A., & Nishida, E. (2001). Polo-like kinase 1 phosphorylates cyclin B1 and targets it to the nucleus during prophase. *Nature*, *410*(6825), 215-220. https://doi.org/10.1038/35065617

Trabucco, S. E., Gerstein, R. M., Evens, A. M., Bradner, J. E., Shultz, L. D., Greiner, D. L., & Zhang, H. (2015). Inhibition of bromodomain proteins for the treatment of human diffuse large B-cell lymphoma. *Clin Cancer Res*, *21*(1), 113-122. https://doi.org/10.1158/1078-0432.Ccr-13-3346

Trivedi, A., Mehrotra, A., Baum, C. E., Lewis, B., Basuroy, T., Blomquist, T., Trumbly, R., Filipp, F. V., Setaluri, V., & de la Serna, I. L. (2020). Bromodomain and extra-terminal domain (BET) proteins regulate melanocyte differentiation. *Epigenetics & Chromatin*, *13*(1), 14. https://doi.org/10.1186/s13072-020-00333-z

Ucar, D., & Lin, D. I. (2015). Amplification of the bromodomain-containing protein 4 gene in ovarian high-grade serous carcinoma is associated with worse prognosis and survival. *Mol Clin Oncol*, *3*(6), 1291-1294. https://doi.org/10.3892/mco.2015.622

Van de Sande, B., Lee, J. S., Mutasa-Gottgens, E., Naughton, B., Bacon, W., Manning, J., Wang, Y., Pollard, J., Mendez, M., Hill, J., Kumar, N., Cao, X., Chen, X., Khaladkar, M., Wen, J., Leach, A., & Ferran, E. (2023). Applications of single-cell RNA sequencing in drug discovery and development. *Nature Reviews Drug Discovery*, *22*(6), 496-520. https://doi.org/10.1038/s41573-023-00688-4

van de Weerdt, B. C., & Medema, R. H. (2006). Polo-like kinases: a team in control of the division. *Cell Cycle*, *5*(8), 853-864. https://doi.org/10.4161/cc.5.8.2692

Vousden, K. H., & Prives, C. (2009). Blinded by the Light: The Growing Complexity of p53. *Cell*, *137*(3), 413-431. https://doi.org/10.1016/j.cell.2009.04.037

Ward, A., Khanna, K. K., & Wiegmans, A. P. (2015). Targeting homologous recombination, new pre-clinical and clinical therapeutic combinations inhibiting RAD51. *Cancer Treat Rev*, *41*(1), 35-45. https://doi.org/10.1016/j.ctrv.2014.10.006

Warnke, S., Kemmler, S., Hames, R. S., Tsai, H. L., Hoffmann-Rohrer, U., Fry, A. M., & Hoffmann, I. (2004). Polo-like kinase-2 is required for centriole duplication in mammalian cells. *Curr Biol*, *14*(13), 1200-1207. https://doi.org/10.1016/j.cub.2004.06.059

Weichert, W., Schmidt, M., Jacob, J., Gekeler, V., Langrehr, J., Neuhaus, P., Bahra, M., Denkert, C., Dietel, M., & Kristiansen, G. (2005). Overexpression of polo-like kinase 1 is a common and early event in pancreatic cancer. *Pancreatology*, *5*(2), 259-265. https://doi.org/https://doi.org/10.1159/000085280

Weinberg, R. A. (2013). *The Biology of Cancer*. W.W. Norton & Company. https://doi.org/10.1201/9780429258794

Werner, M. T., Wang, H., Hamagami, N., Hsu, S. C., Yano, J. A., Stonestrom, A. J., Behera, V., Zong, Y., Mackay, J. P., & Blobel, G. A. (2020). Comparative structure-function analysis of bromodomain and extraterminal motif (BET) proteins in a gene-complementation system. *Journal of Biological Chemistry*, *295*(7), 1898-1914. https://doi.org/10.1074/jbc.ra119.010679

Weroha, S. J., & Haluska, P. (2008). IGF-1 Receptor Inhibitors in Clinical Trials—Early Lessons. *Journal of Mammary Gland Biology and Neoplasia*, *13*(4), 471-483. https://doi.org/10.1007/s10911-008-9104-6

Wickham, H. (2016). *ggplot2*. Springer International Publishing. https://doi.org/10.1007/978-3-319-24277-4

World Health Organization. (2019). *Cancer*. https://www.who.int/health-topics/cancer#tab=tab_1

World Health Organization. (2020a). *Cancer Today* https://gco.iarc.fr/today/online-analysis-table?v=2020&mode=cancer&mode_population=continents&population=900&populations=826&key=asr&sex=2&cancer=39&type=0&statistic=5&prevalence=0&population_group=0&ages_group%5B%5D=0&ages_group%5B%5D=17&group_cancer=1&include_nmsc=0&include_nmsc_other=1#collapse-group-0-4

World Health Organization. (2020b). *Cancer Tomorrow*. https://gco.iarc.fr/tomorrow/en/dataviz/trends?types=0_1&sexes=2&mode=cancer&group_populations=0&multiple_populations=0&multiple_cancers=1&cancers=23_24_25&populations=826&group_cancers=0&single_unit=500&key=total&show_bar_mode_prop=0&bar_mode=stacked

Xie, S., Xie, B., Lee, M. Y., & Dai, W. (2005). Regulation of cell cycle checkpoints by polo-like kinases. *Oncogene*, *24*(2), 277-286. https://doi.org/10.1038/sj.onc.1208218

Xu, D., Wang, Q., Jiang, Y., Zhang, Y., Vega-SaenzdeMiera, E., Osman, I., & Dai, W. (2012). Roles of Polo-like kinase 3 in suppressing tumor angiogenesis. *Experimental Hematology & Oncology*, *1*(1), 5. https://doi.org/10.1186/2162-3619-1-5

Yokoyama, Y., Zhu, H., Lee, J. H., Kossenkov, A. V., Wu, S. Y., Wickramasinghe, J. M., Yin, X., Palozola, K. C., Gardini, A., Showe, L. C., Zaret, K. S., Liu, Q., Speicher, D., Conejo-Garcia, J. R., Bradner, J. E., Zhang, Z., Sood, A. K., Ordog, T., Bitler, B. G., & Zhang, R. (2016). BET Inhibitors Suppress ALDH Activity by Targeting ALDH1A1 Super-Enhancer in Ovarian Cancer. *Cancer Res*, *76*(21), 6320-6330. https://doi.org/10.1158/0008-5472.Can-16-0854

Zeidan, A. M., Ridinger, M., Lin, T. L., Becker, P. S., Schiller, G. J., Patel, P. A., Spira, A. I., Tsai, M. L., Samuëlsz, E., Silberman, S. L., Erlander, M., & Wang, E. S. (2020). A Phase Ib Study of Onvansertib, a Novel Oral PLK1 Inhibitor, in Combination Therapy for Patients with Relapsed or Refractory Acute Myeloid Leukemia. *Clin Cancer Res*, *26*(23), 6132-6140. https://doi.org/10.1158/1078-0432.Ccr-20-2586

Zhan, L., Li, J., & Wei, B. (2018). Long non-coding RNAs in ovarian cancer. *J Exp Clin Cancer Res*, *37*(1), 120. https://doi.org/10.1186/s13046-018-0793-4

Zhang, R., Shi, H., Ren, F., Liu, H., Zhang, M., Deng, Y., & Li, X. (2015). Misregulation of polo-like protein kinase 1, P53 and P21WAF1 in epithelial ovarian cancer suggests poor prognosis. *Oncology Reports*, *33*(3), 1235-1242. https://doi.org/10.3892/or.2015.3723

Zhang, Y., Cao, L., Nguyen, D., & Lu, H. (2016). TP53 mutations in epithelial ovarian cancer. *Transl Cancer Res*, *5*(6), 650-663. https://doi.org/10.21037/tcr.2016.08.40

Zhang, Y., Liu, T., Meyer, C. A., Eeckhoute, J., Johnson, D. S., Bernstein, B. E., Nusbaum, C., Myers, R. M., Brown, M., Li, W., & Liu, X. S. (2008). Model-based Analysis of ChIP-Seq (MACS). *Genome Biology*, *9*(9), R137. https://doi.org/10.1186/gb-2008-9-9-r137

Zhang, Z., Ma, P., Jing, Y., Yan, Y., Cai, M. C., Zhang, M., Zhang, S., Peng, H., Ji, Z. L., Di, W., Gu, Z., Gao, W. Q., & Zhuang, G. (2016). BET Bromodomain Inhibition as a Therapeutic Strategy in Ovarian Cancer by Downregulating FoxM1. *Theranostics*, *6*(2), 219-230. https://doi.org/10.7150/thno.13178

Zhou, J., Wang, Y., Wang, Y., Yin, X., He, Y., Chen, L., Wang, W., Liu, T., & Di, W. (2014). FOXM1 modulates cisplatin sensitivity by regulating EXO1 in ovarian cancer. *PLoS One*, *9*(5), e96989. https://doi.org/10.1371/journal.pone.0096989

Zitouni, S., Nabais, C., Jana, S. C., Guerrero, A., & Bettencourt-Dias, M. (2014). Polo-like kinases: structural variations lead to multiple functions. *Nature Reviews Molecular Cell Biology*, *15*(7), 433-452. https://doi.org/10.1038/nrm3819